String Stable Constant-Spacing Platoon with Robustness to Communication Delays and Cutoff

Yudong Lin

A dissertation
submitted in partial fulfillment of the
requirements for the degree of

Doctor of Philosophy

University of Washington

2024

Reading Committee:

Santosh Devasia, Chair

Brian Fabien, Chair

Xuegang (Jeff) Ban

Per Reinhall

Xu Chen

Program Authorized to Offer Degree:
Department of Mechanical Engineering

University of Washington

Abstract

String Stable Constant-Spacing Platoon with Robustness to Communication Delays and Cutoff

Yudong Lin

Co-Chairs of the Supervisory Committee:
Santosh Devasia
Mechanical Engineering, University of Washington

Brian Fabien
Mechanical Engineering,University of Portland

This dissertation develops a string stable, constant-spacing control strategy for connected autonomous vehicle networks with robustness to communication delays and cutoff. It is well-known that decentralized constant-spacing strategies cannot achieve string stability, which requires the error to decrease as it propagates downstream. Introducing a centralized approach could achieve string stability in constant-spacing platoons. However, the benefits of introducing centralized control are questionable under communication limitations, like delays and cutoffs, which are common in modern traffic networks. Therefore, this thesis develops a new constant-spacing control approach that is robust to communication delays and cutoff. Moreover, this thesis develops conditions for guaranteeing string stability for constant-spacing policy (CSP) under communication delays. Furthermore, this dissertation applies the proposed control approach to a mixed vehicle network at a signalized intersection with vehicle-to-infrastructure (V2I) connectivity, as well as a human-led platoon.

TABLE OF CONTENTS

Page

List of Figures iii

Chapter 1: Introduction 1
1.1 Research Goal 2
1.2 RQ1: Can we achieve string stable CSP with robustness to communication delays and cutoff? 6
1.3 MC1: String stable and robust connected CSP using blended DSR 6
1.4 RQ2: Can blended DSR improve the CSP tracking with partial connectivity? 7
1.5 MC2: Safely improving the velocity cohesion of a mixed autonomous vehicle network at signalized intersections with blended DSR 7
1.6 RQ3: Can blended DSR improve the CSP tracking of a mixed traffic with human? 8
1.7 MC3: Increasing the traffic capacity of mixed traffic with human-driven vehicles at signalized intersections using blended DSR 8
1.8 Research summary 8
1.9 Structure of the thesis 8

Chapter 2: Background 10
2.1 String stable and robust connected CSP using blended DSR (MC1) 10
2.2 Improve velocity cohesion using the blended DSR with partial connectivity (MC2) 11
2.3 Improve response time of mixed traffic network with blended DSR (MC3) . . 12

Chapter 3: MC1: String stable and robust connected CSP using blended DSR . . 14
3.1 Problem Formulation 14
3.2 Analysis of blended DSR for PLF networks 21
3.3 Results and Discussion 48
3.4 Conclusion 57

Chapter 4: MC2 An efficient AV network at signalized intersection with partial connectivity using blended DSR. 59
4.1 Problem Formulation 60
4.2 Proposed Approach 66
4.3 Results 69
4.4 Conclusion 74

Chapter 5: MC3: An efficient mixed network at real-world signalized intersections 75
5.1 Introduction 76
5.2 Problem Formulation 78
5.3 Traffic capacity analysis 85
5.4 Simulation Results and Discussion 96
5.5 Conclusion 110

Chapter 6: Conclusion and Future Work 112

Bibliography 113
.1 A:Car-following dynamics of CAV followers 122
.2 B: Human Intelligent Driver Model 124

LIST OF FIGURES

Figure Number Page

1.1 Decentralized CSP ($\lambda = 0$) results in string instability. Left: The maximum of the spacing error $\delta_i(t)$ amplified as vehicle index i increases. Right: The maximum magnitude of the transfer function $G(s)$ in Eq.(1.1) is greater than 1, which fails the string stability condition in Eq. (1.1). 4

1.2 Centralized vehicle platoon with n vehicles. Each follower vehicle $i \geq 2$ gets (i) centralized information about its desired position $\tilde{x}_{d,i} = x_0(t) - (i-1)d_s$ where x_0 is the desired position of the lead vehicle and (ii) decentralized local sensing information of its own position x_i and the relative positioning error $\delta_i = x_{i-1} - x_i$ in Eq. (1.2) with respect to its predecessor vehicle. 5

1.3 Compare Decentralized approach Eq. (1.3)and centralized approach Eq.(1.4) 5

1.4 Research Timeline, publication [1], [2] 9

3.1 Stable pole-zero cancellations using controllers $C_{ff,i}$, $C_{fb,i}$ in Eqs. (3.10), (3.11) reduces the vehicle dynamics $\tilde{L}_i$ to a single-integrator system L depicted inside the red dashed box. x_i is the deviation from the ideal spacing $(i-1)d_s$ with respect to the lead vehicle, as in Eq. (3.17). 16

3.2 Predecessor-Leader-Follower (PLF) vehicle platoon with n vehicles. Each follower vehicle $i \geq 2$ gets (i) centralized information about its desired position $\tilde{x}_{d,i} = x_0(t) - (i-1)d_s$ in Eq. (3.14) where x_0 is the desired position of the lead vehicle and (ii) decentralized local sensing information of its own position x_i in Eq. (3.17) and the relative positioning error $\delta_i = x_{i-1} - x_i$ in Eq. (3.26) with respect to its predecessor vehicle. 22

3.3 The block diagram of PLF with DSR for the follower vehicles $i \geq 2$ in Eq. (3.30), with communication delay τ_c, local sensing delay τ_l, and DSR delay τ_d. The vehicle control $u_{c,i}$ using centralized information is depicted in blue and control $u_{dsr,i}$ using decentralized sensing is in red. The DSR augmentation of the traditional feedback is shown in yellow shaded blocks, and the blending of centralized and decentralized control is shown in green shaded blocks. When centralized communication is lost $u_{c,i}$ is set to zero. For PLF without DSR, the yellow blocks are set to zero and the green blocks are set to 1. 23

3.4 For comparative evaluations, the blending gain γ for PLF with DSR is selected (vertical cyan dashed line) to achieve the same acceptable communication delay τ_c^* as PLF without DSR (horizontal black dashed line) for string stability found from Eq. (3.159), Lemma 12. The vertical purple dashed line marks the maximum acceptable blending gain γ^* from Eq. (3.160), Lemma 8. The string-stable region (the red shaded area) is computed from Eq. (3.158), Lemma 5. The internally-stable region (the blue shaded area) is found numerically by checking for finite settling time of the step response using MATLAB and can be estimated by Lemmas 2 and 3. 52

3.5 Comparison of maximum deviation δ_m (left plots) and settling time T_s (right plots) for PLF with DSR (black lines) and PLF without DSR (blue lines) as communication delay increases till string instability (vertical cyan lines). Horizontal dashed lines represent communication loss case. Left: With communication loss, PLF with DSR has less steady state spacing error δ_m (horizontal black line) than PLF without DSR (horizontal blue line). Right: Settling time T_s variation with communication delay is substantially smaller with DSR compared to the case without DSR. 54

3.6 DSR (left plots) leads to more cohesive tracking performance and smaller spacing errors δ_i when compared to the case without DSR (right plots) under large communication delays $\tau_c = 2.5$ s (top plots) or communication loss (bottom plots). 55

3.7 Impact of the DSR gain β on the maximum deviation δ_m (left plots) and settling time T_s (right plots) under small communication delay (black lines), large communication delay (blue lines) and communication loss (red lines). Dashed line indicates when the CVS is string unstable. Increasing the DSR gain β can improve the performance, but can also make the system string unstable. 57

4.1 The inter-spacing between trucks. Left: The two trucks maintain target inter-spacing $d_i = d_0 = 2l_0$. Right: The two trucks collide when their inter-spacing $d_i \leq l_0$ 70

4.2 DSR without TLVC communication (left plots (a),(c)) leads to more cohesive tracking performance (top plots) and smaller spacing errors (bottom plots) when compared to the case without DSR and without TLVC communication (right plots, (b),(d)). 72

4.3 Comparison with (blue circles) and without blended DSR (red circles and crosses): (top) the maximum normalized spacing error $\Delta_{d,max}$ defined in Eq. (4.25) and (bottom) the time for passing the intersection T_p defined in Eq. (4.26). With blended DSR, both (i) the maximum normalized spacing error $\Delta_{d,max}$ and (ii) the time T_p for passing through the intersection, have less variations and smaller values, for all cases with partial connectivity to the TLVC. 73

5.1 DSR improves traffic capacity (right vertical azis) over a wide range of desired time period T_s (horizontal axis), and target traffic speed V (left vertical axis), according to Eq. (5.81). 99

5.2 The mean capacity (for both cases with and without DSR) converges within ± 0.25 vehicles when the number of simulations are greater than 65 runs. . . 101

5.3 All DSR AV network achieves better traffic capacity N_p by reducing the cumulative spacing loss. The solid lines are the numerical solutions of the cumulative spacing loss $f_{c,i}(T)$ from Eq. (5.48) for ideal network, $f_{d,i}(T)$ from Eq. (5.72) for All DSR AV network and $f_{n,i}(T)$ from Eq. (5.60) for no-DSR AV network. Dashlines are the analytical approximation of the spacing loss $\tilde{f}_{d,i}(T)$ for All DSR AV network and $\tilde{f}_{n,i}(T)$ for no-DSR AV network. The star markers are the estimated traffic capacity $N_{p,idl} = 36$ for ideal network (green) from Eq. (5.49), $\tilde{N}_{p,n} = 11$ for no-DSR network (black) from Eq. (5.62) and $\tilde{N}_{p,d} = 32$ for DSR network (black) from Eq. (5.73). 103

5.4 DSR improves the traffic capacity compared without the use of DSR on AVs with different target speed V (left plot) The dotted data points are from MATLAB simulations, while the dash-lines are computed from the capacity prediction Eqs. (5.49), (5.62) and (5.73), as well as the prediction of improvement I Eq. (5.81)(right plot) 104

5.5 DSR AV network maintains higher traffic capacity compared with no-DSR network: With the target speed $V = 34$ mph and 10 s after the traffic signal turns green, the DSR AV network (bottom plot) has less spacing loss from the leader (the green box) and thus allows more vehicles (12) compared with the no-DSR AV network (top plot) with 5 vehicles during the same amount of time. Therefore, the use of DSR on AVs improves the traffic capacity of the all-AV network. Video is available at `https://youtu.be/xGiAI4IXVns` , as well as in supplementary material. 105

5.6 Mixed traffic capacity with $V = 34$ mph. DSR guarantees improvements on the traffic capacity N_p when the mixed traffic has no more than 50% of HDVs, or when the mixed traffic has at least 20% of the AVs with the use of DSR. DSR results in improvements even with 70% HDVs and 30% AVs 107

5.7 Standard deviation (as a percentage of the mean capacity) for the mixed traffic simulation. 108
5.8 Satellite view [3] of the intersection (left) at Fairview and Denny way in Seattle, USA, evaluated with the intersection model in SUMO platform (right). 109
5.9 The phase information of the traffic light (one cycle). 109
5.10 DSR improves the traffic capacity compared without the use of DSR on AVs from SUMO simulations. Capacity is evaluated after the intersection is loaded, for cycles 2-8. 111
1 The value of $S(d_0)$ with $\epsilon = 10^{-3}$ 123

Chapter 1

INTRODUCTION

Longitudinal cruise control with constant spacing policy (CSP) enables platoons with small inter-vehicle distances, resulting in improved fuel efficiency, and increased traffic throughput [4, 5, 6]. However, it is well-known that constant spacing cannot be maintained together with string stability when using decentralized approaches, which rely only on local sensing information about the preceding vehicle [7, 8]. Using centralized communication from the leader vehicle to the followers, resolves the problem and enables constant spacing with string stability [9, 10]. However, the performance of the resulting connected autonomous vehicles (CAVs) network is vulnerable to communication issues [11], e.g. (i) large communication delays can lead to slower oscillatory convergence to consensus and (ii) communication loss can lead to large spacing errors. Large communication delays and communication loss can be caused by environmental jamming or during transmission over long distances. For example, in locations with a high rate of jamming, the system needs to reduce the packet delivery rate in order to reject unwanted messages [12]. Furthermore, large transmission and receiving distances in the hundreds of meters, which is anticipated for truck platooning on highways, can greatly increase the path loss and communication delay of vehicle-to-vehicle communication [13]. Therefore, there is a need to develop control protocols with robust performance in the presence of such communication problems.

This thesis develops a blended control approach for achieving string stability CSP for CAV networks, in the presence of local sensing delays and large communication delays and cutoffs. Furthermore, the proposed approach is shown to achieve better traffic capacity in a mixed traffic network with only partial connectivity to the source and interventions from human participants.

A brief discussion of the research goals and main contributions of the thesis is presented below. Detailed information is discussed in subsequent chapters.

1.1 Research Goal

The main goal of the research is presented, which leads to the development of the research questions and main contributions of this thesis. String stability of the network describes the propagation of the spacing error. The vehicle network is said to be string stable if the spacing errors do not amplify along the vehicle platoon downstream, i.e. the magnitudes of the error propagation transfer functions $G_i(s)$ of the followers ($i \geq 2$) satisfy

$$\left| G_i(j\omega) = \frac{\delta_{i+1}(s)}{\delta_i(s)} \right| < 1, \qquad \forall \omega > 0, \tag{1.1}$$

where the spacing error $\delta_i(s)$ defined as

$$\delta_i(s) = x_{i-1}(s) - (1 + \lambda s) x_i(s). \tag{1.2}$$

where λ is the headway time of the network, x_i is the longitudinal position of the vehicle. Depending on the selection of the headway time λ, the tracking control policy can be categorized by

1. constant-spacing policy (CSP): $\lambda = 0$, the target inter-distance between the vehicles of the network do not expected to amplified as the speed of the network increases.

2. constant-headway-time policy (CTH): $\lambda > 0$, the target inter-distance between the vehicles of the network amplifies as the speed of the network increases.

The traffic capacity with the use of CSP is better than the one with the use of CTH, because CSP results in more compact space utilization. However, CSP platooning is a more challenging problem for autonomous platooning compared with CTH platooning, since it results in higher requirements on spacing control in order to maintain a fixed distance among the vehicles and avoid unnecessary stop-and-go actions, regardless of the traffic speed. Given

the odometer information of the vehicle $x_i(s)$ and local sensing information to the predecessor $d_i = x_{i-1}(s) - x_i(s)$, a standard controller can be given by [8]

$$x_i^{(3)}(s) = u_i(s) = (C_p + C_v s)\delta_i(s) + (K_v s + K_a s^2)x_i(s). \tag{1.3}$$

Standard control approach like Eq. (1.3) is decentralized since Eq. (1.3) do not require information from a remote source, like information from the state of the leader $x_1(s)$ and tracking error $x_1(s) - x_i(s)$. However, it cannot achieve string stability and constant-spacing tracking together.

1.1.1 Decentralized CSP platoon leads to string instability

Decentralized approach Eq. (1.3) does not satisfy the string stability condition Eq. (1.1) with CSP policy $\lambda = 0$, with any selection of the control parameters [8], as illustrated by Fig. 1.1. The maximum spacing error of the fifth follower $\|\delta_5(t)\|_\infty$ is about 2.2 meters, which is amplified compared with the maximum spacing error of the first follower $\|\delta_1(t)\|_\infty$, which is about 1.6 meters. Such amplification of the spacing error continues along the downstream of the network, which can not be bounded without giving the length of the network. The bode plots of the error propagation transfer function $G(s)$ show that the controller Eq.(1.3) amplifies a specific range of low-frequency components (0 - 2 rad/s) of the input, which finally results in the amplification of the spacing error. Furthermore, the conclusion has been extended in [7], such that string stable decentralized CSP is not achievable with any linear feedback control law for a vehicle system with the relative degree $r \geq 2$.

On the other hand, string stability can be guaranteed using CTH policy. The minimum headway time can be derived in order to guarantee string stability [8]. However, the presence of the headway time results in additional inter-distance among the vehicles as the cruise speed of the network increases, which is not applicable in some scenarios like vehicle formation control and fuel-efficient truck platooning, which requires accurate constant-spacing control in order to improve fuel economy using the drag effect on highways [14].

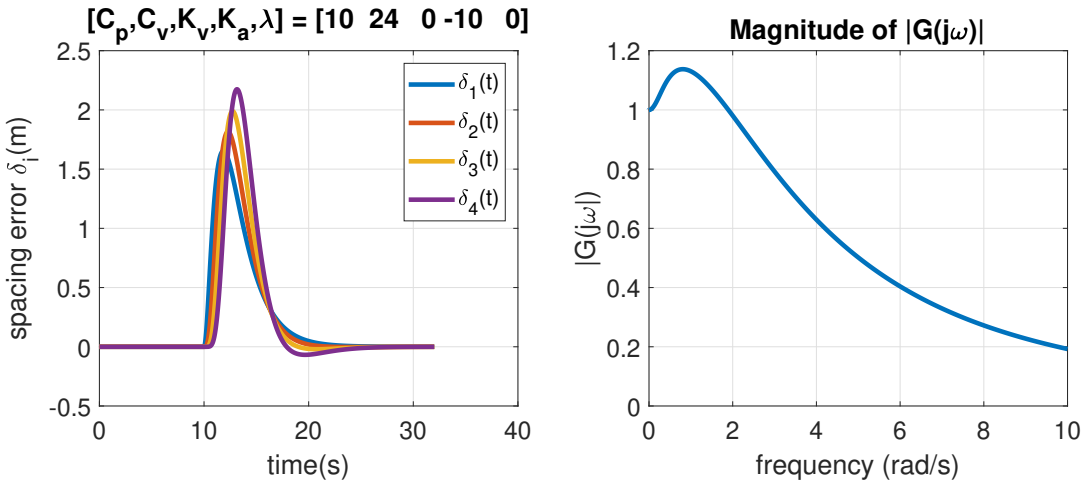

Figure 1.1: Decentralized CSP ($\lambda = 0$) results in string instability. Left: The maximum of the spacing error $\delta_i(t)$ amplified as vehicle index i increases. Right: The maximum magnitude of the transfer function $G(s)$ in Eq.(1.1) is greater than 1, which fails the string stability condition in Eq. (1.1).

1.1.2 Centralized control CSP Platoon Achieves String Stability

Centralized information, i.e. the target distance of the i^{th} vehicle $\tilde{x}_{d,i}$, could be used to augment the decentralized control approach Eq. (1.3), as illustrated in Fig. 1.2, in order to achieve string stability and constant-spacing control together, for example,

$$x_i^{(3)}(s) = (C_p + C_v s+)\delta_i(s) + (K_v s + K_a s^2)x_i(s) + D_p(\tilde{x}_{d,i}(s) - x_i(s)) \tag{1.4}$$

However, such centralized approaches need to establish inter-agent communications between the leader and all the followers in order to compute the target state $\tilde{x}_{d,i}$, which increases additional costs for the communication infrastructure. Besides, communication delays and cutoffs from long-distance transmissions, jamming, and cyber-threats could cause the vehicle system internally unstable and string unstable [10].

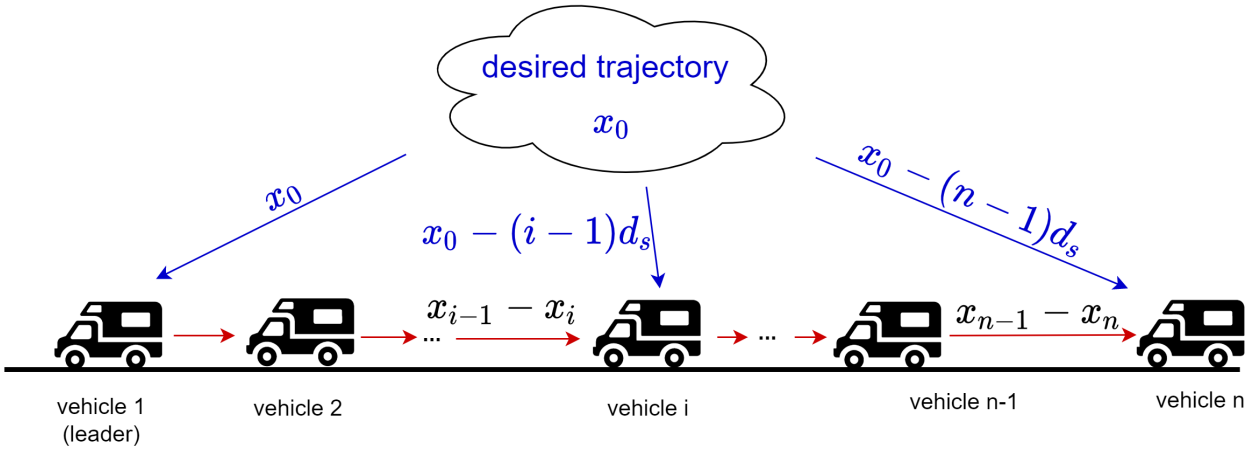

Figure 1.2: Centralized vehicle platoon with n vehicles. Each follower vehicle $i \geq 2$ gets (i) centralized information about its desired position $\tilde{x}_{d,i} = x_0(t) - (i-1)d_s$ where x_0 is the desired position of the lead vehicle and (ii) decentralized local sensing information of its own position x_i and the relative positioning error $\delta_i = x_{i-1} - x_i$ in Eq. (1.2) with respect to its predecessor vehicle.

Decentralized network	Centralized network
Pros: Only use local sensing for control	Pros: Achieve string stability and CSP together
Cons: cannot achieve string stability and CSP together	Cons: not robust to communication delays and cutoff

Figure 1.3: Compare Decentralized approach Eq. (1.3)and centralized approach Eq.(1.4)

1.1.3 Research Goal

The goal of this research is to present a centralized approach that guarantees string stability Eq. (1.1), as well as robustness to large communication delays. Additionally, the proposed method also reduces the additional inter-spacing Eq. (1.2) when centralized communication is cut off or not available, compared with standard decentralized platooning.

Based on the research goal, the research questions (RQs) of this thesis, and the main contributions (MCs) and proposed research to address the questions are given below.

1.2 RQ1: Can we achieve string stable CSP with robustness to communication delays and cutoff?

It is well-known that decentralized approaches cannot achieve string stability together with constant-spacing tracking. Therefore, it is necessary to use centralized approaches in order to achieve string stability for CSP. The degraded performance from the communication delays can be mitigated by blending the centralized command with a decentralized approximation of it, which only uses already available local sensing information in historical data.

1.3 MC1: String stable and robust connected CSP using blended DSR

This section introduces the first main contribution together with Anuj Tiwari, Brian Fabien and Santosh Devasia. It has been published in IEEE Transactions on Intelligent Transportation Systems [1]. This work proposes a control approach which (i) enlarges the acceptable upper bound of communication delays for maintaining string stability and constant spacing, and (ii) reduces the constant-spacing error Eq. (1.2) when the centralized vehicle network degrades to decentralized network due to communication loss. The main idea is to use the delayed self reinforcement (DSR) approach [15] for decentralized control. The main contribution of this work is the following.

(i) Development of a new blended DSR approach with both (a) decentralized DSR and (b) centralized communication as opposed to purely decentralized cases studied in prior work [15].

(ii) Finding conditions for the blended DSR-based, constant-spacing network to guarantee internal stability and string stability with delayed centralized command and loss of communication. Moreover, the steady-state spacing error under communication loss is also quantified.

(iii) Illustration of the DSR parameter selection and impact under different communication conditions using a simulation example.

1.4 RQ2: Can blended DSR improve the CSP tracking with partial connectivity?

MC1 can be applied to CSP platooning since it guarantees string stability. Furthermore, it improves the CSP tracking by reducing the steady-state spacing error when the communication is lost. However, before the vehicular communication technology popularizes, it is challenging to guarantee all the agents in the traffic network have communication capability to the source command as assumed in **MC1**. The second main research question addressed in this thesis is to examine the benefits brought by the blended DSR approach in such mixed traffic networks with CAVs and AVs.

1.5 MC2: Safely improving the velocity cohesion of a mixed autonomous vehicle network at signalized intersections with blended DSR

This section introduces the second main contribution together with Anuj Tiwari, Brian Fabien and Santosh Devasia. It has been published in IEEE 8th Indian Control Conference (ICC 2022) [2]. The main contribution of this work is to improve the performance of the mixed AVs network which only has partial connectivity to the source for longitudinal spacing control by improving the velocity cohesion using the blended DSR approach proposed in **MC1**. The blended DSR is shown to improve the response speed of each AV in a mixed AV network for a more cohesive response to desired velocity changes which leads to smaller longitudinal spacing variations in such networks, and therefore, to better traffic capacity and improved safety.

1.6 RQ3: Can blended DSR improve the CSP tracking of a mixed traffic with human?

In the near future, the traffic network will include CAVs, AVs and traditional vehicles driven by human. **MC2** shows that the blended DSR approach can improve the mixed AV network with CAVs and AVs. However, the presence of HDVs will introduce uncertain behaviors to the mixed traffic network since human drivers perceive the driving environment and make decisions in very different ways. The third main research question addressed in this thesis is to quantify the benefits brought by the blended DSR approach, as well as verifying the improvements in traffic throughput of the mixed traffic with HDVs, with the use of the blended DSR approach.

1.7 MC3: Increasing the traffic capacity of mixed traffic with human-driven vehicles at signalized intersections using blended DSR

The main goal of this proposed work, is to improve the traffic throughput of the mixed traffic network with CAVs, AVs and HDVs by improving the response time of the network using a DSR-based approach [15]. It has been shown that DSR can improve the settling time of partially-connected AV networks by increasing the response time of the decentralized AVs in the network from **MC2.1** [2]. Therefore, it can be used to improve the throughput of the mixed traffic network with HDVs for a faster response to desired traffic speed change, which results in smaller longitudinal spacing loss and thus better traffic capacity.

1.8 Research summary

The outline of the dissertation contribution is provided in Fig. 1.4.

1.9 Structure of the thesis

The subsequent chapters begin with a background in Chapter 2 which provides a brief review of the **MCs**. Chapter 3 introduces **MC1** in detail, including the formulation of the blended DSR approach, the derivations of the upper bounds on communication delays, as well as an

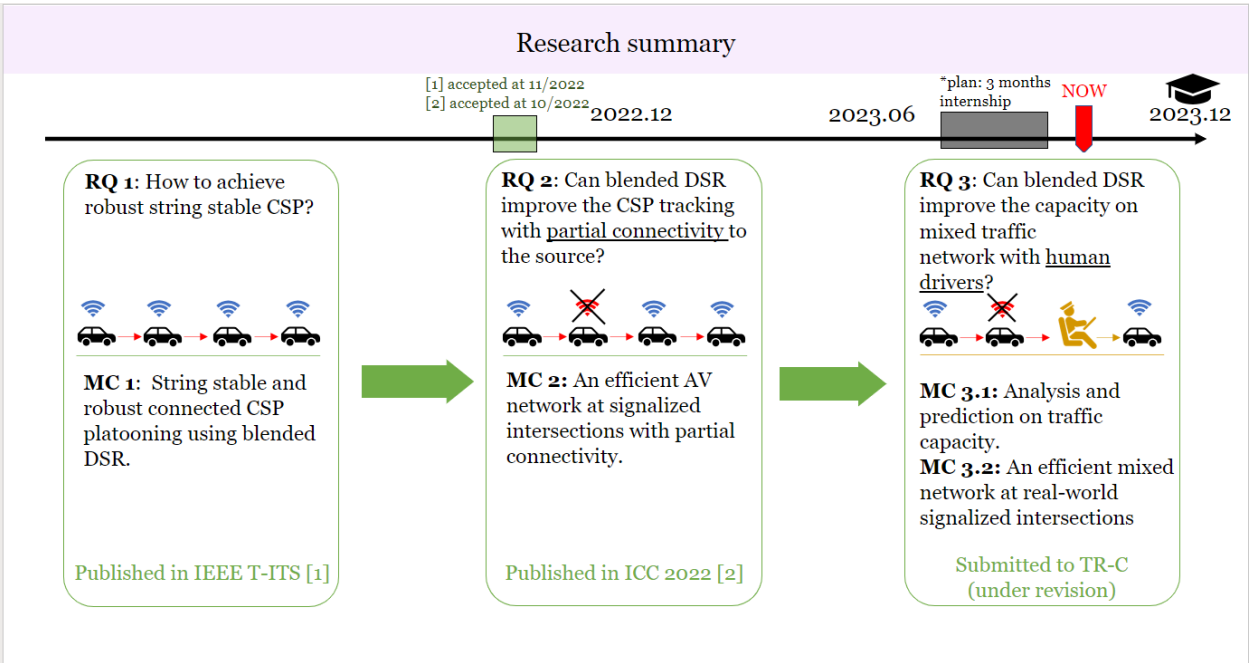

Figure 1.4: Research Timeline, publication [1], [2]

illustration of the parameter selections. Chapter 4 introduces **MC2**, which examines the blended DSR approach in **MC1** with only partial connectivity, with an application on a signalized intersection. Chapter 5 introduces the last main contribution **MC3**, including the analysis and prediction of traffic capacity, as well as the simulation results using Simulation of Urban MObility (SUMO) platform.

Chapter 2

BACKGROUND

This chapter provides a background of the available literature concerning each of the research questions (**RQ1**, **RQ2** and **RQ3**) addressed in this thesis, taken from the main contributions (**MC1**, **MC2** and **MC3**).

2.1 String stable and robust connected CSP using blended DSR (MC1)

String stable CSP can be achieved by introducing centralized command. However, the connected CSP network can be string unstable again with communication limitations like delays [11]. Previous works have addressed the issue of small communication delays or short periods of communication loss on the performance of the CAV network. For example, an upper bound of communication delay to maintain string stability depends on the vehicle dynamics and can be found numerically [16] or analytically depending on the selected headway time [17]. Furthermore, sufficient conditions on the communication delay can be derived analytically to guarantee the internal stability [18] and string stability [10]. However, for large communication delays, even with string stability and internal stability, the performance in terms of settling time (for converging to consensus) can be large. Similarly, short term communication loss can be addressed using estimation techniques to infer the lost centralized command [19, 20, 21]. However, such methods are not applicable for large delays in communication or when communication is lost for long periods of time. In particular, when the communication is lost for extended periods of time, the centralized control structure degrades to the decentralized ones, which cannot maintain both constant-spacing and string stability as discussed before. Thus, current CSP has challenges when dealing with large communication delays or loss in communication for extended periods of time.

The main idea is to use the delayed self reinforcement (DSR) approach for the decentralized control. The DSR approach seeks to implement the ideal, non-delayed centralized command which results in ideal platooning from the current and delayed local sensing information, and to improved cohesion. Since the DSR approximates the ideal centralized command, it leads to low spacing errors in the platoon with large communication delays and even when the communication is lost.

2.2 Improve velocity cohesion using the blended DSR with partial connectivity (MC2)

As connected autonomous vehicles (CAVs) with communication capabilities become available [22, 23], traffic-light scheduling information can be broadcast to vehicles approaching an intersection using traffic-light-to-vehicle-communication (TLVC) to improve fuel economy and journey time, as studied in [24, 25]. Specifically, vehicles adjust their velocities according to the upcoming traffic-light time and phase information to reach the intersection during its green phase and avoid braking, using predictive cruise control (PCC) [25], which reduces fuel consumption and time for operation. However, it is impossible to cover all the vehicles in the traffic network with communication capability in the near future. Based on the development and adoption of autonomous vehicle (AV) technologies, AVs with moderate price are expected to constitute only 20% - 50% of the traffic around 2040s [26, 27]. Therefore, the traffic-signal information might not be available to every vehicle in a network, due to unavailability of dedicated communication capabilities in some vehicles. Furthermore, not all vehicles might be secure for wireless communication due to cyber-physical security threats [28]. Therefore, it is crucial to develop a protocol for such mixed AVs networks, with a mix of CAVs with communications capabilities, and non-cooperative AVs which only use local sensing using radar, lidar or vision to gather information about neighboring vehicles and environment to navigate in traffic, such as adaptive cruise control [29].

Cohesive velocity transitions, where all vehicle maintain similar velocities during velocity changes, is essential for efficient traffic flows and fuel savings [30]. However mixed

autonomous vehicle networks have limits on the cohesion during such maneuvers due to heterogeneity in communication capabilities, which results in increased possibility of varying spacing between vehicles and undesirable braking, and therefore lower traffic flow capacity [26]. The main contribution of the article is to improve the performance of the mixed AVs network for longitudinal spacing control and velocity tracking by improving velocity cohesion using delayed self reinforcement (DSR). The advantage of using DSR, which has been used for cohesive transitions with faster responses in networked systems in [15, 31], is that it can be implemented using the already existing information in the vehicle network without network-connectivity modifications. Thus, DSR can be used to improve the response speed of each vehicle in a mixed autonomous vehicle network for a more cohesive response to desired velocity changes. A more cohesive response leads to smaller longitudinal spacing variations in such networks, and therefore, to better traffic capacity and improved safety.

2.3 Improve response time of mixed traffic network with blended DSR (MC3)

As vehicular communication techniques become more available, traffic light information can be broadcast to autonomous vehicles (AVs) approaching the signalized intersection to improve their mobility, fuel economy and traffic capacity[32]. Connected autonomous vehicles (CAVs) with connectivity to traffic light scheduling information are able to adjust their velocities based on the phase information and avoid unnecessary braking activities, which reduces fuel consumption and time for re-acceleration [33]. However, it is neither possible to implement communication techniques on all the autonomous vehicles, nor create a traffic environment without human driven vehicles (HDVs) in the near future. According to the development and adoption rate of AV technologies, AVs and CAVs with moderate price are expected to consist 20% to 50% of the market around 2040s [26][27]. Therefore, it brings questions to the benefits brought by vehicular communication techniques under a mixed traffic environment with AVs, CAVs and HDVs. Furthermore, the connectivity to traffic scheduling information is vulnerable to signal jamming and cyber-security attacks, which might cause temporary loss of communication on CAVs [28] and degrades CAVs to

AVs [20, 34]. Therefore, it is critical to develop a vehicle control protocol for mixed traffic networks including (1) CAVs with connectivity to traffic scheduling information, and (2) AVs which only relies on local sensing techniques like radar, camera to gather surrounding information to navigate in traffic, and (3) HDVs with stochastic human driver features.

Response time of the vehicle, which describes the time for the vehicle to transit to the target speed, is closely related to the traffic capacity. Larger response time results in additional spacing loss among the agents of the network during the transition, which is one of the reason for low traffic capacity [35]. Currently, the traffic capacity of the mixed traffic is limited by the response time of HDVs and the minimum designed headway time of decentralized AVs [26, 36]. The main contribution of this paper is to improve the traffic throughput of the mixed traffic network by improving the response time of the network using delayed self reinforcement (DSR), which approximates the centralized-based control by decentralized control which uses already-available information from historical data, without changing the network topology and connectivity to the source [15]. It has been shown that DSR can improve the settling time of partially-connected AVs network by increasing the responses time of the decentralized AVs in the network[2]. Therefore, it can be used to improve the throughput of the mixed traffic network with human for a faster response to desired traffic speed change, which results in smaller longitudinal spacing loss and thus better traffic capacity.

Chapter 3

MC1: STRING STABLE AND ROBUST CONNECTED CSP USING BLENDED DSR

This chapter proposes an approach to make constant-spacing vehicle platoons robust to large delays and loss of communication (**MC1**) and is based on a work published in IEEE Transactions on Intelligent Transportation Systems [1]. It is well known that centralized communication of the desired trajectory is important to simultaneously guarantee both string stability and constant-spacing in platoons. However, the performance of the resulting connected vehicle system (CVS) is vulnerable to large communication delays and communication loss. The main contribution of this work is a new delayed-self-reinforcement-based (DSR-based) approach that approximates the centralized communication based control by a decentralized predecessor follower (PF) control. The resulting blending of centralized communication with the decentralized DSR approach results in predecessor-leader follower (PLF) control with (i) robustness of the convergence to consensus under large communication delays and (ii) substantially-smaller spacing errors under loss of communication. Comparative simulations show that, for the same level of robustness to internal-stability and string-stability, the variation in settling time to consensus for PLF with DSR under large communication delays is 95% less than PLF without DSR and the steady-state error with DSR under loss of communication is 80% less than PLF without DSR.

3.1 Problem Formulation

3.1.1 Individual vehicle dynamics

The individual heterogeneous nonlinear vehicle dynamics is changed into a first-order homogeneous dynamics using feedback linearization followed by stable pole-zero cancellations.

Let the dynamics of each vehicle $i \in \{1, 2 \ldots\} = S_n$ have the general form [37, 38]

$$\dot{\xi}_i(t) = f_i\left(\xi_i(t)\right) + g_i\left(\xi_i(t)\right)\hat{u}_i(t), \tag{3.1}$$

$$\tilde{x}_i(t) = h_i\left(\xi_i(t)\right), \tag{3.2}$$

where $\xi_i \in \mathbb{R}^m$, $\tilde{x}_i \in \mathbb{R}$ and $\hat{u}_i \in \mathbb{R}$ are the state, output position and input of the system. We assume that each vehicle system has relative degree m, i.e.,

$$L_{g_i} L_{f_i}^k h_i(\xi_i) = 0, \qquad \forall\ 0 \leq k \leq m-2, \tag{3.3}$$

$$L_{g_i} L_{f_i}^{m-1} h_i(\xi_i) \neq 0, \tag{3.4}$$

where L_f^h stands for the Lie derivative of $h(\xi_i)$ w.r.t the vector field $f(\xi_i)$. Then, the m^{th} derivative of the output $\tilde{x}_i$ is given by

$$\frac{d^m}{dt^m}\tilde{x}_i(t) = L_{f_i}^m h_i(\xi_i) + L_{g_i} L_{f_i}^{m-1} h_i(\xi_i)\hat{u}_i, \tag{3.5}$$

and selecting the control input $\tilde{u}_i$ as

$$\tilde{u}_i(t) = L_{f_i}^m h_i(\xi_i) + L_{g_i} L_{f_i}^{m-1} h_i(\xi_i)\hat{u}_i(t), \tag{3.6}$$

yields the linear m-integrator form of the system [38][39]

$$\frac{d^m}{dt^m}\tilde{x}_i(t) = \tilde{u}_i(t). \tag{3.7}$$

Therefore, each vehicle's input-to-output dynamics can be made homogeneous using input-output feedback linearization even if the original dynamics is heterogeneous and nonlinear to obtain in the Laplace domain

$$\tilde{L}_i(s) = \frac{\tilde{x}_i(s)}{\tilde{u}_i(s)} = \frac{1}{s^{m_i}}, \tag{3.8}$$

where m_i is the relative degree. Stable pole-zero cancellation is achieved by selecting the control law

$$\tilde{u}_i(s) = C_{ff,i}(s)u_i(s) - C_{fb,i}(s)\tilde{x}_i(s) \tag{3.9}$$

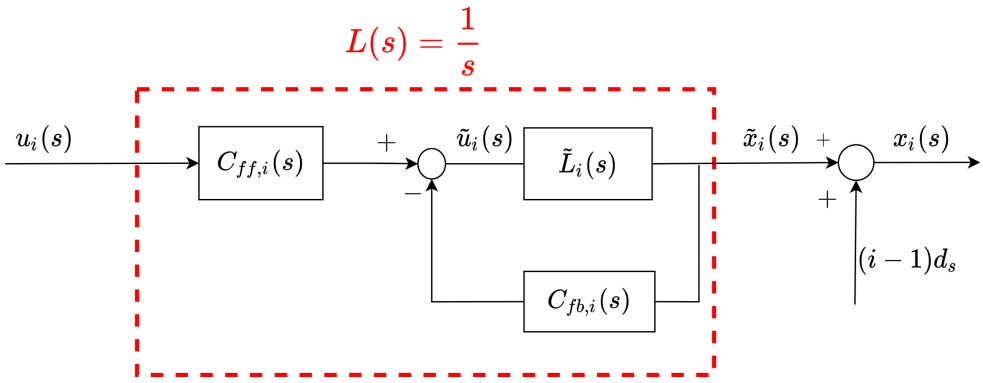

Figure 3.1: Stable pole-zero cancellations using controllers $C_{ff,i},\ C_{fb,i}$ in Eqs. (3.10), (3.11) reduces the vehicle dynamics $\tilde{L}_i$ to a single-integrator system L depicted inside the red dashed box. x_i is the deviation from the ideal spacing $(i-1)d_s$ with respect to the lead vehicle, as in Eq. (3.17).

as in Fig. 3.1 with feedback controllers $C_{ff,i}, C_{fb,i}$

$$C_{ff,i}(s) = s^{m_i-1} + k_1 s^{m_i-2} + \cdots + k_{m_i-1}, \tag{3.10}$$

$$C_{fb,i}(s) = k_1 s^{m_i-1} + k_2 s^{m_i-2} + \ldots k_{m_i-1} s, \tag{3.11}$$

resulting in a first-order closed-loop dynamics $L_i(s)$

$$\begin{aligned} L_i(s) = \frac{\tilde{x}_i(s)}{u_i(s)} &= \frac{\tilde{L}_i(s) C_{ff,i}(s)}{1 + \tilde{L}_i(s) C_{fb,i}(s)} \\ &= \frac{(s^{m_i-1} + k_1 s^{m_i-2} + k_2 s^{m_i-3} + \ldots k_{m_i-1})}{s(s^{m_i-1} + k_1 s^{m_i-2} + k_2 s^{m_i-3} + \ldots k_{m_i-1})} \\ &= \frac{1}{s} = L(s). \end{aligned} \tag{3.12}$$

The controller gains $k_1, \ldots, k_{m_i-1}$ are designed to avoid unstable pole-zero cancellations by ensuring that the cancelled polynomial $p_i(s) = s^{m_i-1} + k_1 s^{m_i-2} + \cdots + k_{m_i-1}$ has roots in the open left-half of the complex-plane. For example, if each individual vehicle dynamics is a second-integrator model $\tilde{L}_i(s) = s^{-2}$ as in [38, 10], then the controllers

$$C_{ff,i}(s) = s + k_1, \qquad C_{fb,i}(s) = k_1 s, \tag{3.13}$$

with $k_1 > 0$, would achieve the reduction to the single-integrator system in Eq. (3.12).

Remark 1 (Heterogeneous dynamics)**.** *Each vehicle's input-to-output dynamics can be made homogeneous using input-output feedback linearization even if the original dynamics is heterogeneous and nonlinear – provided each vehicle dynamics has the same relative degree [37].*

Remark 2 (Stable-pole-zero cancellation)**.** *If the relative degree of the vehicle dynamics is varying, then the above stable pole-zero cancellation via feedback controller design can be used to convert the input-output response to the same first order system.*

3.1.2 Ideal Centralized CSP

To maintain constant-spacing in a platoon, an ideal scenario is for each vehicle i in the set of positive integers $\mathcal{N}$, i.e., $i \in \mathcal{N}$ to receive information about its desired position $\tilde{x}_{d,i}$ from a virtual source as

$$\tilde{x}_{d,i}(t) = x_0(t) - (i-1)d_s, \tag{3.14}$$

where x_0 is the desired position of the lead vehicle $i = 1$ and d_s is the desired spacing between adjacent vehicles. Then, each vehicle in the platoon applies the control law

$$u_i(t) = -\alpha(\tilde{x}_i(t) - \tilde{x}_{d,i}(t)), \tag{3.15}$$

and $\alpha > 0$ defines the time constant $1/\alpha$. The resulting dynamics can be written as, from Eqs. (3.12) and (3.15),

$$\dot{x}_i(t) = -\alpha x_i(t) + \alpha x_0(t) \quad = u_{c,i}(t), \tag{3.16}$$

where the position x_i is defined as the deviation from the ideal spacing with respect to the lead vehicle, i.e.,

$$x_i(t) = \tilde{x}_i(t) - (-(i-1)d_s) = \tilde{x}_i(t) + (i-1)d_s. \tag{3.17}$$

It is assumed that all vehicles have the desired spacing initially, i.e., $x_i(0) = x_0(0)$ for all $i \in \mathcal{N}$. With the ideal centralized input $u_{c,i}$ in Eq. (3.16), all vehicle responses are the

same, i.e., $x_i(t) = x_j(t)$, and therefore, the constant-spacing policy (CSP) can be maintained for a given desired position trajectory x_0. In matrix form, the ideal centralized control in Eq. (3.16) can be written as

$$\dot{X}(t) = -\alpha \mathbf{I} X(t) + \alpha \mathbf{1} x_0(t) \ = u_c(t), \tag{3.18}$$

where $X = [x_1, x_2, \ldots, x_n]^T$, $\mathbf{I}$ is the $n \times n$ identity matrix, and $\mathbf{1}$ is an $n \times 1$ vector of ones.

3.1.3 Decentralized CSP with Delayed Self Reinforcement

The ideal centralized approach in Eq. (3.18) can be approximated to be decentralized (e.g., where only the lead vehicle has access to the desired trajectory x_0) using the delayed self reinforcement (DSR) approach in [15], as described below. Multiplying Eq. (3.18) with βK, where β is the DSR gain and K is the pinned graph Laplacian of the CVS network without the virtual source, with nonzero off-diagonal elements $K_{i,j} = -1$ only if vehicle i receives information (through sensing or communication) about vehicle j where $i \neq j$, and the diagonal elements are $K_{i,i} = B_i - \sum_j K_{i,j}$ with nonzero $B_i = 1$ only if vehicle i receives information about the desired position d_s from the virtual source $i = 0$, the ideal centralized dynamics can be rewritten as

$$\beta K \dot{X}(t) = -\alpha \beta K X(t) + \alpha \beta K \mathbf{1} x_0(t). \tag{3.19}$$

If the CVS connectivity contains information paths from the virtual source node $i = 0$ (providing the desired position information) to each vehicle in the platoon, then the pinned Laplacian K of the graph without the source node $i = 0$ is invertible, i.e., $\det(K) \neq 0$ from the Matrix-Tree Theorem in [40]. Moreover, the vehicles will achieve consensus eventually, i.e., $K^{-1}B = \mathbf{1}$, where B is the source connectivity vector (i.e. row element is nonzero $B_i = 1$ only if vehicle i is connected to the source and is zero otherwise). Finally, adding $\dot{X}(t)$ on both sides of Eq. (3.19) and rearranging, results in

$$\dot{X}(t) = (\mathbf{I} - \beta K)\dot{X}(t) - \alpha \beta K X(t) + \alpha \beta B x_0(t). \tag{3.20}$$

The DSR approach [15] uses delayed versions of already available information to implement the derivative on the right hand side of Eq. (3.20) as

$$\begin{aligned}\dot{X}(t) &= (\mathbf{I} - \beta K)\frac{X(t) - X(t-\tau_d)}{\tau_d} \\ &\quad - \alpha\beta K X(t) + \alpha\beta B x_0(t), \\ &= u_{dsr}(t). \end{aligned} \tag{3.21}$$

If there is local sensing delay to measure relative distances, then the terms multiplying K will get modified as

$$\begin{aligned}\dot{X}(t) &= (I - \beta K)\frac{X(t-\tau_l) - X(t-\tau_l-\tau_d)}{\tau_d} \\ &\quad - \alpha\beta K X(t-\tau_l) + \alpha\beta B x_0(t-\tau_l) \\ &= u_{dsr}(t-\tau_l). \end{aligned} \tag{3.22}$$

The above DSR approach can be implemented in a decentralized manner, e.g., with source information available only to the leader vehicle, and it approximates the performance of the centralized approach when the desired trajectories vary slowly compared to the time delay $\tau_d > 0$ in Eq. (3.21). Conditions for stability in terms of the DSR gain β and delay τ_d have been established in [15].

Remark 3 (DSR implementation)**.** *An advantage of the DSR approach is that it does not require additional sensing or communication. Rather, current and delayed versions of the sensed signals KX and the vehicles position x_i, already available to the vehicle controller, are sufficient for implementation.*

Remark 4 (DSR for higher-order vehicle dynamics)**.** *The DSR approach to decentralize the ideal cohesive dynamics as in Eq.* (3.21) *can be applied even if the homogeneous dynamics L in Eq.* (3.12) *of the vehicle is higher order [15].*

3.1.4 Problem statement

In this article, we consider the blending of the centralized and decentralized DSR approach to achieve good performance even when communication about the desired trajectory x_0 is not always available for all the vehicles. With the blended approach, from Eqs. (3.18) and (3.21),

$$\begin{aligned} \dot{x}_i(t) &= \gamma u_{dsr,i}(t-\tau_l) + (1-\gamma)u_{c,i}(t-\tau_c), \quad \forall i \geq 2 \\ \dot{x}_1(t) &= \gamma u_{dsr,1}(t-\tau_l) + (1-\gamma)u_{c,1}(t-\tau_l), \end{aligned} \tag{3.23}$$

where $0 \leq \gamma \leq 1$ is the blending gain, $\tau_c > 0$ is the communication delay, $\tau_l > 0$ is the local sensing delay, and, $u_{dsr,i}$ and $u_{c,i}$ are the i^{th} elements of the DSR and centralized control inputs respectively. Since the leader has the source information x_0, the local sensing delay τ_l is applied instead of the communication delay τ_c in Eq. (3.23). The blended approach Eq. (3.23) is referred to as PLF with DSR in the following.

Remark 5 (Small communication delay to the leader)**.** *Typically, the leader can compute and generate the source trajectory locally before broadcasting to the followers[41]. Therefore, the communication delay of the leader to the source trajectory is assumed to be small, and is considered to be the same as the local sensing delay τ_l.*

Remark 6 (Homogeneous time delays)**.** *The time delays τ_c, τ_l, τ_d can be varying for each vehicle. However, they are assumed to be the same for all vehicles to promote cohesive responses. If the actual delays are different, each vehicle can add intentional buffer delays (as needed) to maintain homogeneity in the delays for all vehicles as in Ref. [10].*

The following three research questions are addressed next.

(1) Internal stability of CVS: What are the conditions on the blended protocol in Eq. (3.23) to ensure internal stability of the CVS, i.e., for the real parts of the poles of the individual-vehicle transfer functions

$$T_i(s) = \frac{x_i(s)}{x_0(s)} \tag{3.24}$$

to be negative?

(2) String stability: What are the conditions on the blended protocol in Eq. (3.23) to guarantee string stability of the CVS? The CVS is said to be string stable if the spacing errors do not amplify along the vehicle platoon downstream, i.e. the magnitudes of the error propagation transfer functions $G_i(s)$ of the followers ($i \geq 2$) satisfy

$$\left| G_i(j\omega) = \frac{\delta_{i+1}(s)}{\delta_i(s)} \right| < 1, \qquad \forall \omega > 0, \tag{3.25}$$

where the spacing error δ_i defined as

$$\delta_i(s) = x_{i-1}(s) - x_i(s). \tag{3.26}$$

(3) Steady-state error: Does the steady-state error converge to zero under the blended protocol in Eq. (3.23)? Given a step change in the desired velocity, i.e. $v_0(s) = V/s$, the CVS has no steady state error if the spacing error δ_i in Eq. (3.26) converges to zero for all vehicles, i.e.,

$$\lim_{t \to \infty} \delta_i(t) = \lim_{s \to 0} s\delta_i(s) = 0 \qquad \forall i \in \mathcal{N}. \tag{3.27}$$

3.2 Analysis of blended DSR for PLF networks

Internal stability, string stability and steady-state errors for the CVS are established in this section.

3.2.1 Internal Stability of CVS

Conditions for internal stability of the CVS are developed by (i) finding the transfer functions T_i in Eq. (3.24) of the vehicle responses x_i to the desired lead vehicle position x_0, and then (ii) finding requirements to ensure that the poles of the transfer functions T_i are on the open left half of the complex plane.

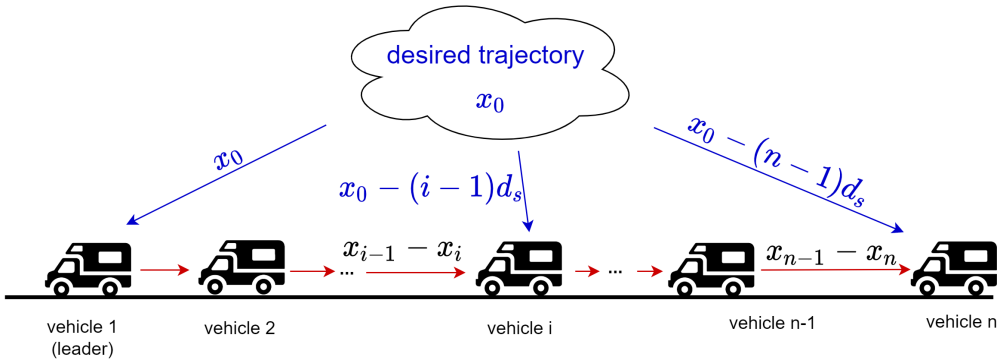

Figure 3.2: Predecessor-Leader-Follower (PLF) vehicle platoon with n vehicles. Each follower vehicle $i \geq 2$ gets (i) centralized information about its desired position $\tilde{x}_{d,i} = x_0(t) - (i-1)d_s$ in Eq. (3.14) where x_0 is the desired position of the lead vehicle and (ii) decentralized local sensing information of its own position x_i in Eq. (3.17) and the relative positioning error $\delta_i = x_{i-1} - x_i$ in Eq. (3.26) with respect to its predecessor vehicle.

1) Dynamics of the vehicles

Each vehicle uses both the relative positioning error (with respect to the predecessor) and the source positioning error in control, as illustrated in Fig. 3.2

with the predecessor leader follower network, where the associated pinned graph Laplacian $K \in \mathbb{R}^{n\times n}$ in Eq. (3.21) and the source connectivity vector $B \in \mathbb{R}^n$ are given by [42]

$$K = \begin{bmatrix} 1 & \dots & & 0 \\ -1 & 1 & & \\ \vdots & \ddots & \ddots & \\ 0 & \dots & -1 & 1 \end{bmatrix}, \quad B = \begin{bmatrix} 1 \\ 0 \\ \vdots \\ 0 \end{bmatrix}. \tag{3.28}$$

The leader ($i = 1$) vehicle's state equation with the DSR approach (Eq. (3.21)), for the pinned graph Laplacian K and source connectivity vector B as defined in Eq. (3.28), is found to be,

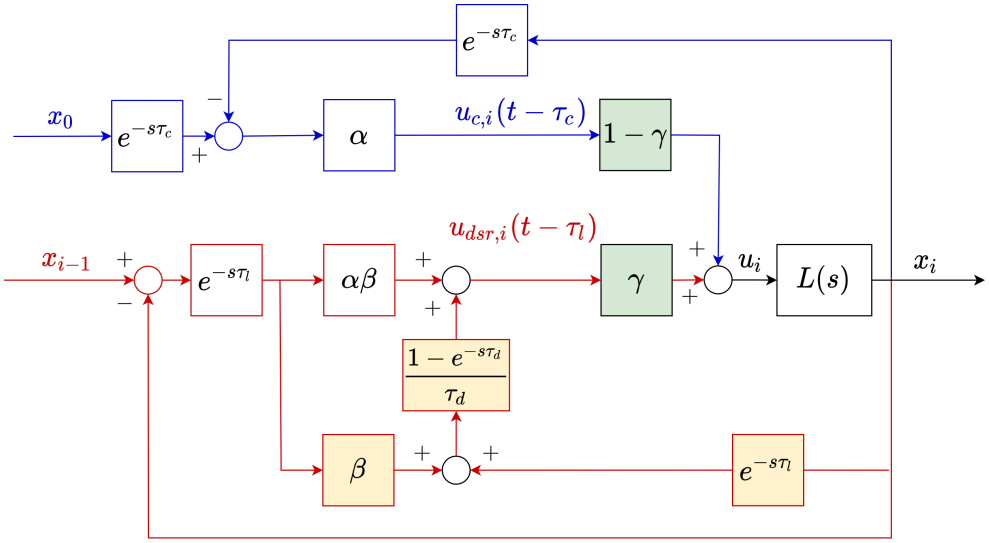

Figure 3.3: The block diagram of PLF with DSR for the follower vehicles $i \geq 2$ in Eq. (3.30), with communication delay τ_c, local sensing delay τ_l, and DSR delay τ_d. The vehicle control $u_{c,i}$ using centralized information is depicted in blue and control $u_{dsr,i}$ using decentralized sensing is in red. The DSR augmentation of the traditional feedback is shown in yellow shaded blocks, and the blending of centralized and decentralized control is shown in green shaded blocks. When centralized communication is lost $u_{c,i}$ is set to zero. For PLF without DSR, the yellow blocks are set to zero and the green blocks are set to 1.

$$\begin{aligned}\dot{x}_1(t) =&(1-\beta)\frac{x_1(t)-x_1(t-\tau_d)}{\tau_d} - \alpha\beta\left(x_1(t)-x_0(t)\right)\\ =&u_{dsr,1}(t),\end{aligned} \tag{3.29}$$

and the state equation for the followers $i > 1$ is obtained as,

$$\begin{aligned}\dot{x}_i(t) =&(1-\beta)\frac{x_i(t)-x_i(t-\tau_d)}{\tau_d} + \beta\frac{x_{i-1}(t)-x_{i-1}(t-\tau_d)}{\tau_d}\\ &- \alpha\beta(x_i(t)-x_{i-1}(t)) \quad = u_{dsr,i}(t).\end{aligned} \tag{3.30}$$

The dynamics of the i^{th} vehicle $\dot{x}_i(t)$ can be found by substituting the DSR command from

Eqs. (3.29), (3.30) and the centralized command from Eq. (3.18) into the blended protocol in Eq. (3.23) to obtain, in the Laplace domain,

for $i = 1$,

$$\frac{x_1(s)}{x_0(s)} = \frac{G_{c0}(s)}{s - (1-\beta)G_m(s) + G_{c0}(s)} = \frac{G_{c0}(s)}{D_0(s)} = T_1(s), \tag{3.31}$$

where $T_1(s)$ is the position-transfer function for the lead vehicle, and for the follower vehicles, $i \geq 2$,

$$\begin{aligned} x_i(s) &= \frac{G_c(s)x_0 + G_f(s)x_{i-1}}{s - G_m(s) + G_f(s) + G_c(s)} \\ &= \frac{G_c(s)x_0 + G_f(s)x_{i-1}}{D(s)}, \end{aligned} \tag{3.32}$$

with

$$G_m(s) = \gamma e^{-s\tau_l}\frac{1 - e^{-s\tau_d}}{\tau_d}, \tag{3.33}$$

$$G_f(s) = \beta\gamma e^{-s\tau_l}(\alpha + \frac{1 - e^{-s\tau_d}}{\tau_d}), \tag{3.34}$$

$$G_{c0}(s) = \alpha(1 - \gamma(1-\beta))e^{-s\tau_l}, \tag{3.35}$$

$$G_c(s) = \alpha(1-\gamma)e^{-s\tau_c}, \tag{3.36}$$

$$D_0(s) = s - (1-\beta)G_m(s) + G_{c0}, \tag{3.37}$$

$$D(s) = s - G_m(s) + G_f(s) + G_c(s). \tag{3.38}$$

Lemma 1. *The position transfer functions $T_i(s)$ in (3.24) for the follower vehicles $i \geq 2$ are given by*

$$T_i(s) = \left[\frac{G_c(s)}{D(s)}\sum_{j=0}^{i-2}\left(\frac{G_f(s)}{D(s)}\right)^j\right] + \left(\frac{G_f(s)}{D(s)}\right)^{i-1} T_1(s), \tag{3.39}$$

where $T_1(s)$ is the lead-vehicle transfer function in Eq. (3.31).

Proof. Eq. (3.39) can be shown by induction

1. Base case ($i = 2$): The position transfer function $T_2(s)$ can be computed from Eqs. (3.31) and (3.32) as

$$T_2(s) = \frac{G_c(s)}{D(s)} + \frac{G_f(s)}{D(s)} T_1(s), \tag{3.40}$$

which is equal to Eq. (3.39) with $i = 2$.

2. Induction step: Assume Eq. (3.39) is true when $i = k \geq 2$. Then, from Eq. (3.32)

$$T_{k+1}(s) = \frac{G_c(s) + G_f(s) T_k(s)}{D(s)}, \tag{3.41}$$

and using Eq. (3.39) for $T_k(s)$ results in

$$\begin{aligned} T_{k+1}(s) &= \frac{G_c(s)}{D(s)} + \frac{G_f(s)}{D(s)} \left(\frac{G_c(s)}{D(s)} \sum_{j=0}^{k-2} \left(\frac{G_f(s)}{D(s)} \right)^j \right) \\ &\quad + \left(\frac{G_f(s)}{D(s)} \right)^k T_1(s) \\ &= \frac{G_c(s)}{D(s)} \sum_{j=0}^{k-1} \left(\frac{G_f(s)}{D(s)} \right)^j + \left(\frac{G_f(s)}{D(s)} \right)^k T_1(s), \end{aligned} \tag{3.42}$$

which is equivalent to Eq. (3.39) with $i = k + 1$.

□

2) Internal stability conditions

The following lemma shows that the CVS can be made internally stable if the delays in the vehicle control are small compared to the CVS time constant.

Lemma 2. *The internal stability of the CVS protocol is independent of the DSR delay τ_d if the DSR gain β is selected as*

$$\beta = 1. \tag{3.43}$$

Moreover, with this DSR-gain selection, the CVS with the blended protocol in Eq. (3.23) *can always be stabilized if the local sensing delay* τ_l *and the communication delay* τ_c *are small compared to the CVS time constant* $1/\alpha$*,*

$$\max\{\tau_l, \tau_c\} < \frac{\pi}{2}\left(\frac{1}{\alpha}\right). \tag{3.44}$$

Proof. The poles $s \in \mathbb{C}$ of the transfer functions T_1 in Eq. (3.31) and $T_i(s)$ in Eq. (3.39) correspond to the roots of $D_0(s) = 0$ and $D(s) = 0$. Then, substituting from Eqs. (3.33)-(3.36) into Eqs. (3.37) and (3.38) and using the condition $\beta = 1$ results in

$$D_0(s) = \quad s + \alpha e^{-s\tau_l} \qquad = 0, \tag{3.45}$$

$$D(s) = \quad s + \alpha(\gamma e^{-s\tau_l} + (1-\gamma)e^{-s\tau_c}) \qquad = 0. \tag{3.46}$$

The CVS is stable with poles (i.e., roots of Eqs. (3.45), (3.46)) at $s = -\alpha$ when the local sensing delay τ_l and the communication delay τ_c are zero and $\alpha > 0$. Therefore, from continuity of roots with parameter variations, the CVS will remain stable provided there is no imaginary axis crossing, i.e., there is no frequency ω such that Eq. (3.45) or Eq. (3.46) is satisfied at $s = j\omega$ with $j = \sqrt{-1}$, i.e.,

$$\begin{aligned} D_0(j\omega) &= j\omega + \alpha e^{-j\omega\tau_l} \\ &= j\omega + \alpha[\cos(\tau_l\omega) - j\sin(\tau_l\omega)] \ = 0, \end{aligned} \tag{3.47}$$

$$\begin{aligned} D(j\omega) &= j\omega + \alpha(\gamma e^{-j\omega\tau_l} + (1-\gamma)e^{-j\omega\tau_c}) \\ &= \alpha(\gamma\cos(\tau_l\omega) + (1-\gamma)\cos(\tau_c\omega)) \\ &\quad + j(\omega - \alpha\gamma\sin(\tau_l\omega) - \alpha(1-\gamma)\sin(\tau_c\omega)) \\ &= 0. \end{aligned} \tag{3.48}$$

which are known as D-curves in the D-subdivision method[43]. First, conditions are found for $D_o(j\omega) = 0$ to not have imaginary axis roots. Equating, the real and imaginary parts of

$D_o(j\omega)$ to zero results in, from Eq. (3.47)

$$\alpha \cos(\tau_l \omega) = 0, \tag{3.49}$$

$$\omega - \alpha \sin(\tau_l \omega) = 0. \tag{3.50}$$

Eq. (3.49) is satisfied if

$$\tau_l \omega = \frac{\pi}{2} + n\pi, \tag{3.51}$$

for $n \in \{0, 1, 2, 3, \ldots\}$, which when substituted in Eq. (3.50) identifies the (positive) imaginary-axis crossing frequency as $\omega^* = \alpha$, and the corresponding local sensing delays leading to imaginary-axis-crossing at $\omega^* = \alpha$, from Eq. (3.51), is

$$\tau_l^* = \frac{\pi}{2\alpha} + n\pi. \tag{3.52}$$

Therefore, the imaginary axis crossing can be avoided if the the local sensing delay τ_l is smaller than the smallest τ_l^* value in Eq. (3.52) $\tau_l^* = \pi/(2\alpha)$, which leads to Eq. (3.44) of the current lemma.

Second, conditions are found for $D(j\omega) = 0$ to not have imaginary axis roots through the following three steps.

(i) There are no imaginary axis roots when $|\omega| > \alpha$. Equating the real and imaginary parts of $D(j\omega)$ to zero results in, from Eq. (3.48)

$$\alpha(\gamma \cos(\tau_l \omega) + (1-\gamma)\cos(\tau_c \omega)) = 0, \tag{3.53}$$

$$\alpha(\gamma \sin(\tau_l \omega) + (1-\gamma)\sin(\tau_c \omega)) = \omega. \tag{3.54}$$

Any solution ω satisfying Eq. (3.54) is bounded by α in magnitude, for $\gamma \in [0, 1]$, as shown below,

$$\omega = \alpha(\gamma \sin(\tau_l \omega) + (1-\gamma)\sin(\tau_c \omega)) \in [-\alpha, \alpha], \tag{3.55}$$

since,

$$\begin{aligned} -1 &= \gamma(-1) + (1-\gamma)(-1) \\ &\leq \gamma \sin(\tau_l \omega) + (1-\gamma)\sin(\tau_c \omega) \\ &\leq \gamma + (1-\gamma) = 1. \end{aligned} \tag{3.56}$$

Therefore, there can be no roots outside $[-\alpha, \alpha]$.

(ii) If there is an imaginary-axis crossing with $\omega \in [0, \alpha]$, then $-\omega$ would also be a solution since

$$\begin{aligned} &\alpha(\gamma \cos(-\tau_l \omega) + (1-\gamma)\cos(-\tau_c \omega)) \\ &= \alpha(\gamma \cos(\tau_l \omega) + (1-\gamma)\cos(\tau_c \omega)) = 0, \end{aligned} \tag{3.57}$$

$$\begin{aligned} &\alpha(\gamma \sin(-\omega \tau_l) + (1-\gamma)\sin(-\omega \tau_c)) \\ &= -\alpha(\gamma \sin(\omega \tau_l) + (1-\gamma)\sin(\omega \tau_c)) = -\omega. \end{aligned} \tag{3.58}$$

(iii) There are no imaginary axis roots with $\omega \in [0, \alpha]$. Assume that there exists $\omega \in [0, \alpha]$ such that Eq.(3.53) is satisfied. Then,

$$\alpha(\gamma \cos(\tau_l \omega) + (1-\gamma)\cos(\tau_c \omega)) = 0. \tag{3.59}$$

However, both cosine terms are positive, i.e., $\cos(\tau_l \omega) > 0$ and $\cos(\tau_c \omega) > 0$ since $\tau_l \omega \in [0, \frac{\pi}{2})$ and $\tau_c \omega \in [0, \frac{\pi}{2})$ when $\omega \in [0, \alpha]$ from the condition in Eq. (3.44) of the lemma. Therefore, the positively weighted sum of the cosines cannot be zero, and therefore,

$$\alpha(\gamma \cos(\tau_l \omega) + (1-\gamma)\cos(\tau_c \omega)) > 0, \tag{3.60}$$

which contradicts the assumption that there exists $\omega \in [0, \alpha]$ that satisfies Eq. (3.53). Therefore, there is no imaginary axis crossing of the poles under the condition in Eq.(3.44) of the lemma, resulting in internal stability of the CVS. □

Internal stability is guaranteed when both the local sensing delay τ_l and the communication delay τ_c are bounded as in Eq. (3.44) of Lemma 2. For larger communication delays,

the internal stability of CVS can still be guaranteed by using a sufficiently-large blending gain γ, as shown in the next lemma.

Lemma 3. *The CVS with the blended protocol in Eq.* (3.23) *is internally stable, for any communication delay τ_c, if the local sensing delay τ_l and the blending gain γ satisfy*

$$\tau_l < \frac{\pi}{2\alpha}, \tag{3.61}$$

$$\frac{1}{1+\cos(\tau_l \alpha)} < \gamma \leq 1 \tag{3.62}$$

with the DSR gain $\beta = 1$ as in Remark 8.

Proof. Internal stability of the lead vehicle is established from Eq. (3.52) in the proof of Lemma 2, since the condition $\tau_l < \pi/(2\alpha)$ guarantees that there is no frequency $\omega \in \mathbb{R}$ such that $D_0(j\omega) = 0$ (Eq. (3.47)) is satisfied. For the followers, internal stability can be examined by judging whether there exists $\omega \in \mathbb{R}$ such that Eq. (3.53) and (3.54) are satisfied. With the blending gain γ selection as in Eq. (3.62), there is no $\omega \in [0, \alpha]$ that satisfies Eq. (3.53) since

$$\begin{aligned} &\alpha(\gamma \cos(\tau_l \omega) + (1-\gamma)\cos(\tau_c \omega)) \\ &\quad \geq \alpha(\gamma \cos(\tau_l \omega) - (1-\gamma)) \\ &\quad \geq \alpha((\cos(\tau_l \alpha) + 1)\gamma - 1) \ > \alpha(1-1) = 0. \end{aligned} \tag{3.63}$$

The second inequality in Eq.(3.63) follows since $\cos(\tau_l \omega)$ monotonically decreases on $\omega \in [0, \alpha]$, and $\tau_l \omega \leq \tau_l \alpha < \pi/2$, from Eq. (3.61). Besides, using arguments in Steps 1 and 2 in the proof of Lemma 2, there can be no imaginary axis crossing when the frequency is large, $\omega > \alpha$ or negative, $\omega \leq 0$. Thus, there is no imaginary axis crossing under the conditions of the lemma, resulting in internal stability of the CVS. □

Remark 7 (Blending gain selection)**.** *The CVS is internally stable for any selection of the blending gain $\gamma \in [0, 1]$ if the communication delay τ_c and local-sensing delays τ_l are small with respect to the time constant $1/\alpha$, i.e., smaller than $\pi/(2\alpha)$, according to Lemma 2. In*

the presence of large communication delay τ_c with respect to the time constant $1/\alpha$, i.e., $\tau_c \geq \pi/(2\alpha)$, sufficient use of the DSR input u_{dsr} (with a sufficiently-large blending gain as in Eq. (3.62)*) also ensures internal stability.*

Remark 8 (Internal stability assumption)**.** *The CVS is assumed to be internally stable in the rest of the article by satisfying the stability conditions of either Lemma 2 or Lemma 3 – including, $\beta = 1$.*

3.2.2 String stability of CVS

This section begins by finding the error propagation transfer functions $G_i(s)$, using which the conditions for string stability are established.

1) Error dynamics of CVS

To assess string stability, the error propagation transfer functions $G_i, \forall i \in \mathcal{N}$ are obtained using the definition of the spacing error in Eq. (3.26) and the position transfer functions T_i in Eq. (3.24), as for $i = 1$,

$$G_1(s) = \frac{x_1(s) - x_2(s)}{x_0(s) - x_1(s)} = \frac{T_1(s) - T_2(s)}{1 - T_1(s)}, \tag{3.64}$$

and for $i \geq 2$,

$$G_i(s) = \frac{x_i(s) - x_{i+1}(s)}{x_{i-1}(s) - x_i(s)} = \frac{T_i(s) - T_{i+1}(s)}{T_{i-1}(s) - T_i(s)}. \tag{3.65}$$

The following existence lemma shows that the CVS can be made string stable if the delays in the vehicle control are small.

Lemma 4. *The CVS, with the blended protocol in Eq.* (3.23) *satisfying the internal stability conditions as in Remark 8, meets the string stability condition in Eq.* (3.25) *on the error-propagation transfer function $G_i(s)$ provided the time delays in local sensing τ_l, communication τ_c and DSR τ_d are sufficiently small compared to the time constant $1/\alpha$ of the CVS, and the blending gain is less than one*

$$\gamma < 1. \tag{3.66}$$

Proof. The approach is to find the error transfer function G_i in Eq. (3.65) and then find conditions to bound it to be less than one in three main steps. First, for all the follower vehicles ($i \geq 2$), the difference in the position transfer functions T_i can be found from Eq. (3.39) as

$$\begin{aligned} T_{i-1} - T_i =& \frac{G_c(s)}{D(s)} \left(\sum_{j=0}^{i-3} \left(\frac{G_f(s)}{D(s)} \right)^j - \sum_{j=0}^{i-2} \left(\frac{G_f(s)}{D(s)} \right)^j \right) \\ &+ T_1(s) \left(\left(\frac{G_f(s)}{D(s)} \right)^{i-2} - \left(\frac{G_f(s)}{D(s)} \right)^{i-1} \right) \\ =& \left(\frac{G_f(s)}{D(s)} \right)^{i-2} \left(\frac{G_c(s)}{D(s)} + T_1(s) \left(1 - \frac{G_f(s)}{D(s)} \right) \right), \end{aligned} \tag{3.67}$$

and since only the first term relates to the order of the vehicle i, the error transfer function in Eq. (3.65) becomes, for $i \geq 2$,

$$G_i(s) = \frac{T_i(s) - T_{i+1}(s)}{T_{i-1}(s) - T_i(s)} = \frac{G_f(s)}{D(s)}. \tag{3.68}$$

Second, the error transfer function G_i can be found by replacing G_f and D from Eq. (3.37) and Eqs. (3.33)-(3.36) with $\beta = 1$, as

$$G_i(s) = \frac{e^{-s\tau_l}\gamma(\alpha\tau_d + 1 - e^{-s\tau_d})}{\tau_d(s + \alpha(\gamma e^{-s\tau_l} + (1-\gamma)e^{-s\tau_c}))} = G(s), \tag{3.69}$$

which is independent of the vehicle number i. Third, from Eqs. (3.25) and (3.69), the string stability condition is

$$|G(j\omega)| = \left| \frac{e^{-j\omega\tau_l}\gamma(\alpha\tau_d + 1 - e^{-j\omega\tau_d})}{\tau_d(j\omega + \alpha(\gamma e^{-j\omega\tau_l} + (1-\gamma)e^{-j\omega\tau_c}))} \right| < 1,$$

for all $\omega > 0$, which is equivalent to (by squaring both sides and multiplying the denominator)

$$\begin{aligned} f(\omega, \gamma, \tau_c) =& \left| \tau_d(j\omega + \alpha(\gamma e^{-j\omega\tau_l} + (1-\gamma)e^{-j\omega\tau_c})) \right|^2 \\ &- \left| e^{-j\omega\tau_l}\gamma(\alpha\tau_d + 1 - e^{-j\omega\tau_d}) \right|^2 \\ =& \alpha^2(1-\gamma)^2\tau_d^2 + 2\alpha^2\tau_d^2\gamma(1-\gamma)\cos((\tau_c - \tau_l)\omega) \\ &+ \tau_d^2\omega^2 - 2\tau_d^2\alpha\omega(\gamma\sin(\tau_l\omega) + (1-\gamma)\sin(\tau_c\omega)) \\ &- 2\gamma^2(\alpha\tau_d + 1)(1 - \cos(\tau_d\omega)) \\ &> 0. \end{aligned} \tag{3.70}$$

Since $\cos(z) \leq 1$ integrating both sides from 0 to z yields $\sin(z) \leq z$ when $z \geq 0$ and integration again yields $1 - \cos(z) \leq z^2/2$ when $z > 0$. Therefore,

$$1 - \cos(\tau_d \omega) \leq \frac{1}{2}(\tau_d \omega)^2, \tag{3.71}$$

$$\cos((\tau_c - \tau_l)\omega) \geq 1 - \frac{(\tau_c - \tau_l)^2 \omega^2}{2}, \tag{3.72}$$

$$\sin(\tau_l \omega) \leq \tau_l \omega, \quad \sin(\tau_d \omega) \leq \tau_d \omega, \quad \sin(\tau_c \omega) \leq \tau_c \omega, \tag{3.73}$$

since the frequency ω are positive. Substituting these inequalities into Eq. (3.70) yields

$$\begin{aligned} f(\omega, \gamma, \tau_c) \geq & \omega^2 \tau_d^2 \left[1 - \alpha^2 \gamma (1-\gamma)(\tau_c - \tau_l)^2 - \gamma^2(\alpha \tau_d + 1)\right. \\ & \left. -2\alpha(\gamma \tau_l + (1-\gamma)\tau_c)\right] + \alpha^2 \tau_d^2 (1-\gamma)^2 \\ & > 0, \qquad \forall \omega > 0, \end{aligned} \tag{3.74}$$

which is satisfied if the coefficient of the ω^2 term is positive, i.e.,

$$\begin{aligned} p(\gamma) = & 1 - \alpha^2 \gamma (1-\gamma)(\tau_c - \tau_l)^2 - 2\alpha(\gamma \tau_l + (1-\gamma)\tau_c) \\ & - \gamma^2(\alpha \tau_d + 1) > 0. \end{aligned} \tag{3.75}$$

By collecting all the time-delay terms to one side of the equation, the above inequality can be rewritten as

$$\begin{aligned} \gamma(1-\gamma)\left(\frac{\tau_c}{1/\alpha} - \frac{\tau_l}{1/\alpha}\right)^2 + 2\left(\gamma \frac{\tau_l}{1/\alpha} + (1-\gamma)\frac{\tau_c}{1/\alpha}\right) \\ + \gamma^2\left(\frac{\tau_d}{1/\alpha}\right) \quad < \left(1 - \gamma^2\right). \end{aligned} \tag{3.76}$$

Note that this inequality cannot be satisfied with the blending gain $\gamma = 1$, since the right hand side becomes zero, and the time delays and the time constant $1/\alpha$ are non-negative, which leads to the condition in Eq. (3.66) of the lemma. However, with $\gamma < 1$, the inequality in Eq. (3.76) is always satisfied provided all the delays are sufficiently small since the left hand side tends to zero. □

Lemma 4 ensures string stability if the delays are small. String stability can be numerically assessed for a given set of delay values by directly evaluating the condition on $f(\omega)$ in Eq. (3.70) over a finite frequency interval, as shown next.

Lemma 5. *The CVS, with the blended protocol in Eq.* (3.23) *satisfying the internal stability conditions as in Remark 8, meets the string stability condition in Eq.* (3.25) *on the error-propagation transfer function $G_i(s)$ provided the minimum value of $f(\omega)$ over the bounded interval $[0, \omega^*]$ in Eq.* (3.70) *is positive, i.e.,*

$$\min_{\omega \in (0,\omega^*]} f(\omega, \gamma, \tau_c) > 0, \tag{3.77}$$

where

$$\omega^* = \alpha \left(1 + 2\sqrt{\frac{1}{3} + \frac{\alpha\tau_d + 1}{\alpha^2 \tau_d^2}} \right). \tag{3.78}$$

Proof. The string stability condition $f(\omega) > 0$ in Eq. (3.70) is always satisfied if ω is large, as the condition can be rewritten as (since sine and cosine are bounded functions)

$$\begin{aligned} f(\omega, \gamma, \tau_c) >& \alpha^2(1-\gamma)^2\tau_d^2 - 2\alpha^2\tau_d^2\gamma(1-\gamma) + \tau_d^2\omega^2 - 2\tau_d^2\alpha\omega \\ & - 4\gamma^2(\alpha\tau_d + 1) \\ >& 0, \end{aligned} \tag{3.79}$$

which is equivalent to

$$\begin{aligned} (\omega - \alpha)^2 >& \alpha^2(4\gamma - 3\gamma^2) + 4\frac{\gamma^2}{\tau_d^2}(\alpha\tau_d + 1), \\ & \text{or } \omega > \alpha \left(1 + 2\sqrt{(\gamma - \frac{3}{4}\gamma^2) + \frac{\gamma^2(\alpha\tau_d + 1)}{\tau_d^2\alpha^2}} \right), \end{aligned} \tag{3.80}$$

and is always satisfied if $\omega > \omega^*$ in Eq. (3.78) since $\max_{0 \le \gamma \le 1}(\gamma - 3\gamma^2/4) = 1/3$ and $\gamma \le 1$. □

Remark 9 (String stability assumption)**.** *The CVS is assumed to be string stable in the rest of the article by satisfying the stability condition in Lemma 5, esp., $\gamma < 1$ from Lemma 4.*

3.2.3 Steady-state error of CVS

The proposed approach maintains constant steady-state spacing between vehicles.

Lemma 6. *Constant steady-state spacing between vehicles for a desired trajectory with constant velocity is maintained with the blended protocol in Eq.* (3.23) *satisfying the internal stability conditions in Remark 8. Specifically, with desired trajectory* $x_0(t) = Vt$ *and*

$$x_0(s) \ = v_0(s)/s \ = V/s^2 \tag{3.81}$$

the relative spacing error δ_i *is zero,* $\lim_{t\to\infty} \delta_i(t) = 0$*, for all follower vehicles, i.e.,* $i \geq 2$*.*

Proof. The steady-state spacing error $\delta_i = x_{i-1} - x_i$ for each follower vehicle ($i \geq 2$) can be found from Eq.(3.25) as,

$$\begin{aligned}
\delta_i(s) = G_{i-1}\delta_{i-1}(s) \ &= \left(\prod_{j=1}^{i-1} G_j(s)\right)\delta_1(s) \\
&= G^{i-2}(s)G_1(s)\delta_1(s) \quad \text{(using Eq. (3.69))} \\
&= G^{i-2}(s)G_1(s)G_0(s)v_0(s), \\
&= G^{i-2}(s)G_1(s)G_0(s)\frac{V}{s},
\end{aligned} \tag{3.82}$$

where

$$\begin{aligned}
G_0(s) = \frac{\delta_1(s)}{v_0(s)} &= \frac{x_0(s) - x_1(s)}{sx_0(s)} = \frac{1 - T_1(s)}{s} \\
&= \frac{1}{s + \alpha e^{-s\tau}} \quad \text{(using Eqs. (3.31), (3.35), (3.45)).}
\end{aligned} \tag{3.83}$$

Similarly, the transfer function $G_1(s)$ can be found from Eq. (3.64). The denominator of G_1 in Eq. (3.64) can be obtained from the expression of T_1 in Eq.(3.31), and G_{c0} in Eq. (3.35) and $D_0(s)$ in Eq. (3.37), with $\beta = 1$,

$$\begin{aligned}
1 - T_1(s) = 1 - \frac{G_{c0}(s)}{D_0(s)} &= 1 - \frac{\alpha e^{-s\tau_l}}{s + \alpha e^{-s\tau_l}} \\
&= \frac{s}{s + \alpha e^{-s\tau_l}} = \frac{s}{D_0(s)}.
\end{aligned} \tag{3.84}$$

The numerator of G_1 in Eq. (3.64) can be found from Eq. (3.40), resulting in, using Eq.(3.31),

and Eqs.(3.33)-(3.38), with $\beta = 1$,

$$\begin{aligned} & T_1(s) - T_2(s) \\ &= \left(1 - \frac{G_f(s)}{D(s)}\right) \frac{G_{c0}(s)}{D_0(s)} - \frac{G_c(s)}{D(s)} \\ &= \frac{(D(s) - G_f(s))G_{c0}(s) - G_c(s)D_0(s)}{D(s)D_0(s)} \\ &= \frac{\alpha s e^{-s\tau_l}((1 - (1-\gamma)e^{-s(\tau_c - \tau_l)}) - \gamma e^{-s\tau_l}\frac{1-e^{-s\tau_d}}{s\tau_d})}{(s + \alpha e^{-s\tau_l})(s + \alpha(\gamma e^{-\tau_l} + (1-\gamma)e^{-s\tau_c}))}. \end{aligned} \tag{3.85}$$

Substituting Eqs. (3.84) and (3.85) into Eq. (3.64) yields

$$G_1(s) = \frac{\alpha e^{-s\tau_l}(1 - (1-\gamma)e^{-s(\tau_c - \tau_l)} - \gamma e^{-s\tau_l}\frac{1-e^{-s\tau_d}}{s\tau_d})}{(s + \alpha(\gamma e^{-s\tau_l} + (1-\gamma)e^{-s\tau_c}))}. \tag{3.86}$$

The limit as s tends to zero for the error transfer functions in Eqs.(3.69) and (3.83) are given by

$$\begin{aligned} \lim_{s\to 0} G(s) &= \lim_{s\to 0} \frac{e^{-s\tau_l}\gamma(\alpha\tau_d + 1 - e^{-s\tau_d})}{\tau_d(s + \alpha(\gamma e^{-s\tau_l} + (1-\gamma)e^{-s\tau_c}))} \\ &= \gamma, \end{aligned} \tag{3.87}$$

$$\lim_{s\to 0} G_0(s) = \lim_{s\to 0} \frac{1}{s + \alpha e^{-s\tau_l}} = \frac{1}{\alpha}. \tag{3.88}$$

and from Eq. (3.86)

$$\begin{aligned} \lim_{s\to 0} G_1(s) &= \lim_{s\to 0} \frac{\alpha\gamma(s - e^{-s\tau_l}\frac{1-e^{-s\tau_d}}{\tau_d})}{s\alpha} \\ &= \lim_{s\to 0} \frac{\alpha\gamma(s - \frac{1-e^{-s\tau_d}}{\tau_d})}{s\alpha}. \end{aligned} \tag{3.89}$$

Note that the Taylor expansion of $e^{-s\tau_d}$

$$e^{-s\tau_d} = 1 - \tau_d s + \frac{1}{2}(\tau_d s)^2 + \ldots, \tag{3.90}$$

and therefore, from Eq. (3.89),

$$\begin{aligned} \lim_{s\to 0} G_1(s) &= \lim_{s\to 0} \frac{\alpha\gamma(\frac{1}{2}\tau_d s^2 - \frac{1}{6}\tau_d^2 s^3 + \ldots)}{s\alpha} \\ &= \lim_{s\to 0} \frac{\alpha\gamma(\frac{1}{2}\tau_d s - \frac{1}{6}\tau_d^2 s^2 + \ldots)}{\alpha} = 0. \end{aligned} \tag{3.91}$$

Finally, substituting Eqs. (3.87), (3.88) and (3.91) into Eq. (3.82), the steady state spacing error of all follower vehicles $i \geq 2$ is

$$\begin{aligned}\lim_{t\to\infty} \delta_i(t) &= \lim_{s\to 0} s\delta_i(s) \\ &= \lim_{s\to 0} s[G_1(s)] \left(G^{i-2}(s)G_0(s)\right) \frac{V}{s} \\ &= \lim_{s\to 0} [G_1(s)] \left(G^{i-2}(s)G_0(s)\right) V = 0, \end{aligned} \tag{3.92}$$

since the limit as s tends to zero of $G_1(s)$ is zero and the limits of $G(s) = G_i(s)$ and $G_0(s)$ are bounded, resulting in the maintaining of constant spacing by all the followers. □

3.2.4 Loss of centralized communication (use of DSR alone)

This subsection considers the impact when DSR alone is used due to the loss of centralized communication of the desired trajectory to the followers. Specifically, this section considers the case when the blended protocol in Eq. (3.23) is reduced to the purely predecessor-follower DSR case (and referred to as PF with DSR), for the followers, i.e.,

$$\begin{aligned}\dot{x}_i(t) &= \gamma u_{dsr}(t-\tau_l), \qquad i \geq 2 \\ \dot{x}_1(t) &= \gamma u_{dsr,1}(t-\tau_l) + (1-\gamma) u_{c,1}(t-\tau_l) \\ &= -\alpha(x_1(t-\tau_l) - x_0(t-\tau_l)). \end{aligned} \tag{3.93}$$

This PF with DSR can be represented by the block diagram in Fig. 3.3 without the blue centralized control, i.e., $u_{c,i}(t) = 0$.

It is well known that, without centralized control, constant spacing cannot be maintained while remaining string stable. In the following, it is shown that even under full communication loss, the DSR-based approach to constant spacing platooning (i) remains internally stable (Lemma 7), and (ii) is string stable (Lemma 8). The cost of this string stability is an increase in steady state spacing error similar to standard PLF (where the steady state spacing error is proportional to the time constant $1/\alpha$ [44]), and quantified in Lemma 9. The steady state error is also shown to decrease with larger values of blending gain γ.

Internal stability with DSR alone

Lemma 7. *Internal stability is maintained if centralized communication to the followers is lost as in Eq.* (3.93) *when the local sensing delay* τ_l *satisfies the internal stability condition with the centralized communication in Lemmas 2 and 3, i.e.,* $\tau_l < \frac{\pi}{2\alpha}$, *as in Eq.* (3.61).

Proof. With loss of the centralized communication and the control as in Eq. (3.93), the relationship between the spacing of adjacent vehicles can be obtained from Eqs. (3.29), (3.30) with $\beta = 1$ as, for $i \geq 2$

$$x_i(s) = \frac{\gamma e^{-s\tau_l}}{\tau_d} \left(\frac{(1 - e^{-s\tau_d}) + \alpha\tau_d}{s + \alpha\gamma e^{-s\tau_l}} \right) x_{i-1}(s). \tag{3.94}$$

From Eq. (3.93), the dynamics of the leader is not impacted. Therefore, the characteristic function $D_0(s)$ for the leader is the same as in Eq. (3.45), which requires $\tau_l < \pi/(2\alpha)$ for the internal stability of the leader. From Eq. (3.94), the characteristic function $D(s)$ of the dynamics of the followers are given by

$$D(s) = s + \alpha\gamma e^{-s\tau_l}. \tag{3.95}$$

The result follows using arguments similar to the proof of Lemma 2 to ensure that there are no imaginary axis crossing of the poles. □

String stability with DSR alone

Lemma 8. *String stability is maintained if centralized communication to the followers is lost as in Eq.* (3.93) *when satisfying the string stability condition* $\gamma < 1$ *in Eq.* (3.66) *and satisfying the internal stability conditions as in Remark 8, provided the blending gain* $\gamma > 0$ *is sufficiently small, i.e.,*

$$0 < \gamma < \gamma^* = \frac{-\alpha\tau_l + \sqrt{\alpha^2\tau_l^2 + \alpha\tau_d + 1}}{\alpha\tau_d + 1}, \tag{3.96}$$

where the upper bound γ^* *is less than one,* $\gamma^* < 1$.

Proof. Following arguments similar to the proof of Lemma 4, string stability can be ensured if $G_i(j\omega) < 1$ for all $\omega > 0$, or if the function $f(\omega, \gamma)$ with $1 - \gamma$ terms (corresponding to centralized communication) removed satisfies the $f(\omega) > 0$ condition for string stability in Eq. (3.70), i.e.,

$$\begin{aligned} f(\omega,\gamma) =& \tau_d^2\omega^2 - 2\tau_d^2\alpha\omega\gamma\sin(\tau_l\omega) \\ & - 2\gamma^2(\alpha\tau_d+1)(1-\cos(\tau_d\omega)) \\ \geq& \tau_d^2\omega^2 - 2\tau_d^2\alpha\omega^2\gamma\tau_l - \gamma^2(\alpha\tau_d+1)\tau_d^2\omega^2 \\ & \text{(from Eqs. (3.71), (3.73))} \\ =& \tau_d^2\omega^2\left(1 - 2\alpha\gamma\tau_l - \gamma^2(\alpha\tau_d+1)\right) > 0. \end{aligned} \tag{3.97}$$

The above condition is always satisfied if the blending gain γ is sufficiently small. A bound on the blending gain γ can be found by noting that Eq. (3.97) is satisfied if the coefficient of ω^2 is positive

$$-\gamma^2(\alpha\tau_d+1) - 2\alpha\tau_l\gamma + 1 > 0, \tag{3.98}$$

where the maximum gain $\gamma^* \in [0, 1]$ is found by

$$\begin{aligned} \gamma^* &= \arg\max_{\gamma\in[0,1]}\{-\gamma^2(\alpha\tau_d+1) - 2\alpha\tau_l\gamma + 1 = 0\} \\ &= \frac{-\alpha\tau_l + \sqrt{\alpha^2\tau_l^2 + \alpha\tau_d + 1}}{\alpha\tau_d+1} \\ &< \frac{-\alpha\tau_l + \sqrt{\alpha^2\tau_l^2 + (\alpha\tau_d+1)^2 + 2\alpha\tau_l(\alpha\tau_d+1)}}{\alpha\tau_d+1} \\ &= \frac{-\alpha\tau_l + (\alpha\tau_l + \alpha\tau_d + 1)}{\alpha\tau_d+1} = 1, \end{aligned} \tag{3.99}$$

which proves the assertion in the lemma that the blending gain γ needs to be less than one for string stability when communication is lost. □

Steady-state error with DSR alone

Lemma 9. *When the communication to the followers is lost, the relative spacing error of the i^{th} vehicle at the steady state for the desired trajectory in Eq.* (3.81)*, is given as*

$$\lim_{s\to 0} s\delta_i(s) = \frac{V}{\alpha}\left(\frac{1}{\gamma} - 1\right). \tag{3.100}$$

Proof. The position transfer functions $T_1(s), T_2(s)$ can be found from Eqs. (3.31), (3.94), with $\beta = 1$ as

$$T_1(s) = \frac{\alpha e^{-s\tau_l}}{s + \alpha e^{-s\tau_l}}, \tag{3.101}$$

$$T_2 = \frac{\gamma e^{-s\tau_l}}{\tau_d}\left(\frac{(1 - e^{-s\tau_d}) + \alpha\tau_d}{s + \alpha\gamma e^{-s\tau_l}}\right) T_1(s). \tag{3.102}$$

resulting in the error transfer function from Eq. (3.64)

$$\begin{aligned} G_1(s) &= \frac{T_1(s) - T_2(s)}{1 - T_1(s)} \\ &= \frac{\alpha e^{-s\tau_l}(\tau_d s - \gamma e^{-s\tau_l}(1 - e^{-s\tau_d}))}{\tau_d s(s + \alpha\gamma e^{-s\tau_l})}. \end{aligned} \tag{3.103}$$

Additionally, the error propagation is, from Eq. (3.94), for $i \geq 2$,

$$\begin{aligned} G_i(s) =& \frac{x_i(s) - x_{i+1}(s)}{x_{i-1}(s) - x_i(s)} \\ =& \gamma\frac{e^{-s\tau_l}((1 - e^{-s\tau_d}) + \alpha\tau_d)}{\tau_d(s + \alpha\gamma e^{-s\tau_l})} = G(s). \end{aligned} \tag{3.104}$$

Therefore, substituting from Eqs. (3.88), (3.103) and (3.104) into Eq. (3.82), the relative spacing error of the i^{th} vehicle at the steady state is given as

$$\begin{aligned} \lim_{t\to\infty} \delta_i(t) &= \lim_{s\to 0} s\delta_i(s) = \lim_{s\to 0}[G_1(s)]\,(G(s))^{i-2}\,[G_0(s)]\,V \\ &= \left[\frac{1-\gamma}{\gamma}\right](1)^{i-2}\left[\frac{1}{\alpha}\right]V = \frac{V}{\alpha}\left(\frac{1}{\gamma} - 1\right). \end{aligned}$$

□

Remark 10 (Limitations of pure decentralized control)**.** *String stability and constant spacing cannot be guaranteed simultaneously when communication is lost based on Lemmas 8*

and 9. The relative spacing error converges to zero only when the blending gain $\gamma = 1$ *from Eq.* (3.100)*. However, string stability requires a smaller blending gain* $\gamma < \gamma^* < 1$ *in Eq.* (3.96)*.*

3.2.5 PLF without DSR

This section derives the standard first-order protocol for constant spacing platoon without DSR, develops conditions for internal stability and string stability and quantifies the steady-state error. This standard protocol for first-order constant spacing tracking, referred to as PLF without DSR, is given as

$$\begin{aligned} \dot{x}_i(t) &= u_{std,i}(t-\tau_l) + u_{c,i}(t-\tau_c), \quad \forall i \geq 2 \\ \dot{x}_1(t) &= u_{std,1}(t-\tau_l), \end{aligned} \tag{3.105}$$

where $u_{std,i}(t) = \alpha(x_{i-1}(t) - x_i(t))$. Similarly, when the second term in Eq. (3.105) for $i \geq 2$ is dropped due to communication loss, the method is referred to as PF without DSR in the followings. The PLF without DSR corresponds to the block diagram in Fig. 3.3 with the yellow blocks removed, $\beta = 1$, and gains of both the green blocks (γ and $1-\gamma$) set to 1. The position transfer function of the standard protocol in Eq. (3.105) has the same general form as Eq. (3.32), arguments similar to the DSR case can be used to establish internal stability if the delays are small, and the ability to maintain constant spacing. The dynamics of the i^{th} vehicle $\dot{x}_i(t)$ can be found as

$$\begin{aligned} sx_1(s) &= \alpha e^{-s\tau_l}(x_0(s) - x_1(s)), \\ sx_i(s) &= \alpha e^{-s\tau_c}((x_0(s) - x_i(s)) + \alpha e^{-s\tau_l}(x_{i-1}(s) - x_i(s)). \end{aligned} \tag{3.106}$$

resulting in,

$$x_1(s) = \frac{\alpha e^{-s\tau_l}}{s + \alpha e^{-s\tau_l}} x_0(s) = \frac{G_{c0(s)}}{D_0(s)} T_1(s) x_0(s), \tag{3.107}$$

$$\begin{aligned} x_i(s) &= \frac{\alpha e^{-s\tau_l} x_{i-1}(s) + \alpha e^{-s\tau_c} x_0(s)}{s + \alpha(e^{-s\tau_l} + e^{-s\tau_c})} \\ &= \frac{G_c(s) x_0(s) + G_f(s) x_{i-1}(s)}{D(s)}, \end{aligned} \tag{3.108}$$

where

$$G_f(s) = \alpha e^{-s\tau_l}, \tag{3.109}$$

$$G_c(s) = \alpha e^{-s\tau_c}, \tag{3.110}$$

$$G_{c0}(s) = \alpha e^{-s\tau_l}, \tag{3.111}$$

$$D_0(s) = s + \alpha e^{-s\tau_l}, \tag{3.112}$$

$$D(s) = s + \alpha(e^{-s\tau_l} + e^{-s\tau_c}). \tag{3.113}$$

Similar to Eq. (3.32), the position transfer function $T_1(s)$ and $T_i(s)$ for the standard protocol has the same general expression in terms of G_f, G_c, G_{c0}, D_0 and D. The position transfer functions $T_1(s)$ and $T_i(s)$ are given by

$$T_1(s) = \frac{G_{c0}}{D_0(s)} = \frac{\alpha e^{-\tau_l}}{s + \alpha e^{-s\tau_l}}, \tag{3.114}$$

$$T_i(s) = \left[\frac{G_c(s)}{D(s)} \sum_{j=0}^{i-2} \left(\frac{G_f(s)}{D(s)}\right)^j\right] + \left(\frac{G_f(s)}{D(s)}\right)^{i-1} T_1(s). \tag{3.115}$$

Conditions on the standard protocol Eq. (3.105) are derived for guaranteeing internal stability, string stability and maintaining steady-state spacing.

1) Internal Stability

The following lemma derives the conditions to guarantee internal stability.

Lemma 10. *The CVS with the standard protocol Eq.* (3.105) *is internally stable if the local sensing error is small compared to the time constant* $1/\alpha$

$$\tau_l < \frac{1}{2\alpha}. \tag{3.116}$$

Proof. From the position transfer functions in Eq. (3.114), (3.115), the internal stability of the CVS corresponds to the location of the roots of the characteristic function, i.e.,

$$D_0(s) = s + \alpha e^{-s\tau_l} = 0.$$

$$D(s) = s + \alpha(e^{-s\tau_l} + e^{-s\tau_c}) = 0. \tag{3.117}$$

The characteristic equation $D_0(s) = 0$ is the same as the $D_0(s)$ in Lemma 2. Therefore, the leader dynamics is guaranteed to be internally stable with the same condition as in Lemma 2, which is satisfied with the small bound in Eq. (3.116).

When the sensing delay is zero, $\tau_l = 0$, the CVS is internally stable for any communication delay $\tau_c > 0$. Assume that there is an unstable pole $s = a+bj$ with $a \geq 0, b \in \mathbb{R}$ s.t. $D(s) = 0$. Then, substituting $s = a + j\omega$ and $\tau_l = 0$ into Eq. (3.117) results in

$$D(a + j\omega) = (a + j\omega) + \alpha(1 + e^{-\tau_c a}e^{-j\tau_c\omega}) = 0. \tag{3.118}$$

Requiring both the real and the imaginary part be 0, results in

$$a + \alpha e^{-\tau_l a}(1 + \cos(\tau_c\omega)) = 0, \tag{3.119}$$

$$\alpha(e^{-\tau_c a}\sin(\tau_c\omega)) = \omega. \tag{3.120}$$

Eq. (3.119) requires $a = 0$ and $\cos(\tau_c\omega) = -1$, which results in $\sin(\tau_c\omega) = 0$. From Eq. (3.120)

$$\alpha(e^{-\tau_c a}s\sin(\tau_c\omega)) = \omega = 0. \tag{3.121}$$

It also requires $\omega = 0$, which contradicts $\cos(\tau_c\omega) = -1$. Therefore, there is no unstable poles $s = a + j\omega, a > 0, \omega \in \mathbb{R}$ satisfying $D(s) = 0$, and CVS is internally stable when $\tau_l = 0$. Next, the proof focuses on when there a pole could be on the imaginary axis for some nonzero sensing delay $\tau_l > 0$.

Substituting $s = j\omega, \omega \in \mathbb{R}$ into into Eq. (3.117) results in

$$\begin{aligned} D(j\omega) =& \alpha(\cos(\tau_c\omega) + \cos(\tau_c\omega)) \\ &+ j(\omega - \alpha(\sin(\tau_c\omega) + \sin(\tau_l\omega))) = 0. \end{aligned} \tag{3.122}$$

Requiring both the real and the imaginary part be 0, results in

$$\alpha(\cos(\tau_c\omega) + \cos(\tau_l\omega)) = 0, \tag{3.123}$$

$$\alpha(\sin(\tau_c\omega) + \sin(\tau_l\omega)) = \omega. \tag{3.124}$$

From Eq. (3.123)

$$cos(\tau_c\omega) = -\cos(\tau_l\omega) = \cos(\pi - \tau_l\omega), \tag{3.125}$$

$$\pm\tau_c\omega = 2k\pi + (\pi - \tau_l\omega), \qquad k = 0, \pm1, \ldots \tag{3.126}$$

or

$$(\tau_l \pm \tau_c)\omega = 2k\pi + \pi. \tag{3.127}$$

Substituting Eq. (3.126) into Eq. (3.124) yields

$$\begin{aligned} &\alpha(\sin(\tau_c\omega) + \sin(\tau_l\omega)), \\ =&\alpha(\pm\sin(\pi - \tau_l\omega) + \sin(\tau_l\omega)) = \omega. \end{aligned} \tag{3.128}$$

1. if $-\tau_c\omega = 2k\pi + (\pi - \tau_l\omega)$, then Eq. (3.127) becomes

$$(\tau_l - \tau_c)\omega = 2k\pi + \pi, \tag{3.129}$$

   and Eq. (3.128) becomes

$$\begin{aligned} &\alpha(\sin(\tau_c\omega) + \sin(\tau_l\omega)) \\ =&\alpha(-\sin(\pi - \tau_l\omega) + \sin(\tau_l\omega)) \\ =&\alpha(-\sin(\tau_l\omega) + \sin(\tau_l\omega)) = 0 = \omega, \end{aligned} \tag{3.130}$$

   which contradicts to Eq. (3.129). Therefore, there is no $\omega \in \mathbb{R}$ which makes $s = j\omega$ a root of $D(s) = 0$.

2. if $\tau_c\omega = 2k\pi + (\pi - \tau_l\omega)$, then Eq. (3.127) becomes

$$\begin{aligned} (\tau_l + \tau_c)\omega &= 2k\pi + \pi \\ \omega &= \frac{2k\pi + \pi}{\tau_l + \tau_c}, \end{aligned} \tag{3.131}$$

and Eq. (3.128) becomes

$$\begin{aligned}
&\alpha(\sin(\tau_c\omega)+\sin(\tau_l\omega)) \\
=&\alpha(\sin(\pi-\tau_l\omega)+\sin(\tau_l\omega)) \\
=&\alpha(\sin(\tau_l\omega)+\sin(\tau_l\omega)) \\
=&2\alpha\sin(\tau_l\omega) \qquad (3.132)\\
=&\omega. \qquad (3.133)
\end{aligned}$$

Denote

$$x=\tau_l\omega=\frac{(2k\pi+\pi)\tau_l}{\tau_l+\tau_c}, \qquad x>0. \tag{3.134}$$

Substituting Eq. (3.131) (3.134) into Eq. (3.133) yields

$$\sin(x)=\frac{1}{2\alpha\tau_l}x>x. \tag{3.135}$$

The inequality is true with $\tau_l<1/(2\alpha)$. However, $\sin(z)<z, \forall z>0$, which contradicts Eq. (3.135). Therefore, there is no imaginary axis crossing under Eq. (3.116).

□

2) String Stability

The following lemma derives the conditions to guarantee string stability.

Lemma 11. *The CVS with the standard protocol Eq.* (3.105) *is string stable if the local sensing delay τ_l and τ_c are small, i.e., satisfy*

$$\alpha(\tau_c-\tau_l)^2+2(\tau_l+\tau_c)<\frac{1}{\alpha}. \tag{3.136}$$

Proof. Since the position transfer function of the standard protocol in Eq. (3.105) has the same general form as Eq. (3.32). The error transfer function of the protocol Eq. (3.105) is given as

$$G_i(s)=\frac{G_f(s)}{D(s)}=\frac{\alpha e^{-s\tau_l}}{s+\alpha(e^{-s\tau_l}+e^{-s\tau_c})}=G(s). \tag{3.137}$$

Combine with Eq. (3.25), the string stability of CVS requires

$$|G(j\omega)| = \left| \frac{\alpha e^{-j\omega\tau_l}}{j\omega + \alpha(e^{-s\tau_l} + e^{-j\omega\tau_c})} \right| < 1, \qquad \forall \omega > 0, \tag{3.138}$$

which is equivalent to require

$$\begin{aligned} f(\omega, \tau_c) &= |j\omega + \alpha(e^{-s\tau_l} + e^{-j\omega\tau_c})|^2 - |\alpha e^{-j\omega\tau_l}|^2 \\ &= |j\omega + \alpha(e^{-s\tau_l} + e^{-j\omega\tau_c})|^2 - \alpha^2 > 0, \qquad \omega > 0, \end{aligned} \tag{3.139}$$

where the square of the denominator is given as

$$\begin{aligned} & |j\omega + \alpha(e^{-s\tau_l} + e^{-j\omega\tau_c})|^2 \\ =& |\alpha(\cos(\tau_l\omega) + \cos(\tau_c\omega)) + j(\omega - \alpha(\sin(\tau_c\omega) + \sin(\tau_l\omega))|^2 \\ =& \alpha^2(\cos^2(\tau_l\omega) + \cos^2(\tau_c\omega) + 2\cos(\tau_c\omega)\cos(\tau_l\omega)) \\ & + \omega^2 - 2\alpha\omega(\sin(\tau_l\omega) + \sin(\tau_c\omega)) \\ & + \alpha^2(\sin^2(\tau_l\omega) + \sin^2(\tau_c\omega) + 2\sin(\tau_c\omega)\sin(\tau_l\omega)) \\ =& 2\alpha^2 + 2\alpha^2\cos((\tau_c - \tau_l)\omega) + \omega^2 - 2\alpha\omega(\sin(\tau_l\omega) + \sin(\tau_c\omega)) \\ \geq& 2\alpha^2 + 2\alpha^2(1 - \frac{1}{2}(\tau_c - \tau_l)^2\omega^2) + \omega^2 \\ & - 2\alpha\omega(\tau_c\omega + \tau_l\omega) \qquad \text{Use Eqs. (3.72),(3.73)} \\ =& (1 - 2\alpha(\tau_c + \tau_l) - \alpha^2(\tau_c - \tau_l)^2)\omega^2 + 4\alpha^2. \end{aligned} \tag{3.140}$$

Therefore the string stability Eq. (3.139) can be guaranteed via the lower bound polynomial $f_l(\omega)$

$$\begin{aligned} f(\omega, \tau_c) &= |j\omega + \alpha(e^{-s\tau_l} + e^{-j\omega\tau_c})|^2 - \alpha^2 \\ &\geq f_l(\omega) \\ &= (1 - 2\alpha(\tau_c + \tau_l) - \alpha^2(\tau_c - \tau_l)^2)\omega^2 + 4\alpha^2 - \alpha^2 \\ &= (1 - 2\alpha(\tau_c + \tau_l) - \alpha^2(\tau_c - \tau_l)^2)\omega^2 + 3\alpha^2, \end{aligned} \tag{3.141}$$

which requires the coefficient of ω^2 to be positive

$$1 - 2\alpha(\tau_c + \tau_l) - \alpha^2(\tau_c - \tau_l)^2 > 0, \tag{3.142}$$

resulting in Eq. (3.136) of the Lemma. □

Lemma 12. *The CVS, with the standard protocol in Eq.* (3.93) *satisfying the internal stability conditions as in Lemma 3.116, meets the string stability condition in Eq.*(3.25) *on the error- propagation transfer function* $G_i(s)$ *provided the minimum value of* $f(\omega)$ *over the bounded interval* $[0, \omega^*]$ *in Eq.* (3.139) *is positive, i.e.*

$$\min_{\omega \in [0,\omega^*]} f(\omega, \tau_c) > 0, \tag{3.143}$$

where $\omega^* = 4\alpha$.

Proof. The string stability condition $f(\omega) > 0$ in Eq. (3.139) is always satisfied if ω is large, as the condition can be rewritten as

$$\begin{aligned} f(\omega, \tau_c) &= 2\alpha^2 + 2\alpha^2 \cos((\tau_c - \tau_l)\omega) + \omega^2 \\ &\quad - 2\alpha\omega(\sin(\tau_l\omega) + \sin(\tau_c\omega)) \\ &\geq 2\alpha^2 - 2\alpha^2 + \omega^2 - 4\alpha\omega \\ &= \omega^2 - 4\alpha\omega > 0, \end{aligned} \tag{3.144}$$

which is equivalent to $\omega > 4\alpha = \omega^*$. □

3) Steady-state error

The following lemma derives the conditions for estimating the steady-state error.

Lemma 13. *Constant steady-state spacing between vehicles for a constant-velocity, desired trajectory is maintained with the protocol in Eq.*(3.105) *satisfying the internal stability conditions in Lemma 10. Specifically, with desired trajectory* $x_0(t) = Vt$ *and*

$$x_0(s) = V/s^2. \tag{3.145}$$

The relative spacing error δ_i is zero,

$$\lim_{t\to 0}\delta_i(t) = 0, \tag{3.146}$$

for all follower vehicles, i.e. $i \geq 2$.

Proof. Substituting Eqs. (3.111) (3.112) into Eq. (3.84), the error transfer function $G_0(s)$ is given as

$$G_0(s) = \frac{1 - T_1(s)}{s} = \frac{1}{s + \alpha e^{-s\tau_l}}. \tag{3.147}$$

From Eqs. (3.64), the second error transfer function is given as

$$G_1(s) = \frac{T_1(s) - T_2(s)}{1 - T_1(s)}. \tag{3.148}$$

where substituting Eqs. (3.109)-(3.113) into Eq. (3.85) yields

$$\begin{aligned}
&T_1(s) - T_2(s) \\
&= \frac{(D(s) - G_f(s))G_{c0}(s) - G_c(s)D_0(s)}{D(s)D_0(s)} \\
&= \frac{(s + \alpha e^{-s\tau_c})\alpha e^{-s\tau_l} - \alpha e^{-s\tau_c}(s + \alpha e^{-s\tau_l})}{(s + \alpha e^{-s\tau_l})(s + \alpha(e^{-s\tau_l} + e^{-s\tau_c}))} \\
&= \frac{\alpha s(e^{-s\tau_l} - e^{-s\tau_c})}{(s + \alpha e^{-s\tau_l})(s + \alpha(e^{-s\tau_l} + e^{-s\tau_c}))}.
\end{aligned} \tag{3.149}$$

From Eq. (3.147),

$$1 - T_1(s) = sG_0(s) = \frac{s}{s + \alpha e^{-s\tau_l}}. \tag{3.150}$$

Substituting Eq. (3.150) (3.149) into Eq. (3.148) results in

$$G_1(s) = \frac{\alpha(e^{-s\tau_l} - e^{-s\tau_c})}{(s + \alpha(e^{-s\tau_l} + e^{-s\tau_c}))}. \tag{3.151}$$

From Eqs. (3.137)(3.147)(3.151), the limit as s tends to 0 is given by

$$\lim_{s\to 0} G_0(s) = \lim_{s\to 0} \frac{1}{s + \alpha e^{-s\tau_l}} = \frac{1}{\alpha}, \tag{3.152}$$

$$\lim_{s\to 0} G_1(s) = \lim_{s\to 0} \frac{\alpha(e^{-s\tau_l} - e^{-s\tau_c})}{(s + \alpha(e^{-s\tau_l} + e^{-s\tau_c}))} = 0, \tag{3.153}$$

$$\lim_{s\to 0} G(s) = \lim_{s\to 0} \frac{\alpha e^{-s\tau_l}}{s + \alpha(e^{-s\tau_l} + e^{-s\tau_c})} = \frac{1}{2}. \tag{3.154}$$

Therefore, substituting Eqs. (3.152)-(3.154) into Eq. (3.82), the steady state spacing error of all follower vehicles $i \geq 2$ is

$$\begin{aligned}\lim_{t\to\infty} \delta_i(t) &= \lim_{s\to 0} s\delta_i(s) \\ &= \lim_{s\to 0} s[G_1(s)] \left(G^{i-2}(s)G_0(s)\right) \frac{V}{s} \\ &= \lim_{s\to 0}[G_1(s)] \left(G^{i-2}(s)G_0(s)\right) V \\ &= 0. \end{aligned} \tag{3.155}$$

since the limit as s tends to zero of $G_1(s)$ is zero and the limits of $G_i(s)$ and $G_0(s)$ are bounded, resulting in the maintaining of constant spacing by all the followers. □

3.3 Results and Discussion

In this section, simulations with typical CVS parameters from literature, are used to illustrate the impact of control parameter selections such as blending gain γ as well as DSR gain β, and to estimate the benefits of using the proposed DSR method.

3.3.1 System description

1) CVS parameter selection

The performance of PLF with DSR (Eq. (3.23)) is evaluated through simulations using the MATLAB/Simulink environment. The simulations include the CVS with one leader and four followers. In the following, the different methods are evaluated for a step change in the target velocity, with the platoon accelerating from static to the target velocity of $V = 20$ m/s. Except for the communication delay τ_c and the blending gain γ, the rest of the parameters are selected as typical CVS values, as discussed below.

(i) Control gain α: Depending on the types of the vehicles, the target settling time for accelerating from $V = 0$ to $V = 20$ m/s varies from $5 - 10$ s for typical automobile cruise control systems on passenger cars [45], to $10 - 30$ s for heavy duty trucks [46]. In this paper the controller gain α is selected as $\alpha = 0.4$ to match the settling time of 10 s.

(ii) Local sensing delay τ_l and DSR delay τ_d: The local sensing delay depends on the update rate of the distance sensors and the processors. Typically the local sensor delay τ_l varies between 0.1 to 0.3 s [47, 48]. In the simulations, the DSR delay τ_d is set to be the same as the local sensing delay, $\tau_d = \tau_l = 0.1$ s. It is selected the same as the update rate of the Bosch Mid Range Radar (MRR) sensor, which is widely used in vehicles with Advanced Driver Assistance Systems (ADAS) systems [49]. The controller also outputs the discrete control signal with the sampling time as $\tau_d = 0.1$ s.

2) Vehicle model

The individual vehicle dynamics is selected as a double integrator model as in recent work, e.g., [10] $\tilde{L}_i(s) = \frac{1}{s^2}$, and according to Eqs. (3.10), (3.11), the feedback controllers $C_{ff,i}(s)$ and $C_{fb,i}(s)$ are selected as

$$C_{ff,i}(s) = s + 10\alpha, \qquad C_{fb,i}(s) = 10\alpha\ s, \tag{3.156}$$

with $k_1 = 10\alpha = 4$ for the feedforward controller $C_{ff,i}(s)$ to have a higher bandwidth (by a decade) compared to the velocity dynamics. Note that the choice of $k_1 = 4$ also ensures that the canceled pole $s = -4$ is stable [50]. For real-time simulations, the controller does not have direct access to the derivative of the relative spacing through local sensing. Therefore, a low-pass filter with cutoff frequency $\omega_f = 40\alpha = 16$ rad/s is added to prevent the amplification of the high frequency noise during computations of the derivative[51], which results in a modified feedforward controller $C_{ff,i}(s) = \frac{\omega_f}{(s+\omega_f)}s + 10\alpha$.

3) Metrics

To evaluate the convergence speed to steady-state, the settling time T_s of the CVS is defined as the minimum time required for the states of all the vehicles to settle and remain within 2% of the final steady-state values. Besides, in order to evaluate the ability to maintain constant-spacing during the transient process, the maximum deviation δ_m of the CVS is defined by

$$\delta_m = \max_{t \geq 0} \|X(t) - x_0(t)\mathbf{1}_n\|_\infty, \tag{3.157}$$

where the vector $\mathbf{1}_n = [1, \ldots, 1] \in \mathbb{R}^n$. The step response is selected as the source signal for computing the settling time and comparing the spacing error response.

3.3.2 Impact of varying the blending gain γ

The impact of increasing the blending gain γ, i.e., more reliance on local sensing than the centralized command, on internal and string stability as well as performance are investigated to guide the selection of the blending gain γ.

1) Internal stability

Selecting larger values for the blending gain γ reduces the reliance on the centralized command, and therefore, increases the acceptable communication delay τ_c for internal stability. For example, the acceptable communication delay for internal stability is given as $\tau_c < \pi/(2\alpha) \approx 3.92$ s according to Lemma. 2. However, increasing the blending gain γ such that $\gamma > \frac{1}{1+\cos(\tau_l \alpha)} \approx 0.50$, ensures internal stability regardless of the communication delay τ_c, according to Lemma 3, and indicated in Fig. 3.4.

2) String stability

Selecting larger values for the blended gain γ, i.e., smaller amount of centralized command reduces the acceptable communication delay τ_c for string stability, as shown in Fig. 3.4. This is expected since sufficient centralized command is needed to make constant-spacing PLF string stable, and pure decentralized DSR ($\gamma = 1$) cannot maintain string stability, according to Remark 10.

Given a target acceptable communication delay τ_c^* for string stability, the candidate set of all the available blending gain S_γ can be solved numerically via the following expression,

according to Lemma 5,

$$S_\gamma = \{\gamma \in [0,1] \mid \min_{\omega\in(0,\omega^*]} f(\omega,\gamma,\tau_c^*) > 0\},$$
$$\omega^* = \alpha\left(1+2\sqrt{650.3}\right) = 20.80 \text{ rad/s}, \tag{3.158}$$

with $f(\omega,\gamma,\tau_c)$ defined in Eq. (3.70). The range of the candidate set S_γ reduces as the communication delay τ_c increases, as indicated in the red shaded area in Fig. 3.4.

3) Selection of blending gain

The blending gain γ is selected so that the acceptable communication delay τ_c^* for string stability is the same for PLF, with and without DSR. For PLF without DSR, the acceptable communication delay τ_c^* for string stability can be solved numerically via the following expression, according to Lemma 12,

$$\tau_c^* = \sup_{\tau_c>0} \min_{\omega\in(0,\omega^*]} f(\omega,\tau_c) > 0, \quad \omega^* = 4\alpha = 1.6 \text{ rad/s}, \tag{3.159}$$

with $f(\omega,\tau_c)$ in Eq. (3.139). From Eq. (3.159), the acceptable communication delay for string stability is solved as $\tau_c^* = 2.68$ s. To achieve the same acceptable communication delay for PLF with DSR, the candidate set S_γ can be solved as $0 \le \gamma \le 0.83$ numerically by substituting $\tau_c^* = 2.68$ s into Eq. (3.158). The largest value of $\gamma = 0.83$ is selected for PLF with DSR since this selection reduces the steady-state error when the communication is lost, according to Lemma 9. Lastly, choosing $\gamma = 0.83$ guarantees string stability when the communication is lost, according to Lemma 8,

$$\gamma = 0.83 < \gamma^* = \frac{-\alpha\tau_l + \sqrt{\alpha^2\tau_l^2 + \alpha\tau_d + 1}}{\alpha\tau_d + 1} = 0.94, \tag{3.160}$$

where the upper bound $\gamma^* = 0.94$ is computed from Eq. (3.96).

3.3.3 Robustness to communication delay

Simulations are used to demonstrate that the use of DSR improves CVS performance, with robustness to large communication delays. Moreover, it is shown that the spacing error is reduced substantially by use of DSR when communication is lost.

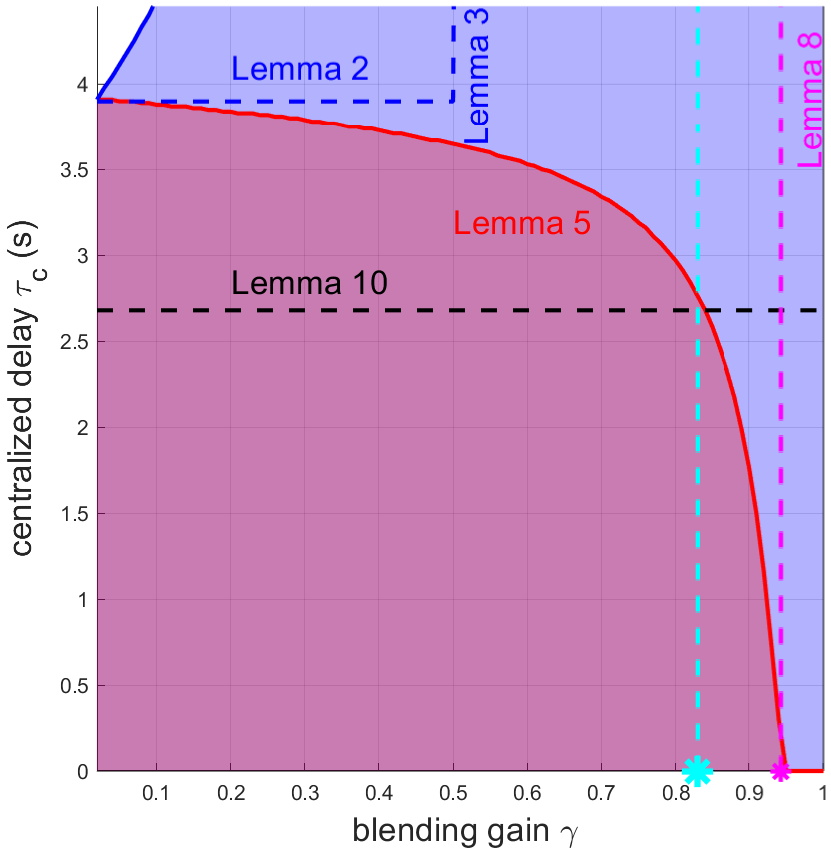

Figure 3.4: For comparative evaluations, the blending gain γ for PLF with DSR is selected (vertical cyan dashed line) to achieve the same acceptable communication delay τ_c^* as PLF without DSR (horizontal black dashed line) for string stability found from Eq. (3.159), Lemma 12. The vertical purple dashed line marks the maximum acceptable blending gain γ^* from Eq. (3.160), Lemma 8. The string-stable region (the red shaded area) is computed from Eq. (3.158), Lemma 5. The internally-stable region (the blue shaded area) is found numerically by checking for finite settling time of the step response using MATLAB and can be estimated by Lemmas 2 and 3.

1) Typical communication delay case

The proposed PLF with DSR enables both string stability and constant spacing, similar to the PLF without DSR in the presence of typical communication delays. In particular, with a communication delay of $\tau_c = 0.5$ s [17, 10], the maximum deviation δ_m for the PLF with DSR during the transition is 2.37 m, compared to the maximum deviation $\delta_m = 2.77$ m for the PLF without DSR. The maximum spacing errors during transients in both cases are less than 10 m, which is typically acceptable for CSP CVS systems in literature, e.g., [18]. The settling time T_s for both methods are 9.4s, which achieves the target settling time of 10s. Therefore, both, PLF with DSR and PLF without DSR have acceptable performance under typical communication delays.

2) Large communication delay case

The PLF with DSR has more robust performance to large communication delays, i.e., maintains constant steady-state spacing with similar convergence rate and the maximum transient deviation as the typical-communication delay case. In contrast, the PLF without DSR results in substantial increase in the settling time T_s and the maximum deviation δ_m as the communication delay τ_c increases. The settling time T_s for the PLF with DSR approach changes from 9.4 s ($\tau_c = 0.1$ s) to 10.7 s ($\tau_c = 2.5$ s), as seen in Fig. 3.6(a). In contrast, for the PLF without DSR, the settling time T_s changes from 9.4 s ($\tau_c = 0.1$ s) to 35.5 s ($\tau_c = 2.5$ s), as seen in Fig. 3.6(b). Therefore, the variation of the settling time with DSR (1.3 s) is about 95% less than the variation of the settling time without DSR (26.1 s). Furthermore, the maximum transient deviation δ_m of the PLF with DSR is 4.69 m, which is 74.05% less than the maximum transient deviation $\delta_m = 18.11$ m of the PLF without DSR, as seen in Fig. 3.6(a), (b). Therefore, the tracking performance of the proposed PLF with DSR approach is more robust to large centralized delay compared with the PLF without DSR.

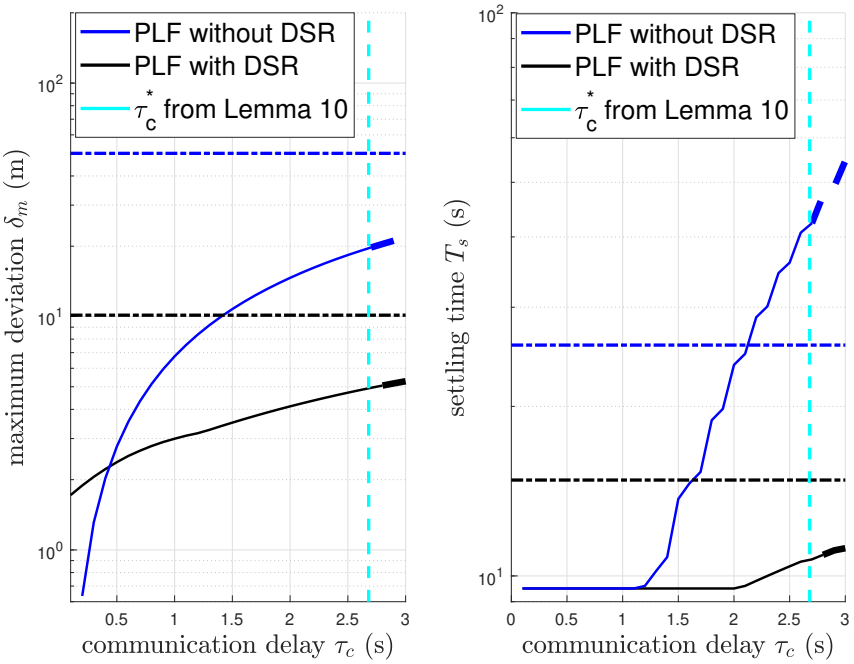

Figure 3.5: Comparison of maximum deviation δ_m (left plots) and settling time T_s (right plots) for PLF with DSR (black lines) and PLF without DSR (blue lines) as communication delay increases till string instability (vertical cyan lines). Horizontal dashed lines represent communication loss case. Left: With communication loss, PLF with DSR has less steady state spacing error δ_m (horizontal black line) than PLF without DSR (horizontal blue line). Right: Settling time T_s variation with communication delay is substantially smaller with DSR compared to the case without DSR.

3) Communication loss case

When communication is lost, the proposed PF with DSR has better tracking performance compared to PF without DSR. The maximum deviation δ_m with DSR approach is 10.22 m, which is an increase of about 0.5 s headway time, as seen in Fig. 3.6(c). This numerically obtained value of 10.22 m is also close to the predicted steady-state error from Eq. (3.100)

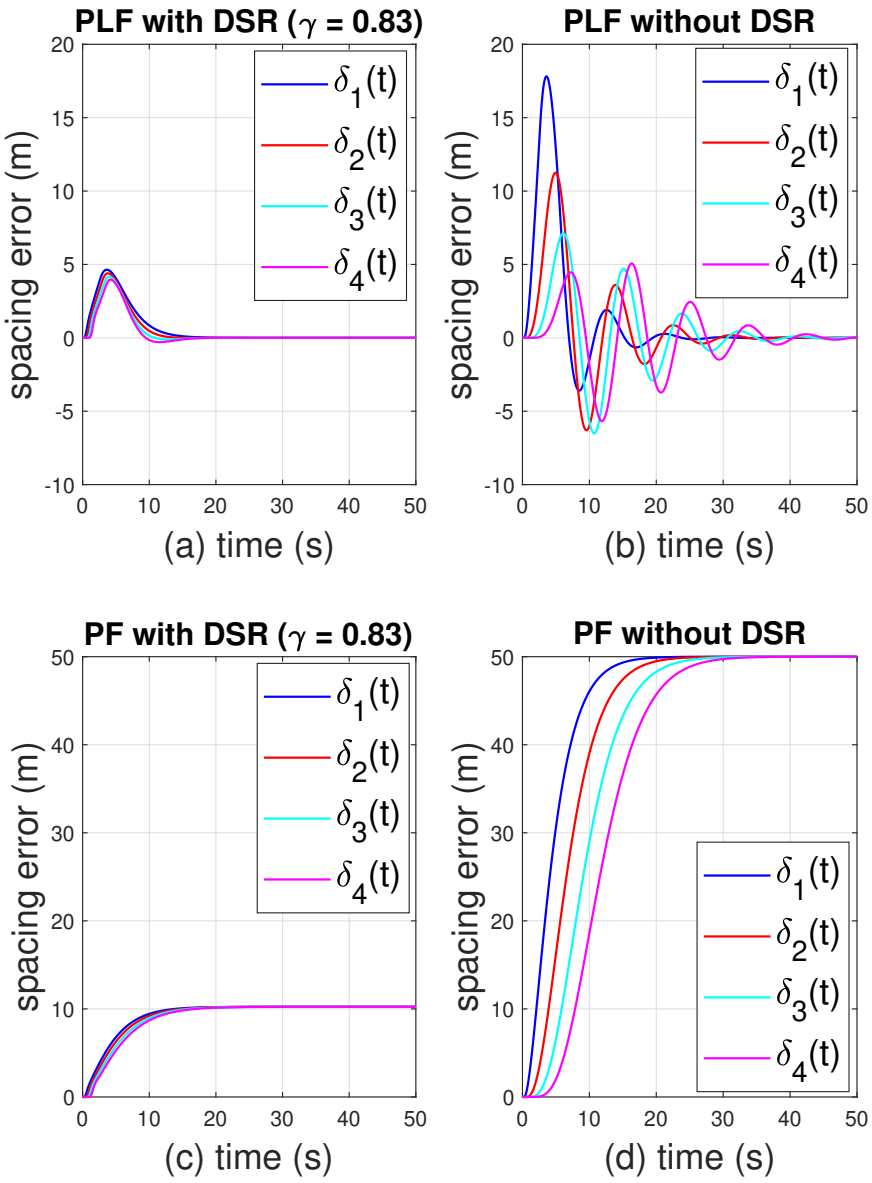

Figure 3.6: DSR (left plots) leads to more cohesive tracking performance and smaller spacing errors δ_i when compared to the case without DSR (right plots) under large communication delays $\tau_c = 2.5$ s (top plots) or communication loss (bottom plots).

in Lemma 9 given by

$$\lim_{s\to 0} s\delta_i(s) = \frac{V}{\alpha}(\frac{1}{\gamma} - 1) = \frac{20}{0.4}\left(\frac{1}{0.83} - 1\right) = 10.24.$$

In contrast, with communication loss, the maximum deviation δ_m is 50 m without DSR, which is about 2.5 s headway time, as seen in Fig. 3.6(d). The speed-dependent spacing error with DSR (10.22m) is about 80% less than the speed-dependent spacing error without DSR (50 m). Thus, the PF with DSR is able to maintain small inter-vehicle spacing in the platoon even without communication.

3.3.4 Impact of varying DSR gain β

The impact of varying the DSR gain β on the CVS performance is shown in Fig. 3.7 for different communication delay conditions. Overall, the performance of the proposed DSR approach can be improved further by increasing the DSR gain, i.e., when $\beta > 1$. However, the CVS can also become string unstable with larger DSR gain β, as seen in Fig. 3.7. In particular, when the communication delay is small ($\tau_c = 0.1$ s), the maximum deviation δ_m can be further reduced to 0.80 m (with $\beta = 1.2$) from $\delta_m = 0.91$ m when $\beta = 1$. However, the settling time T_s increases as DSR gain β increases beyond one. When the communication delay is large ($\tau_c = 2.5$ s), the maximum deviation δ_m can be further reduced to 3.51 m ($\beta = 1.2$) from $\delta_m = 4.15$ m ($\beta = 1$) and the settling time T_s can be further reduced as well to 10.67 s ($\beta = 1.2$) from with $T_s = 10.87$ s ($\beta = 1$). The results are similar when communication is lost. The maximum deviation δ_m can be further reduced to 8.53 m ($\beta = 1.2$) from $\delta_m = 10.24$ m ($\beta = 1$). The settling time T_s can be further reduced to 14.37 s, compared with $T_s = 15.21$ s ($\beta = 1$). In all cases, the maximum deviation δ_m improves (by upto 20%) with increasing DSR gain β, but the improvement is limited by the advent of string instability as shown in Fig. 3.7.

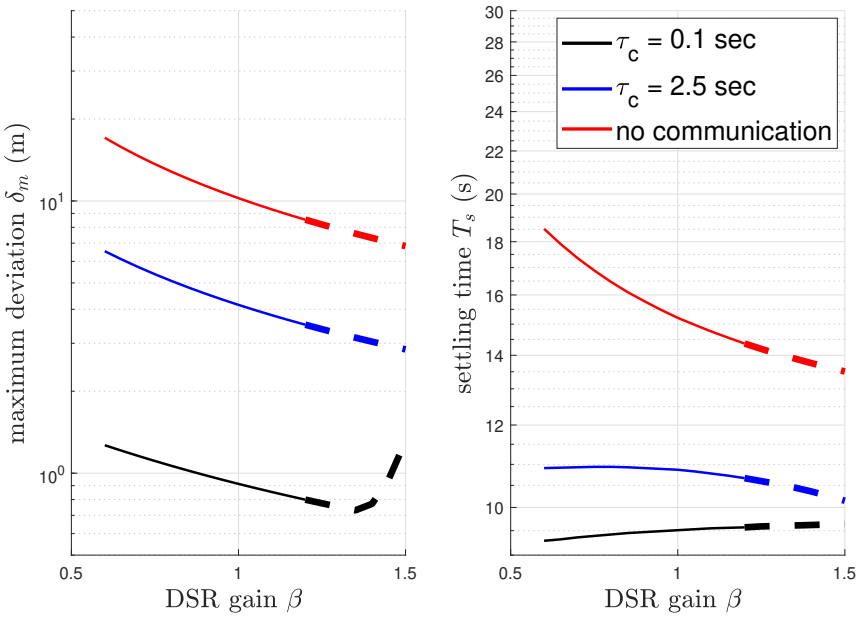

Figure 3.7: Impact of the DSR gain β on the maximum deviation δ_m (left plots) and settling time T_s (right plots) under small communication delay (black lines), large communication delay (blue lines) and communication loss (red lines). Dashed line indicates when the CVS is string unstable. Increasing the DSR gain β can improve the performance, but can also make the system string unstable.

3.4 Conclusion

This work addressed the constant-spacing platooning problem in the presence of large communication delays and loss of communication. Centralized control from the lead vehicle was blended with a new delayed-self-reinforcement (DSR) approach that mimics the ideal centralized control in a decentralized manner. As a result, the DSR-based approach improved performance in the presence of large communication delays as well as communication loss. The article developed conditions for maintaining internal stability, string stability and constant spacing without steady-state error for the proposed blended DSR approach. Simulation

results showed that the tracking performance of predecessor-leader following was more robust to large communication delays and loss with the proposed DSR approach when compared to the case without DSR.

Chapter 4

MC2 AN EFFICIENT AV NETWORK AT SIGNALIZED INTERSECTION WITH PARTIAL CONNECTIVITY USING BLENDED DSR.

Capacity at traffic intersections can be increased if all autonomous vehicles (AVs) have traffic-light-to-vehicle-communication (TLVC), leading to better inter-vehicle spacing control and reduction of time needed to start and move through an intersection. However, with a mix of autonomous vehicles, some vehicles with TLVC and some without TLVC, the capacity improvements of TLVC are lost and safety can be compromised with potential collisions. Such scenarios can be expected during the transition to fully connected autonomous vehicles (CAVs). This chapter shows that the increased capacity of CAVs with TLVC at traffic lights can be recovered safely for mixed AVs network by using delayed self reinforcement (DSR) (**MC2**), and is based on a publication in IEEE 8th Indian Control Conference (ICC 2022) [2].

The advantage of using DSR, where each autonomous vehicles augment its action using delayed versions of past actions, is that it can keep the spacing errors small (i.e., maintain cohesion) even if centralized communication is not available. Therefore, the use of DSR maintains the capacity of traffic intersections even for mixed AVs network, where some vehicles do not have access to the TLVC. Simulation results show the improvement of capacity and safety with the use of DSR when compared to the case without DSR. In particular, DSR improves the traffic capacity by increasing the traffic flow speed by 38% when TLVC is not available. Furthermore, DSR improves safety by reducing the variation in maximum spacing error by 96% under different mixed-connectivity scenarios at the intersection, and thereby, removes the potential for collision seen in the case without DSR.

4.1 Problem Formulation

This section introduces the dynamics used to model each vehicle and presents the performance limits of velocity cohesion and constant-spacing control of a mixed AVs network during velocity transitions. Lastly, the problem statement for the article is stated.

4.1.1 Vehicle model dynamics

The dynamics of each i^{th} vehicle in the network is represented as

$$\begin{aligned}
\hat{x}_i^{(1)}(t) &= \dot{\hat{x}}_i(t) = \hat{v}_i(t) \\
\hat{v}_i^{(1)}(t) &= \dot{\hat{v}}_i(t) = \hat{a}_i(t) \\
\hat{a}_i^{(1)}(t) &= \dot{\hat{a}}_i(t) = f_i\left(\hat{v}_i(t), \hat{a}_i(t)\right) + g_i\left(\hat{v}_i(t)\right)\hat{u}_i(t),
\end{aligned} \tag{4.1}$$

where $\hat{x}_i$, $\hat{v}_i$ and $\hat{a}_i$ are the position, velocity and acceleration of the i^{th} vehicle respectively at time t, the bracketed superscript represents the order of derivative in time. The third equation in Eq. (4.1) with nonlinear functions $f_i(\boldsymbol{.},\boldsymbol{.})$ and $g_i(\boldsymbol{.})$, representing the vehicle dynamics, which can be different for each vehicle, is simplified using feedback linearization (see [52]) with engine input $\hat{u}_i$,

$$\hat{u}_i(t) = g\left(\hat{v}_i(t)\right)^{-1}\left(u_i(t) - f\left(\hat{v}_i(t), \hat{a}_i(t)\right)\right) \tag{4.2}$$

resulting in the following dynamics in the standard output tracking form

$$\dot{\hat{a}}_i(t) = \hat{x}_i^{(r)}(t) = u_i(t), \tag{4.3}$$

where $r = 3$ is the relative degree of the vehicle dynamics, and the control input u_i in Eq. (4.3) can be chosen for desired i^{th} vehicle response. It is assumed that the relative degree for all the vehicles ($i \in \{1, 2, \ldots, N\}$) is the same with $N \geq 1$.

4.1.2 Mixed AVs network dynamics

A constant-spacing policy, with desired inter-vehicle spacing d_0, is implemented as a tracking control problem for a predecessor-follower (PF) network of N AVs, each with dynamics

as described in Section 4.1.1. The network-based update for each vehicle depends on the information available to it, and is different for the non-connected and connected AVs. Each i^{th} vehicle in the network is assumed to have odometer information $\hat{v}_i$ and $\hat{a}_i$ and relative-state information, d_i and its higher derivatives $\dot{d}_i$ and $\ddot{d}_i$, w.r.t. its predecessor vehicle $i-1$ for $1 \leq i \leq N$

$$d_i(t) = \hat{x}_{i-1}(t) - \hat{x}_i(t), \tag{4.4}$$

where $\hat{x}_0(t)$ is the desired position for the leader vehicle $i = 1$. In addition to the above information, CAVs have traffic signal information using TLVC. Let $\mathcal{N}_c$ be the set of CAVs in the network with cardinal number $1 \leq n(\mathcal{N}_c) \leq N$, i.e. every vehicle $j \in \mathcal{N}_c$ has traffic signal time and phase information using TLVC, which can be used to adjust their velocities to reach traffic intersection during green signal phase.

TLVC update

The TLVC information to the i^{th} vehicle is represented as a virtual source of the desired set speed V for passing the intersection such that

$$\hat{x}_0(t) = Vt, \tag{4.5}$$

where $\hat{x}_0(t)$ is the desired position for the leader vehicle at time t. The desired position for the followers can be computed according to the target inter-vehicle spacing d_0 and respective index i

$$\hat{x}_{d,i}(t) = \hat{x}_0(t) - (i-1)d_0, \qquad i \geq 2. \tag{4.6}$$

For more extended applications, the desired velocity $V(t)$ can be computed using TLVC through approaches such as Predictive Cruise Control (PCC) in [25].

To derive the update law for the mixed AVs network, the state of each i^{th} vehicle is represented as the deviation x_i from its desired global position $\hat{x}_i$, where the deviated position x_i is defined as

$$x_i = \hat{x}_i + (i-1)d_0, \tag{4.7}$$

Combining Eq. (4.6) and (4.7) yields

$$\hat{x}_i - \hat{x}_{i-1} + d_0 = x_i - x_{i-1}, \tag{4.8}$$

$$\hat{x}_i - \hat{x}_{d,i} = x_i - \hat{x}_0. \tag{4.9}$$

The position tracking of the vehicles $\hat{x}_i,\ (1 \leq i \leq N)$ in the network can be further simplified as first-order dynamics by stable pole-zero cancellation using the following TLVC-based update law $\dot{a}_{i,T}$ as the control input u_i in Eq. (4.3),

$$\begin{aligned}\dot{a}_i(t) = &-\alpha(\alpha_0(\hat{x}_i(t) - \hat{x}_{d,i}(t)) + \alpha_1(\hat{v}_i(t) - \hat{v}_{d,i}(t)) \\ &+ (\hat{a}_i(t) - \hat{a}_{d,i}(t))) - \alpha_1\hat{a}_i(t) - \alpha_0\hat{v}_i(t) \\ = &-\alpha(\alpha_0(x_i(t) - \hat{x}_0(t)) + \alpha_1(v_i(t) - \hat{v}_0(t)) \\ &+ (a_i(t) - \hat{a}_0(t))) - \alpha_1 a_i(t) - \alpha_0 v_i(t) = \dot{a}_{i,T},\end{aligned} \tag{4.10}$$

where the second equality is obtained using Eq. (4.9). This control results in a first-order vehicle response, as shown next. Consider the Laplace transform of Eq. (4.10)

$$\begin{aligned}s^3 x_i(s) = &-\alpha((\alpha_0 + \alpha_1 s + s^2)(x_i(s) - \hat{x}_0(s))) \\ &- (\alpha_1 s^2 + \alpha_0 s)x_i(s),\end{aligned} \tag{4.11}$$

which can be rearranged as

$$(s^2 + \alpha_1 s + \alpha_0)(s + \alpha)x_i(s) = \alpha(s^2 + \alpha_1 s + \alpha_0)\hat{x}_0(s),$$

leading to the following first-order transfer function between the deviated position x_i and the desired trajectory $\hat{x}_0$

$$\frac{x_i(s)}{\hat{x}_0(s)} = \frac{\alpha(s^2 + \alpha_1 s + \alpha_0)}{(s + \alpha)(s^2 + \alpha_1 s + \alpha_0)} = \frac{\alpha}{s + \alpha}. \tag{4.12}$$

Remark 11 (Stable pole-zero cancellation)**.** *To avoid unstable internal states, the cancelled polynomial* $\mathcal{P}(s)$ *in Eq.* (4.12)

$$\mathcal{P}(s) = s^2 + \alpha_1 s + \alpha_0, \tag{4.13}$$

should have stable roots ($p > 0$). Therefore, from the Routh-Hurwitz criterion, the feedback control gains need to satisfy

$$\alpha_1 > 0, \qquad \alpha_0 > 0. \tag{4.14}$$

Remark 12 (Limit on response speed α)**.** *The location of the root α of the transfer function Eq.* (4.12) *can be chosen to improve the response speed of each vehicle. However, the selection of the control gain α is bounded by the vehicle's time constant from above and the system stability limit from below, as*

$$0 < \alpha \leq 4\tau_e, \tag{4.15}$$

where τ_e is the engine time-constant (see [53]).

Local sensing update

Each vehicle can also track its position by using the locally sensed information d_i in Eq. (4.4), and odometer information of velocity and acceleration $\hat{v}_i$ and $\hat{a}_i$. Combining with Eq. (4.4), (4.8), the local-sensing-based control update $\dot{a}_{i,l}$ for non-connected vehicles are given as

$$\begin{aligned}
\dot{a}_i(t) &= \dot{a}_{i,l}(t) \\
&= -\alpha(\alpha_0(-d_i(t) + d_0) - \alpha_1 \dot{d}_i(t) - \ddot{d}_i(t)) \\
&\quad - \alpha_1 \hat{a}_i(t) - \alpha_0 \hat{v}_i(t) \\
&= -\alpha(\alpha_0(\hat{x}_i(t) - \hat{x}_{i-1}(t) + d_0) \\
&\quad + \alpha_1(\hat{v}_i(t) - \hat{v}_{i-1}(t)) + (\hat{a}_i(t) - \hat{a}_{i-1}(t))) \\
&\quad - \alpha_1 \hat{a}_i(t) - \alpha_0 \hat{v}_i(t) \\
&= -\alpha\left[\alpha_0(x_i(t) - x_{i-1}(t)) + \alpha_1(v_i(t) - v_{i-1}(t))\right. \\
&\quad \left. + (a_i(t) - a_{i-1}(t)\right] - \alpha_1 a_i(t) - \alpha_0 v_i(t).
\end{aligned} \tag{4.16}$$

Similar to Eq. (4.12), the deviated position of the i^{th} vehicle x_i tracks its predecessor x_{i-1} in a first-order manner.

$$\frac{x_i(s)}{x_{i-1}(s)} = \frac{\alpha}{s + \alpha} \tag{4.17}$$

if the feedback gains α_1, α_0 satisfy the conditions Eq. (4.14).

Updates with and without TLVC

The updates for each vehicle, both non-connected and connected, are stated below.

1. If i is a non-connected vehicle ($i \notin \mathcal{N}_c$), then its update only uses the local sensing information as in Eq. (4.16)

$$\dot{a}_i(t) = \dot{a}_{i,l}(t), \tag{4.18}$$

which results in first-order tracking to the preceding vehicles deviated position x_{i-1} as

$$x_i(s) = \frac{\alpha}{s+\alpha} x_{i-1}(s). \tag{4.19}$$

2. If i is a connected vehicle with TLVC information ($i \in \mathcal{N}_c$), then its update is a blending of the local update $\dot{a}_{i,l}$ from Eq. (4.16) and TLVC update $\dot{a}_{i,T}$ from Eq. (4.10)

$$\dot{a}_i(t) = \dot{a}_{i,l}(t) + \dot{a}_{i,T}(t) + \alpha_1 a_i(t) + \alpha_0 v_i(t). \tag{4.20}$$

Substituting $\dot{a}_{i,T}$ from Eq. (4.10) and $\dot{a}_{i,l}$ Eq. (4.16) into Eq. (4.20), taking Laplace transform yields

$$\begin{aligned} s^3 x_i(s) = &- \alpha((\alpha_0 + \alpha_1 s + s^2)(x_i(s) - x_{i-1}(s))) \\ &- (\alpha_1 s^2 + \alpha_0 s) x_i \\ &- \alpha((\alpha_0 + \alpha_1 s + s^2)(x_i(s) - \hat{x}_0(s))), \end{aligned} \tag{4.21}$$

which can be rearranged as

$$\begin{aligned} &(s^2 + \alpha_1 s + \alpha_0)(s + 2\alpha) x_i(s) \\ &\quad = \alpha(s^2 + \alpha_1 s + \alpha_0)(x_{i-1}(s) + \hat{x}_0), \end{aligned} \tag{4.22}$$

leading to the following first-order transfer function between the deviated position x_i and (i) the desired trajectory $\hat{x}_0(s)$ and (ii) the deviated predecessor trajectory $x_{i-1}(s)$

$$x_i(s) = \frac{\alpha}{s+2\alpha}(x_{i-1}(s) + \hat{x}_0(s)). \tag{4.23}$$

In the following, it is assumed that, before the desired velocity v_d changes for the vehicle network, say from $v_{d,o}$ to $v_{d,f}$ e.g., due to a change in the traffic light, all the vehicles have the same initial velocity $v_{d,o}$ and zero initial inter-vehicle spacing error δ_i defined by

$$\delta_i = \hat{x}_{i-1} - \hat{x}_i - d_0. \tag{4.24}$$

4.1.3 Spacing control and traffic speed metrics

The spacing control is evaluated using maximum of normalized absolute inter-vehicle spacing error, averaged over the N vehicles in the network, as,

$$\Delta_{d,max} = \frac{1}{N} \sum_{i=1}^{N} \left(\max_{t \in [0, T_d]} \frac{|d_i(t) - d_0|}{d_0} \right), \tag{4.25}$$

where T_d is the time duration of the transition, and d_0 is the desired spacing. Besides, the traffic flow speed is evaluated as the time for passing through the intersection T_p for all N vehicles of the network,

$$T_p = \arg\min_{t \geq 0} \{\hat{x}_i(t) > \hat{x}_0(0), \forall i = 1, \ldots, N\}. \tag{4.26}$$

4.1.4 Problem statement

The tracking performance of a non-connected autonomous vehicle (AV) with the standard predecessor-following (PF) protocol in Eq. (4.19), can differ from the tracking performance of a connected AV (CAV) with the predecessor-leader following (PLF) protocol using centralized TLVC information in Eq. (4.23). This difference in tracking performance between AV and CAV can lead to large tracking error $\Delta_{d,max}$ (defined in Eq. (4.25)) and even potential collisions.

The research problem is to safely reduce (a) the time T_p in Eq. (4.26) for a set of vehicles to pass through the intersection and (b) the maximum tracking error $\Delta_{d,max}$ in Eq. (4.25) of the mixed AVs network when compared to the standard PLF protocol in stop-and-go scenarios at traffic intersections.

4.2 Proposed Approach

This section introduces the blended delayed-self-reinforcement (DSR) approach to achieve good tracking performance for AVs, with or without the TLVC information.

4.2.1 Decentralized command with DSR

The DSR approach approximates the ideal centralized tracking in a decentralized manner. Consider all vehicles $\hat{x}_i$ are able to track the target position $\hat{x}_{d,i}$ with the desired time constant $1/\alpha$ using feedback linearization from the last section. From Eq. (4.9), the deviated position x_i satisfies

$$\dot{x}_i = -\alpha(x_i(t) - \hat{x}_0(t)). \tag{4.27}$$

The position tracking for all AVs can be written as

$$\dot{X}(t) = -\alpha(X(t) - \mathbf{1}\hat{x}_0) = u_c(t), \tag{4.28}$$

where $X = [x_1, \ldots, x_N]$, and $\mathbf{1}$ is the $n \times 1$ vector of ones. Multiplying Eq. (4.28) by βK, where β is the DSR gain and K is the pinned Laplacian of the vehicle network without the virtual source, we get,

$$\beta K\dot{X}(t) = -\alpha\beta K(X(t) - \alpha\mathbf{1}\hat{x}_0). \tag{4.29}$$

Define the source connectivity vector B such that $K^{-1}B = \mathbf{1}$ ($B_i = 1$ indicates the i^{th} agent is connected to the TLVC information). Adding $(I - \beta K)\dot{X}$ to both sides of Eq. (4.29) yields

$$\begin{aligned} \dot{X}(t) &= (I - \beta K)\dot{X} - \alpha\beta K(X(t) - \alpha\mathbf{1}\hat{x}_0) && (4.30)\\ &\approx (I - \beta K)\frac{X(t) - X(t - \tau_d)}{\tau_d} - \alpha\beta KX(t) - \alpha B\hat{x}_0 \\ &= u_{dsr}(t), && (4.31) \end{aligned}$$

where τ_d is the DSR delay. The resulting decentralized DSR command $u_{dsr}(t)$ only uses delayed local sensing information to approximate the derivative on the right hand side of Eq. (4.30) to enhance the tracking performance.

4.2.2 Blending with centralized TLVC command

The proposed blended DSR method utilizes both the DSR command $u_{dsr}(t)$ from Eq. (4.31) and the centralized command $u_c(t)$ from Eq. (4.28) [54].

1. if i is a connected vehicle ($i \in \mathcal{N}_c$)

$$\dot{X}(t) = \gamma u_{dsr}(t) + (1-\gamma)u_c(t), \tag{4.32}$$

   where $\gamma \in [0,1]$ is the blending gain. In the following section the DSR gain β is selected as $\beta = 1$.

2. if i is a non-connected vehicle ($i \notin \mathcal{N}_c$)

$$\dot{X}(t) = \gamma u_{dsr}(t). \tag{4.33}$$

The blended DSR control law Eq. (4.32), (4.33) needs to guarantee the following control properties

Internal stability

The vehicle network is internally stable if the real parts of the poles of all deviated position transfer function

$$T_i(s) = \frac{x_i(s)}{\hat{x}_0(s)} \tag{4.34}$$

are negative. With the DSR gain $\beta = 1$, the internal stability is guaranteed [54] if

$$\frac{1}{1+\cos(\tau_l \alpha)} < \gamma \leq 1, \tag{4.35}$$

where τ_l is the local sensing delay. Therefore, for sufficiently small local sensing delay (e.g., $\tau_l = 0$), internal stability is guaranteed with $\gamma \in (0.5, 1]$.

String stability

The vehicle network is string stable if the magnitude of the spacing error does not amplify along a chain of vehicles, i.e.,

$$|G_i(j\omega)| = \left| \frac{x_{i-1}(s) - x_i(s)}{x_{i-2}(s) - x_{i-1}(s)} \right|_{s=j\omega} < 1, \quad \forall \omega > 0, \ i \geq 2.$$

For platoons with all AVs connected to TLVC information, string stability is guaranteed if the blending gain γ satisfies [54],

$$\gamma(1-\gamma)\left(\frac{\tau_c}{1/\alpha} - \frac{\tau_l}{1/\alpha}\right)^2 + 2\left(\gamma\frac{\tau_l}{1/\alpha} + (1-\gamma)\frac{\tau_c}{1/\alpha}\right) + \gamma^2\left(\frac{\tau_d}{1/\alpha}\right) < 1 - \gamma^2, \tag{4.36}$$

where τ_c is the TLVC communication delay. For negligible communication delay (e.g., $\tau_c = 0$), the string stability condition in Eq. (4.36) simplifies as

$$\gamma^2\left(\frac{\tau_d}{1/\alpha}\right) < 1 - \gamma^2 \quad \text{or} \quad \gamma < \sqrt{\frac{1}{1+\alpha\tau_d}}. \tag{4.37}$$

For platoons with all decentralized AVs that are not connected to TLVC information, string stability is guaranteed if the blending gain γ satisfies [54]

$$\gamma < \gamma^* = \frac{-\alpha\tau_l + \sqrt{\alpha^2\tau_l^2 + \alpha\tau_d + 1}}{\alpha\tau_d + 1}. \tag{4.38}$$

Again, for negligible local sensing delay τ_l and communication delay τ_c, Eq. (4.38) simplifies to

$$\gamma < \gamma^* = \sqrt{\frac{1}{\alpha\tau_d + 1}}, \tag{4.39}$$

which is the same condition in Eq. (4.37). Thus, the same condition in Eq. (4.39) guarantees string stability for (i) a fully-connected network or (ii) a fully-decentralized networks.

Steady-state error

The vehicle network achieves zero steady-state error for a step change V in velocity ($v_0(s) = V/s$) if

$$\lim_{t\to\infty} x_i(t) - \hat{x}_0(t) = 0, \qquad \forall i = 1, \ldots, N. \tag{4.40}$$

Although CAVs connected to the centralized TLVC have no steady-state error; AVs not connected to the TLVC have non-zero steady state error [54]

$$\lim_{t\to\infty} x_i(t) - \hat{x}_0(t) = \lim_{s\to 0} s(x_i(s) - \hat{x}_0(s)) = \frac{V}{\alpha}(\frac{1}{\gamma} - 1). \tag{4.41}$$

Note that the string stability condition Eq. (4.39) requires $\gamma < 1$, but for non-connected vehicles, their steady-state error is 0 only when $\gamma = 1$. Therefore, zero-steady-state error and string stability cannot be achieved together for non-connected vehicles, which is known as one of the fundamental limits for decentralized constant-spacing platoon [7]. Nevertheless, the steady-state error becomes small as the blending gain γ increases.

4.3 Results

In this section, comparative simulations are used to evaluate the performance of the vehicle network with DSR Eq. (4.32), (4.33) and without DSR Eq. (4.16), (4.20).

4.3.1 Mixed AVs network

The simulation results are evaluated in MATLAB/Simulnk environment. The simulations include 5 vehicles, where the leader vehicle is always connected to the TLVC information (since the lead vehicle can usually visually observe the traffic light) while the connectivity of the rest of the vehicles could be either connected or not – simulations are performed for all possible cases. Different methods are evaluated for a change of the traffic light from stop to go, which provides a step input of the desired cruise velocity $V = 13.41$m/s (30 mph) to all the connected vehicles. The control parameters are selected as discussed below:

(i) Control gain α: The target settling time for accelerating from static to $V = 30$ mph varies from 5 to $10s$, depending on the type of the vehicles [45]. In this paper the controller gain α is selected $\alpha = 2/3$ to match the settling time of 6 seconds.

(ii) Target inter-spacing d_0 and collision: The legal length l_0 of a single unit truck in Washington state is 40 feet (about 12 m) [55]. Therefore, the target constant inter-spacing d_0 is selected as the length of 2 single unit trucks $d_0 = 2l_0 = 24$ m. Two vehicles $i-1$ and

i are considered to have collided if their inter-distance d_i is less than l_0, as illustrated in Fig.4.1.

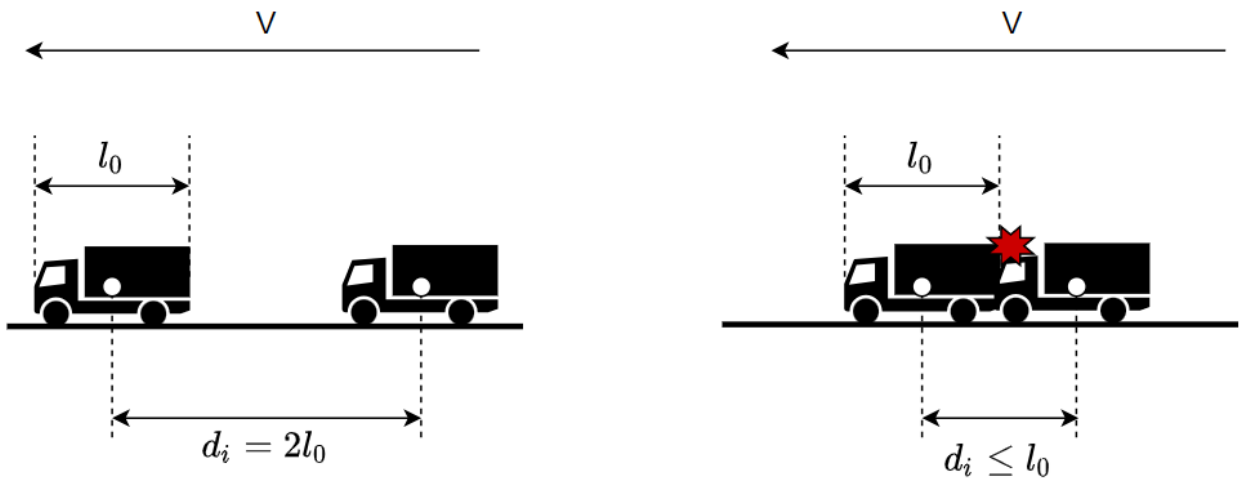

Figure 4.1: The inter-spacing between trucks. Left: The two trucks maintain target inter-spacing $d_i = d_0 = 2l_0$. Right: The two trucks collide when their inter-spacing $d_i \leq l_0$

(iii) DSR delay τ_d: The DSR delay depends on the sampling rate of the local sensors. Typically, the local sensing delay varies between 0.1 - 0.3 s [47, 48]. In this simulation, the DSR delay is selected as $\tau_d = 0.1$s.

(iv) Blended DSR gain γ: The selection of the blending gain γ is restricted by $\gamma \in (0.5, 1]$ for internal stability, according to Eq. (4.35). Additionally, it is restricted by $\gamma < \sqrt{1/(\alpha\tau_d + 1)} = 0.97$ for string stability, according to Eq. (4.39). Therefore, the blending gain γ is selected as $\gamma = 0.95$ to satisfy above conditions and reduce the steady state error for non-connected vehicles according to Eq. (4.41).

4.3.2 Simulation results

Comparative simulations show that the proposed blended DSR method achieves better traffic performance compared with the method without DSR for all scenarios of different mixed AVs networks.

Using DSR leads to smaller steady-state error when TLVC is not available to followers

The proposed blended DSR method has better tracking performance than without DSR when the TLVC is not available. For the cruise speed $V = 13.41$m/s, control gain $\alpha = 2/3$ and the blended DSR gain $\gamma = 0.95$, the steady-state error with blended DSR can be predicted by Eq. (4.41) as

$$\lim_{s\to 0} s(x_i(s) - \hat{x}_0(s)) = \frac{V}{\alpha}(\frac{1}{\gamma} - 1) = 1.06 \text{ m}, \tag{4.42}$$

which is similar to the steady-state error observed in simulations, as seen in plot (c) of Fig.4.2. In contrast, the steady state error of the vehicle network without DSR is 20m, as seen in plot (d) of Fig.4.2. Therefore, even without TLVC communication, the use of DSR results in a 95% reduction of the steady-state error when compared to the case without DSR. This, in turn, results in improved traffic efficiency during stop-and-go scenarios at intersections with DSR when compared to the case without DSR, described below.

Using DSR leads to smaller inter-spacing error and results in safe mixed AVs platooning

The proposed blended DSR method enables safe, string stable constant-spacing mixed AVs platooning, as seen in Fig. 4.3. For different mixed AVs network scenarios, control with DSR maintains robust inter-spacing control and the resulting maximum normalized spacing error $\Delta_{d,max}$ of the vehicle network varies from 0.01 to 0.04. In contrast, the maximum normalized spacing error $\Delta_{d,max}$, without DSR, varies from 0 to 0.75. Therefore, the variation of the maximum inter-spacing error $\Delta_{d,max}$ of the blended DSR method (0.03) is about 96% less than the variation of the maximum spacing error $\Delta_{d,max}$ without DSR (0.75). More significantly, adding DSR avoids collisions in all possible mixed-case simulations, while the mixed-CAVs network without DSR results in collisions under five cases.

Using DSR improves traffic efficiency

The proposed blended DSR method improves the traffic efficiency and allows the mixed AVs network to pass the intersection with significantly shorter time, compared with the mixed

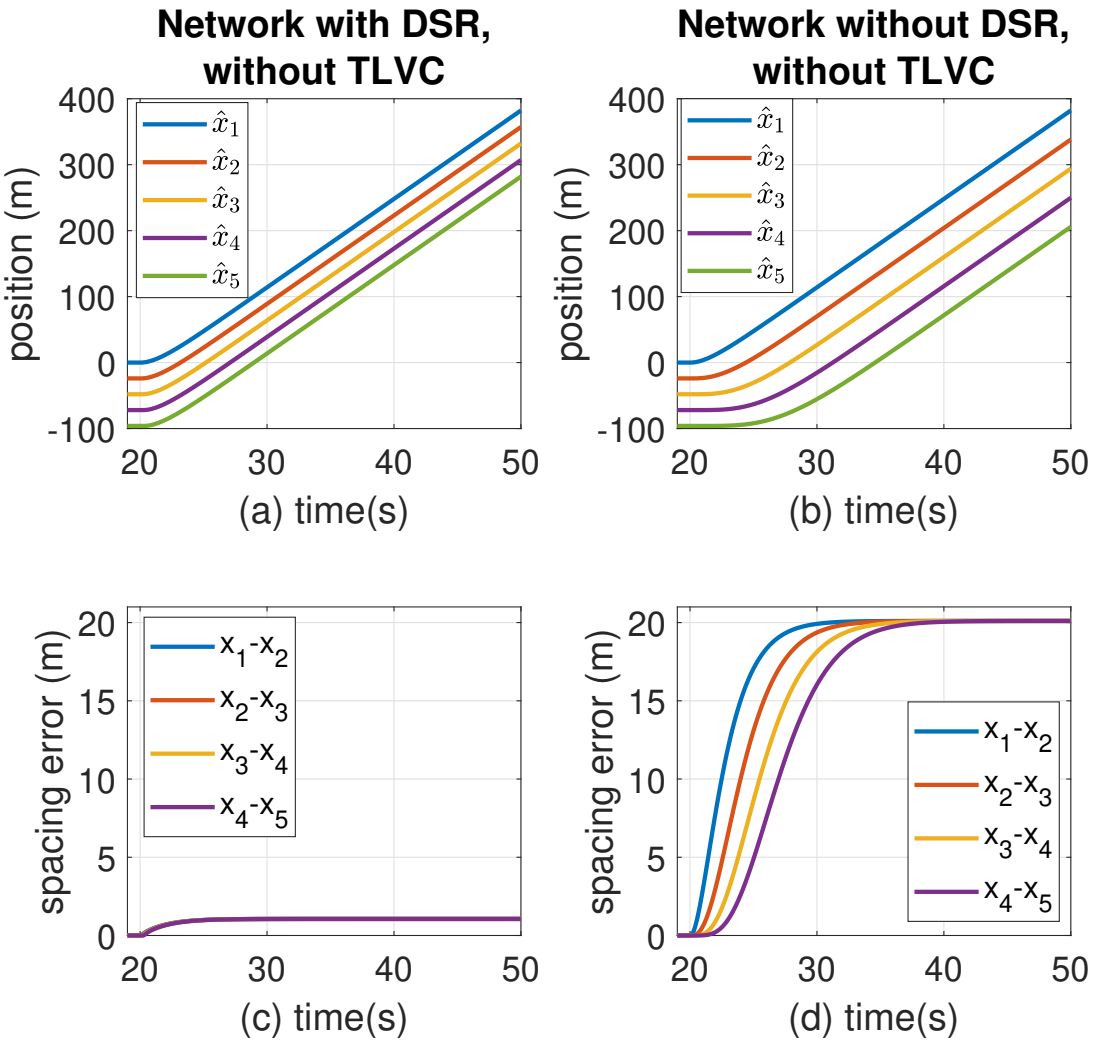

Figure 4.2: DSR without TLVC communication (left plots (a),(c)) leads to more cohesive tracking performance (top plots) and smaller spacing errors (bottom plots) when compared to the case without DSR and without TLVC communication (right plots, (b),(d)).

AVs network without DSR, as seen in Fig. 4.3. With the blended DSR, the resulting time for passing the intersection varies from 8.67 s to 8.98 s, In contrast, the resulting time for passing the intersection T_p without DSR varies from 8.67 s to 14.60 s. Moroeover, the variation of the traffic light passing time T_p with the blended DSR method (0.31 s) is about 95% less than

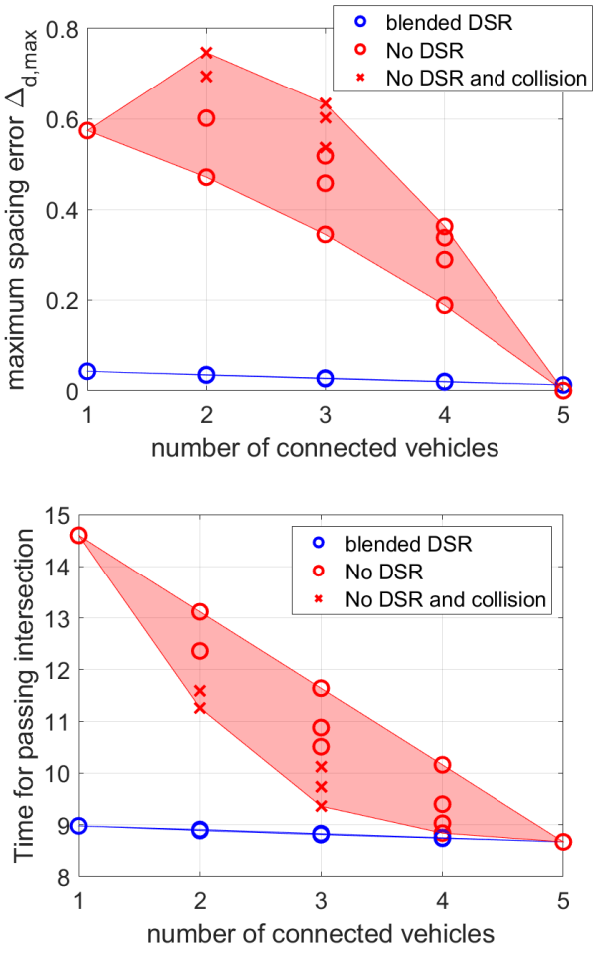

Figure 4.3: Comparison with (blue circles) and without blended DSR (red circles and crosses): (top) the maximum normalized spacing error $\Delta_{d,max}$ defined in Eq. (4.25) and (bottom) the time for passing the intersection T_p defined in Eq. (4.26). With blended DSR, both (i) the maximum normalized spacing error $\Delta_{d,max}$ and (ii) the time T_p for passing through the intersection, have less variations and smaller values, for all cases with partial connectivity to the TLVC.

the variation of the passing time T_p without DSR (5.93 s). Finally, the maximum passing time T_p with DSR (8.98 s) is 38.4% less than the maximum passing time T_p without DSR (14.60 s), as seen in Fig.4.3.

4.4 Conclusion

This work developed an approach to safely increase the flow through a traffic light for mixed autonomous vehicles (AVs), when some of the AVs had access to traffic-light-to-vehicle communication (TLVC) and some did not have access to the TLVC. For connected autonomous vehicles (CAVs), the information from traffic lights was blended with a delayed-self-reinforcement (DSR) approach, which utilizes already available local information to augment the tracking performance. The DSR approach improves spacing-to-predecessor-vehicle control even when the AV is not connected. As a result, the blended DSR approach improved the tracking flow performance and traffic efficiency with mixed AVs. Simulation results showed that the proposed blended DSR approach enables safe mixed AVs platooning with better velocity cohesion and traffic efficiency compared to the case without DSR during stop-and-go scenarios at intersections.

Chapter 5

MC3: AN EFFICIENT MIXED NETWORK AT REAL-WORLD SIGNALIZED INTERSECTIONS

The traffic capacity of signalized intersections can be increased using vehicle to infrastructure (V2I) communication by broadcasting traffic control signals to connected autonomous vehicles (CAVs). However, the potential improvement in traffic capacity with only CAVs can be substantially reduced under mixed traffic environments that include autonomous vehicles (AVs) without V2I communication. The main contribution of this work is to increase the traffic capacity (close to that achieved by CAVs with V2I communication) when there is a substantial number of AVs without V2I communication – by using a delayed-self-reinforcement (DSR) approach for vehicle spacing control with already available history of the AVs own control inputs and sensed information. Moreover, analytical estimates are established to predict the improvements in traffic capacity achieved for AVs with the DSR approach compared to the case without the DSR approach. Simulation results match the analytical predictions and show that AVs using the DSR approach (without V2I communication) are able to recover 88% of intersection capacity achieved with CAVs (with V2I communication) and result in 2.7 times the intersection capacity achieved by AVs without DSR on one way traffic. Moreover, similar improvements with DSR are shown for a real-world intersection using the Simulation of Urban MObility (SUMO) platform. AVs with DSR approach are able to recover 96% of intersection capacity achieved with CAVs (with V2I communication) and result in 1.4 times the intersection capacity achieved by AVs without DSR. Improvements using DSR are also seen with mixed traffic that includes human-driven vehicles (HDVs).

5.1 Introduction

Connected autonomous vehicles (CAVs) have been studied in the existing literature as an approach to improve traffic capacity and stability in transportation networks [22, 56, 23, 57, 58]. More recently, vehicle-to-infrastructure (V2I) communication [59] has been proposed to improve the capacity and safety of signalized intersections using CAVs, for instance, by broadcasting traffic light information to CAVs approaching an intersection to improve fuel economy and reduce journey time by reducing stop-and-go traffic [24, 25, 60, 33], optimizing trajectory planning [61], and ensuring improved inter-vehicle spacing control when going from rest to a cruise speed for increased intersection throughput [62, 2]. However, V2I-based approaches with centralized information are not applicable to autonomous vehicles (AVs) without dedicated communication capability [63]. Furthermore, wireless communication might not be secure on all vehicles due to cyber security threats [28]. AVs without V2I communication may use only local sensing information in a decentralized manner, for instance the relative spacing information with respect to the preceding vehicle for spacing control [64]. Such decentralized approaches in AVs utilize constant time-headway based spacing control similar to adaptive cruise control (ACC) policy, which leads to increased inter-vehicle spacing as speed increases, similar to human-driven vehicles (HDVs), resulting in loss of traffic capacity. In contrast, constant spacing policy doesn't lead to loss of traffic capacity at higher speeds, however it requires communication among vehicles for safe implementation [65]. Therefore, a control protocol for AVs without V2I communication is required that improves the traffic capacity of intersections compared to the standard constant time-headway based spacing control.

The main contribution of this work is to show that the use of the delayed-self-reinforcement (DSR) approach for vehicle spacing control in AVs can substantially recover, without using V2I communication, the improved traffic capacity of intersections achieved with CAVs that rely on V2I communication [15]. The current work is an evolution of preliminary work in [2], where simulation results showed that DSR can improve the capacity of heterogeneous (or

mixed) traffic networks, where only some vehicles are with V2I communication (CAVs) and the rest are without V2I communication (AVs). In the current work, a comparative theoretical analysis of the DSR approach and the standard constant time-headway approach (i.e., the no-DSR approach) is developed (i) to predict the resulting spacing loss of the network and, (ii) to quantify the traffic capacity in terms of target traffic speed and vehicle dynamics. The predictions of the traffic capacity of AV network are verified by simulations, which show that the error between the prediction and the simulations are within ± 2 vehicles (within 10%). Moreover, the analytically predicted improvement in traffic capacity of intersections with AVs (which is almost 88% of that achieved with CAVs) when compared to the AVs without DSR (which is only 33% of that achieved CAVs) is within 3% of the results from simulations. The theoretical predictions of capacity are based on all vehicles in the single lane being the same. The analysis for this ideal scenario gives an estimate of the maximum capacity increase with the use of V2I communication by CAVs and how much of it can be recovered by DSR AVs without the V2I communication. For mixed traffic and for more realistic intersections, the capacity increases with CAVs and DSR AVs cannot be predicted using the theoretical analyses and are estimated through numerical simulations.

Another contribution of this work is to show that AVs with the DSR approach can improve traffic capacity when compared to AVs without DSR – even under mixed traffic conditions with AVs, CAVs and human driven vehicles (HDVs). In general, a similar response for all vehicles can lead to smaller inter-vehicular spacing, and thereby, increase traffic-intersection capacity. However, CAVs and AVs without V2I communication are expected to coexist with human driven vehicles (HDVs) which can lead to further decrease in intersection capacity [66]. For example, heterogeneous vehicles (AVs and CAVs) along with HDVs in mixed traffic conditions may lead to larger inter-vehicle spacing errors and undesirable braking incidents, resulting in lower intersection capacity [26]. Some of the main limiting factors of capacity in mixed traffic are the large response time of HDVs [35], i.e. the time taken to achieve a target speed, capacity uncertainty in HDVs [67], and required minimum time-headway of decentralized AVs [26, 36]. Nevertheless, even in the presence of HDVs in mixed traffic

conditions, DSR maintains smaller inter-vehicle spacing errors for the AVs, compared to AVs without DSR. For instance, it is shown that for one way traffic networks with 30% CAVs and 30% HDVs mixed randomly, AVs implementing DSR for spacing control achieve approximately 1.4 times the intersection capacity achieved by AVs without DSR. Furthermore, for similar mixed traffic conditions, results with a real-world intersection using Simulation of Urban MObility (SUMO) platform show that AVs with DSR for spacing control achieve approximately 1.2 times the intersection capacity achieved by AVs without DSR.

The rest of the paper is organized as follows. Section 5.2 describes the vehicle network dynamics, establishes metrics for evaluating the traffic throughput and formulates the main research problem. Section 5.3 develops the analytical method to quantify the traffic capacity and predict the improvement using DSR when compared with the standard strategy without DSR. Section 5.4 comparatively examines the performance improvement with DSR in a general mixed-traffic environment with CAVs, AVs and HDVs, and the conclusions are provided in Section 5.5. The CAV model and the human driver model used for mixed traffic simulations are described in the Appendices.

5.2 Problem Formulation

This section describes the vehicle dynamics used in this article, as well as the car-following strategies of predecessor-follower (PF) AVs. Here, the follower only uses the spacing information to the predecessor in the car-following strategy for both cases, with and without DSR. Lastly, the problem statement for the article is stated.

5.2.1 Normalized vehicle dynamics

The dynamics [8] of each i^{th} vehicle in the network is given as

$$\hat{x}_i^{(1)}(t) = \hat{v}_i(t), \tag{5.1}$$

$$\hat{v}_i^{(1)}(t) = \hat{x}_i^{(2)}(t) = \hat{a}_i(t), \tag{5.2}$$

$$\hat{a}_i^{(1)}(t) = \hat{x}_i^{(3)}(t) = f(\hat{v}_i(t), \hat{a}_i(t)) + g(\hat{v}_i(t), \hat{a}_i(t))\hat{u}_i(t), \tag{5.3}$$

where $\hat{x}_i, \hat{v}_i$ and $\hat{a}_i$ are the position, speed and acceleration of the i^{th} vehicle. The control command $\hat{u}_i$ represents the target axle torque output of the vehicle. The nonlinear functions $f(\hat{v}_i, \hat{a}_i)$ and $g(\hat{v}_i, \hat{a}_i)$ describe the propulsion dynamics of the vehicle. The vehicle dynamics in Eq. (5.3) can be normalized using feedback linearization [52]

$$x_i^{(3)}(t) = \tilde{u}_i(t), \tag{5.4}$$

where $x_i(t)$ is the deviated position from the target standstill spacing d_0

$$x_i(t) = \hat{x}_i(t) - (i-1)\, d_0, \tag{5.5}$$

and $\tilde{u}_i$ is the normalized control command which is given by

$$\hat{u}_i(t) = g\left(\hat{v}_i(t), \hat{a}_i(t)\right)^{-1} \left(\tilde{u}_i(t) - f\left(\hat{v}_i(t), \hat{a}_i(t)\right)\right). \tag{5.6}$$

5.2.2 Standard car-following strategy

The standard car-following strategy of the normalized dynamics in Eq. (5.4) can be designed using stable pole-zero cancellation [1], which gives the normalized control command $\tilde{u}_i(s)$ in Eq. (5.6) in Laplace domain as,

$$\tilde{u}_i(s) = C_{ff}(s) u_i(s) - C_{fb}(s) x_i(s), \tag{5.7}$$

with the control input $u_i(s)$ chosen according to the standard spacing control policy, and the feedforward and feedback controllers $C_{ff}(s)$ and $C_{fb}(s)$ designed as,

$$u_i(s) = u_{std,i}(s) = \alpha e_i(s), \qquad i \geq 2, \tag{5.8}$$

$$C_{ff}(s) = s^2 + k_1 s + k_0, \tag{5.9}$$

$$C_{fb}(s) = k_1 s^2 + k_0 s, \tag{5.10}$$

where the control gains k_0, k_1 are selected to achieve stable zero-pole cancellation as illustrated in [1], and the spacing error gain is positive $\alpha > 0$ for stability, with the spacing error

$e_i(s)$ defined as

$$e_i(s) = \hat{x}_{i-1}(s) - \hat{x}_i(s) - d_0 = x_{i-1}(s) - x_i(s). \tag{5.11}$$

Substituting Eqs. (5.7)-(5.10) into the normalized dynamics Eq. (5.4) yields the first-order car-following dynamics for the standard approach

$$x_i(s) = \frac{\alpha}{s+\alpha} x_{i-1}(s), \qquad i \geq 2. \tag{5.12}$$

Therefore, given the desired time period T_s within which vehicle i should settle to its target state (which depends on the vehicle performance characteristics), the control gain α is determined by

$$\alpha = \frac{4}{T_s}. \tag{5.13}$$

Eq. (5.12) describes the standard decentralized AV car-following strategy with constant time-headway $\lambda = 1/\alpha$, which indicates the inter-vehicle spacing increases proportionally with headway time λ, as shown next. Given a step target cruise speed $V > 0$, assume the leader vehicle achieves V within the desired time period $T_s = 4/\alpha$ such that,

$$x_1(s) = \frac{V}{s^2} \frac{\alpha}{s+\alpha}. \tag{5.14}$$

Then, the steady state error e_i of the i^{th} vehicle depends on the desired time period T_s, as shown using Final Value Theorem of Laplace Transform,

$$\begin{aligned}
\lim_{t\to\infty} e_i(t) &= \lim_{s\to 0} s e_i(s) = \lim_{s\to 0} s \left(x_{i-1}(s) - x_i(s)\right), \\
&= \lim_{s\to 0} s \left(\frac{\alpha}{s+\alpha}\right) \left(x_{i-2}(s) - x_{i-1}(s)\right), \\
&= \lim_{s\to 0} s \left(\frac{\alpha}{s+\alpha}\right)^{i-2} \left(x_1(s) - x_2(s)\right), \\
&= \lim_{s\to 0} s \left(\frac{\alpha}{s+\alpha}\right)^{i-2} \frac{V\alpha}{s^2\left(s+\alpha\right)} \left(1 - \frac{\alpha}{s+\alpha}\right) \\
&= \lim_{s\to 0} \left(\frac{\alpha}{s+\alpha}\right)^{i-1} \frac{V}{\alpha} = \frac{V}{\alpha} = V\frac{T_s}{4}.
\end{aligned} \tag{5.15}$$

Lastly, the network dynamics of a vehicle network with N follower vehicles (besides the lead $i = 1$ vehicle), each implementing constant time-headway policy as in Eq. (5.12), can be written by stacking the standard control command $u_{std,i}$ from Eq. (5.8) $u_{std} = [u_{std,2}, \ldots, u_{std,N+1}]^T$, and the deviated position x_i $X = [x_2, \ldots, x_{N+1}]^T \in \mathbb{R}^N$ as column vectors, for all the follower vehicles ($i \in \{2, N+1\}$), and taking the inverse Laplace transform to get,

$$\dot{X}(t) = u_{std}(t) = -\alpha K X(t) + \alpha B x_1(t), \tag{5.16}$$

where the matrix $K \in \mathbf{R}^{N \times N}$ is called the pinned Laplacian of the PF vehicle network, and $B \in \mathbf{R}^N$ is the decentralized source communication vector of the network, i.e.,

$$K = \begin{bmatrix} 1 & \ldots & & 0 \\ -1 & 1 & & \\ \vdots & \ddots & \ddots & \\ 0 & \ldots & -1 & 1 \end{bmatrix}, \quad B = \begin{bmatrix} 1 \\ 0 \\ \vdots \\ 0 \end{bmatrix}. \tag{5.17}$$

Note that only the first entry of the communication vector B is non-zero in Eq. (5.17), which indicates that only the first follower has the connected information about the deviated position of the leader $x_1(t)$.

5.2.3 DSR-based car-dollowing dynamics

The DSR control update approximates the ideal centralized control, where all the vehicles in the network have access to the leader (traffic light) information, which is ideal for maintaining inter-vehicle spacing. Therefore, all the vehicles in the network have similar position responses and smaller inter-vehicle spacing error compared to the standard constant time-headway spacing control [15].

Ideal car-following dynamics

The ideal control update $u_{idl,i}(t)$ for each i^{th} vehicle uses the leader information $x_1(s)$, as shown below,

$$u_i(s) = u_{idl,i}(s) = \alpha\left(x_1(s) - x_i(s)\right) + sx_1(s). \tag{5.18}$$

Substituting Eq. (5.18), Eq. (5.6), Eq. (5.7), Eq. (5.9) and Eq. (5.10) into Eq. (5.4) yields the ideal car-following dynamics

$$sx_i(s) = -\alpha\left(x_i(s) - x_1(s)\right) + sx_1(s), \tag{5.19}$$

with error ($\hat{e}_i = x_i - x_1$) dynamics

$$\frac{d}{dt}\hat{e}_i(t) = -\alpha\hat{e}_i(t), \tag{5.20}$$

i.e., exponential correction of tracking errors. Since all vehicles have similar motion, the spacing between vehicles remains constant at d_0. Similar to Eq. (5.16), stacking the states $x_i(s)$ and applying inverse Laplace transform results in the ideal network dynamics in time domain [15],

$$\begin{aligned}\dot{X}(t) &= -\alpha\left(X(t) - \mathbf{1}_N x_1(t)\right) + \mathbf{1}_N\dot{x}_1(t)\\ &= -\alpha X(t) + \alpha\mathbf{1}_N\left(x_1(t) + \dot{x}_1(t)/\alpha\right)\\ &= -\alpha X(t) + \alpha\mathbf{1}_N x_d(t) \qquad = u_{idl}(t)\end{aligned} \tag{5.21}$$

where $\mathbf{1}_N = [1, \ldots, 1]^T \in \mathbf{R}^N$, and $x_d(t)$ is computed by

$$x_d(t) = x_1(t) + \frac{1}{\alpha}\dot{x}_1(t) \tag{5.22}$$

which denotes the centralized information required for ideal tracking. However, the update Eq. (5.21) requires centralized communication of $x_d(t)$.

DSR-based car-following dynamics

An approximation of the update law in Eq. (5.21), which does not require centralized communication, is achieved by multiplying the pinned Laplacian matrix of the vehicle network K from Eq. (5.17) on both sides of Eq. (5.21),

$$K\dot{X}(t) = -\alpha K\left(X(t) - \mathbf{1}_N x_d(t)\right). \tag{5.23}$$

It can be shown from [31] that the pinned Laplacian K and the source communication vector B in Eq. (5.17) satisfy $K^{-1}B = \mathbf{1}_N$. Therefore, Eq. (5.23) can be rewritten using $B = K\mathbf{1}_N$, and addition of $\dot{X}(t)$ on both sides of Eq. (5.23) with some rearrangement of terms, results in the DSR command u_{dsr} as,

$$\begin{aligned}\dot{X}(t) &= (I-K)\,\dot{X}(t) - \alpha K X(t) + \alpha B x_d(t)\\ &\approx (I-K)\,\frac{X(t) - X(t-\tau_d)}{\tau_d} - \alpha K X(t) + \alpha B x_d(t)\\ &= u_{dsr}(t), \qquad u_{dsr} = [u_{dsr,2}, u_{dsr,3}, \ldots, u_{dsr,N+1}]^T,\end{aligned} \tag{5.24}$$

where $\tau_d > 0$ is the DSR delay used to approximate the derivative on the RHS of the equation. The resulting decentralized command $u_{dsr}(t)$ approximates the ideal command $u_{idl}(t)$ in Eq. (5.21). However, DSR command $u_{dsr}(t)$ uses the same connectivity vector B as the decentralized standard constant time-headway car-following policy in Eq. (5.16). Therefore, the DSR network Eq. (5.24) only requires the leader information x_d for the first follower, which has visual access to the leader, and does not require broadcast of the leader trajectory information $x_d(t)$ as in the centralized case Eq. (5.21). Lastly, in order to guarantee string stability of the vehicle network to avoid amplification of disturbances, the DSR command Eq. (5.24) needs to be scaled by a blending gain $\gamma < \gamma^* < 1$, modifying the update equation to

$$\dot{X}(t) = \gamma u_{dsr}(t). \tag{5.25}$$

The upper bound γ^* of the blending gain γ can be found using the control gain α and the DSR delay τ_d as illustrated in [1].

5.2.4 Traffic capacity metric

The traffic capacity N_p is evaluated by the number of vehicles passing through the intersection given a fixed, traffic light signal time T during which the light remains green. Let the initial position of the leader (at the start of the intersection) be the origin, i.e. $\hat{x}_1(0) = 0$. Then, the traffic capacity N_p is given as the number of vehicles passing the intersection, i.e.,

$$\begin{aligned} N_p &= \arg\max_{i\in\mathbb{Z}}\{\hat{x}_i(T) > \hat{x}_1(0)\} \\ &= \arg\max_{i\in\mathbb{Z}}\{x_i(T) - (i-1)d_0 > \hat{x}_1(0) = 0\}, \end{aligned} \tag{5.26}$$

where $\mathbb{Z} = \{0, 1, 2, \dots\}$ is the set of integers.

5.2.5 Problem statement

Ideal connected AVs (CAVs), with network dynamics as in Eq. (5.21), rely on centralized information $x_d(t)$ which can be broadcast from infrastructure devices like cameras at signalized intersections. This enables the CAVs to maintain small inter-vehicle spacing and achieve high traffic capacity N_p at signalized intersections. However, the benefits from the centralized communication can be substantially reduced when not all vehicles are CAVs in a mixed traffic environment, or when V2I communication is not available and the vehicles operate as AVs.

The research problems addressed in this article are the following.

1. Increase the traffic capacity N_p at signalized intersections, defined in Eq. (5.26) using DSR, when vehicles operate as AVs (without V2I communication) instead of CAVs.

2. Predict the traffic capacity improvement for AVs with DSR compared to the case without DSR, i.e., AVs using standard car-following protocol Eq. (5.12).

3. Comparatively evaluate the traffic-intersection capacity N_p, defined in Eq. (5.26), for mixed vehicle networks with CAVs, HDVs, and AVs, where the AVs are using either the standard car-following protocol Eq. (5.12) or DSR.

5.3 Traffic capacity analysis

In this section, the traffic capacity, given a constant target cruise speed V at a one way intersection during the green light phase, is analyzed for the following vehicle networks: (a) ideal connected network using Eq. (5.21), (b) decentralized DSR AVs using Eq. (5.25) and (c) decentralized standard AVs based on Eq. (5.16). To assess the maximum capacity with V2I communication and the capacity loss without V2I communication all vehicles are assumed to be aligned on a single lane with a target standstill distance d_0.

5.3.1 General form of the strategies

This section shows that the car-following dynamics in the different vehicle networks: (a) ideal connected network using Eq. (5.21), (b) decentralized DSR AVs using Eq. (5.25) and (c) decentralized standard AVs based on Eq. (5.16) can be expressed or approximated by the general form

$$\dot{x}_i(t) = u_i(t) = -k\left(x_i(t) + x_{i-1}(t)\right) + b\dot{x}_{i-1}(t), \qquad \forall i = 2, \ldots, N, \tag{5.27}$$

Ideal network

From the ideal network dynamics in Eq. (5.21), individual vehicle i update can written as,

$$\dot{x}_i(t) = u_{idl,i}(t) = -\alpha\left(x_i(t) - x_d(t)\right), \quad i = 2, \ldots, N+1 \tag{5.28}$$

subtracting two consecutive vehicle update equations from Eq. (5.28) yields,

$$\begin{aligned} \dot{x}_i(t) - \dot{x}_{i-1}(t) &= -\alpha\left(x_i(t) - x_d(t)\right) + \alpha(x_{i-1}(t) - x_d(t)) \\ &= -\alpha\left(x_i(t) - x_{i-1}(t)\right) \qquad (5.29) \\ \Rightarrow \dot{x}_i(t) &= -\alpha\left(x_i(t) - x_{i-1}(t)\right) + \dot{x}_{i-1}(t), \qquad \forall i = \{2, \ldots, N\}, \qquad (5.30) \end{aligned}$$

which can be written using the general form in Eq. (5.27), with the parameters as $k = \alpha, b = 1$.

All no-DSR AV network

For a decentralized vehicle network with no-DSR AVs, the update dynamics from Eq. (5.16) for each vehicle i is,

$$\dot{x}_i(t) = -\alpha x_i(t) + \alpha x_{i-1}(t), \qquad i = 2, \ldots, N+1, \tag{5.31}$$

which can be written using the general form in Eq. (5.27) with the parameters as $k = \alpha, b = 0$.

All DSR AV network with gain

The DSR-based update dynamics in Eq. (5.24) leads to a set of delay differential equations (DDEs) for each vehicle in the network. Note that the solutions with the the DSR command Eq. (5.25), approximates the ideal command in Eq. (5.24), i.e.,

$$\frac{1}{\gamma}\dot{X} \approx (I - K)\,\dot{X}(t) - \alpha K X(t) + \alpha B x_d(t), \tag{5.32}$$

and therefore, the DSR network Eq. (5.32) approximates following update dynamics for individual vehicles in the network,

$$\dot{x}_i(t) = \alpha\gamma\,(x_{i-1}(t) - x_i(t)) + \gamma\dot{x}_{i-1}(t), \qquad i = 2, \ldots, N+1, \tag{5.33}$$

which can be written using the general form in Eq. (5.27) with the parameters as $k = \alpha\gamma, b = \gamma$.

5.3.2 Properties of the general form

Solving the general form of the vehicle dynamics in Eq. (5.27) with initial condition $x_i(0) = 0$ results in the solution of the trajectory $x_i(t)$ as follows,

$$x_i(t) = \mathcal{L}\,(x_{i-1}, k, b)\,(t) = e^{-kt}\int_0^t (k x_{i-1}(\tau) + b\dot{x}_{i-1}(\tau))\,e^{k\tau}d\tau \tag{5.34}$$

for $i = 2, \ldots, N+1$, where the operator $\mathcal{L}(u, k, b)$ is defined as

$$\mathcal{L}(u, k, b)(t) = e^{-kt}\int_0^t (ku(\tau) + b\dot{u}(\tau))\,e^{k\tau}d\tau. \tag{5.35}$$

The spacing error e_i from Eq. (5.11) satisfies the following lemmas, which are used in the subsequent derivations of the traffic capacity.

Lemma 14. *The spacing error e_i based on the general car following dynamics in Eq.* (5.27) *satisfies*

$$e_i = \mathcal{L}\left(e_{i-1}, k, b\right), \qquad i = 2, \ldots, N+1 \tag{5.36}$$

Proof. From Eq. (5.35), the operator $\mathcal{L}$ is linear in its first argument since for any $t \geq 0$

$$\begin{aligned}
&\mathcal{L}(a_1u_1 + a_2u_2, k, b)(t) \\
&\quad = e^{-kt}\int_0^t \left(k\left(a_1u_1 + a_2u_2\right) + b(a_1\dot{u}_1 + a_2\dot{u}_2)\right)e^{k\tau}d\tau \\
&\quad = a_1e^{-kt}\int_0^t \left(ku_1(\tau) + b\dot{u}_1(\tau)\right)e^{k\tau}d\tau + a_2e^{-kt}\int_0^t \left(ku_2(\tau) + b\dot{u}_2(\tau)\right)e^{k\tau}d\tau \\
&\quad = a_1\mathcal{L}(u_1, k, b)(t) + a_2\mathcal{L}(u_2, k, b)(t).
\end{aligned} \tag{5.37}$$

Then, from Eq. (5.11)

$$\begin{aligned}
e_i = x_{i-1} - x_i \ &= \mathcal{L}(x_{i-2}, k, b) - \mathcal{L}\left(x_{i-1}, k, b\right) \\
&= \mathcal{L}\left(x_{i-2}, k, b\right) - \mathcal{L}\left(x_{i-2} - e_{i-1}, k, b\right) \\
&= \mathcal{L}\left(x_{i-2}, k, b\right) - \left(\mathcal{L}\left(x_{i-2}, k, b\right) - \mathcal{L}\left(e_{i-1}, k, b\right)\right) \ = \mathcal{L}\left(e_{i-1}, k, b\right).
\end{aligned} \tag{5.38}$$

□

The following lemma develops a general form of the propagation dynamics of the spacing error $e_i(t)$.

Lemma 15. *For the system dynamics in Eq.* (5.27)*, if there exists a constant $c \in \mathbb{R}$ with $k > 0$ such that the spacing error $e_i(t)$ has the form*

$$e_i(t) = c\left(1 - e^{-kt}P_i(t)\right), \tag{5.39}$$

where $P_i(t)$ is an element in the space $\mathcal{P}_i$ of polynomial functions

$$P_i(t) \in \mathcal{P}_i = \left\{ p_i(t) | p_i(t) = \sum_{j=0}^{i-1} k_j t^j, k_j \in \mathbb{R}, t \geq 0 \right\}, \tag{5.40}$$

then the next spacing error $e_{i+1}(t)$ also preserves the same form as in Eq. (5.39) *with the same coefficients c and k, and a polynomial $P_{i+1} \in \mathcal{P}_{i+1}$.*

Proof. From Lemma 14

$$e_{i+1}(t) = \mathcal{L}\left(e_i(t), k, b\right)(t) = e^{-kt} \int_0^t \left(k e_i(\tau) + b\dot{e}_i(\tau)\right) e^{k\tau} d\tau. \tag{5.41}$$

Substituting Eq. (5.39) into Eq. (5.41) yields

$$\begin{aligned} e_{i+1}(t) &= ce^{-kt} \int_0^t \left(k\left(1 - e^{-k\tau} P_i(\tau)\right) + be^{-k\tau} \left(kP_i(\tau) - \dot{P}(\tau) \right) \right) e^{k\tau} d\tau \\ &= ce^{-kt} \left(\left(e^{kt} - 1\right) - k\left(1 - b\right) \int_0^t P_i(\tau) d\tau - bP_i(\tau)|_0^t \right) \\ &= c\left(1 - e^{-kt} \left(1 + k(1-b) \int_0^t P_i(\tau) d\tau + bP_i(\tau) \Big|_0^t \right) \right) \\ &= c\left(1 - e^{-kt} P_{i+1}(t)\right), \end{aligned} \tag{5.42}$$

where the polynomial $P_{i+1}(t) \in \mathcal{P}_{i+1}$ is

$$P_{i+1}(t) = 1 + \left(k\left(1 - b\right) \int_0^t P_i(\tau) d\tau \right) + \left(bP_i(t) - bP_i(0) \right). \tag{5.43}$$

□

As a result of the above Lemma, the spacing error $e_i(t)$ can be solved by computing the polynomial $P_i(t)$ for all follower vehicles with $i > 2$, if the spacing error of the first follower vehicle ($i = 2$), $e_2(t)$, satisfies Eq. (5.39). With the expressions of the spacing error $e_i(t)$, the trajectory of an agent $x_i(t)$ with system dynamics as in Eq. (5.27) can be described by accumulating all the spacing errors from the leader $x_1(t)$,

$$x_i(t) = x_{i-1}(t) - e_i(t) \ = x_{i-2}(t) - \sum_{j=i-1}^{i} e_j(t) \ = x_1(t) - \sum_{j=2}^{i} e_j(t) \tag{5.44}$$

for $i = 2, \ldots, N+1$, where $x_1(t)$ is the leader trajectory that can be found using the inverse Laplace transform of Eq. (5.14).

5.3.3 Traffic capacity

This section derives the estimation of the traffic capacity at an intersection with a constant, target cruise-speed V, for the following networks: (a) ideal connected network Eq. (5.21), (b) decentralized DSR AVs using Eq. (5.25) and (c) decentralized standard AVs Eq. (5.16). The leader position $x_1(s)$ is independent from the selection of the network strategy, which is obtained using Eq. (5.14) in terms of the constant cruise speed V,

$$x_1(s) = \frac{\alpha V}{s^2(s+\alpha)} = V\left(\frac{1}{s^2} - \frac{1}{\alpha s} + \frac{1}{\alpha(s+\alpha)}\right). \tag{5.45}$$

Taking the inverse Laplace transform of Eq. (5.45) yields

$$x_1(t) = V\left(t - \frac{1}{\alpha}(1 - e^{-\alpha t})\right) = Vt - \frac{V}{\alpha}\left(1 - e^{-\alpha t}\right). \tag{5.46}$$

Ideal network

The ideal network-based update law in Eq. (5.30) results in cohesive trajectory responses among all vehicles, where $x_i(t) = x_1(t), \forall i = 2, \ldots, N$, assuming zero initial spacing errors, i.e. $x_i(0) = x_1(0), \forall i \geq 2$. Therefore, the spacing error $e_i(t)$ remains zero for all the followers, i.e., $e_i(t) = 0, \forall i = 2, \ldots, N$. The trajectory $x_i(t)$ is then given using Eq. (5.46) as,

$$x_i(t) = x_1(t) = Vt - \frac{V}{\alpha}\left(1 - e^{-\alpha t}\right) = Vt - \frac{V}{\alpha} f_{c,i}(t), \tag{5.47}$$

where

$$f_{c,i}(t) = 1 - e^{-\alpha t} \tag{5.48}$$

is the cumulative spacing error function for the i^{th} vehicle of the ideal CAV network. Let T be the time duration for which the traffic light signal remains green. Then the traffic capacity $N_{p,idl}$, as defined in Eq. (5.26), which quantifies the number of vehicles that can pass through the intersection in time T, using the ideal CAV network dynamics (Eq. (5.21))

can be given as,

$$\begin{aligned}
N_{p,idl} &= \arg\max_{i\in\mathbb{Z}}\{x_i(T) - (i-1)d_0 > 0\} \\
&= \arg\max_{i\in\mathbb{Z}}\left\{VT - \frac{V}{\alpha}f_{c,i}(T) - (i-1)d_0 > 0\right\} \\
&= \arg\max_{i\in\mathbb{Z}}\left\{f_{c,i}(T) < \alpha\left(T - \frac{d_0(i-1)}{V}\right)\right\} \\
&= \arg\max_{i\in\mathbb{Z}}\left\{1 - e^{-\alpha T} < \alpha\left(T - \frac{d_0(i-1)}{V}\right)\right\} \\
&= \arg\max_{i\in\mathbb{Z}}\left\{\frac{\alpha d_0}{V}i < \alpha T + \frac{\alpha d_0}{V} - (1 - e^{-\alpha T})\right\} \\
&= \text{floor}\left(\frac{\alpha(VT + d_0) - V(1 - e^{-\alpha T})}{\alpha d_0}\right).
\end{aligned} \tag{5.49}$$

All no-DSR AV network

For the followers of the all no-DSR AV network Eq. (5.16), the trajectory of the first follower $x_2(t)$ can be solved by substituting the first vehicle's trajectory $x_1(t)$ from Eq. (5.46) into Eq. (5.34) to get,

$$\begin{aligned}
x_2(t) &= \mathcal{L}(x_1(t), \alpha, 0)(t) \\
&= e^{-\alpha t}\int_0^t \alpha\left(V\tau - \frac{V}{\alpha}(1 - e^{-\alpha\tau})\right)e^{\alpha\tau}d\tau \\
&= e^{-\alpha t}\left(\int_0^t \alpha V\tau e^{\alpha\tau}d\tau - \int_0^t V(1 - e^{-\alpha\tau})e^{\alpha\tau}d\tau\right) \\
&= Ve^{-\alpha t}\left(\tau e^{\alpha\tau}\Big|_0^t - \int_0^t e^{\alpha\tau}d\tau - \frac{1}{\alpha}e^{\alpha\tau}\Big|_0^t + t\right) \\
&= Vt - \frac{V}{\alpha}(1 - e^{-\alpha t}) - \frac{V}{\alpha}(1 - e^{-\alpha t}(1 + \alpha t)) \\
&= x_1(t) - \frac{V}{\alpha}(1 - e^{-\alpha t}(1 + \alpha t)).
\end{aligned} \tag{5.50}$$

Therefore the spacing error for the second vehicle $e_2(t)$ is given as

$$e_2(t) = x_1(t) - x_2(t) = \frac{V}{\alpha}\left(1 - e^{-\alpha t}(1 + \alpha t)\right), \tag{5.51}$$

which satisfies the general form in Eq. (5.39), with $c = V/\alpha$, $P_2(t) = 1 + \alpha t$. From Lemma 15, the spacing error of the rest of the followers $e_i(t), i \geq 3$ has the same form as Eq. (5.39), where the corresponding polynomials $P_i(t), i \geq 3$ can be solved using Eq. (5.43) as

$$P_3(t) = 1 + \alpha \int_0^t 1 + \alpha\tau d\tau = 1 + \alpha \left(t + \frac{\alpha t^2}{2} \right), \tag{5.52}$$

$$P_4(t) = 1 + \alpha \int_0^t P_3(\tau) d\tau = 1 + \alpha \left(t + \frac{\alpha t^2}{2} + \frac{\alpha^2 t^3}{6} \right), \tag{5.53}$$

...

$$P_i(t) = \sum_{m=0}^{i-1} \frac{(\alpha t)^m}{m!}. \tag{5.54}$$

Therefore, from Eq. (5.54) and Eq. (5.39) with $c = V/\alpha, k = \alpha, b = 0$, the spacing error $e_i(t)$ is given as

$$e_i(t) = \frac{V}{\alpha}(1 - e^{-\alpha t} P_i(t)) \ = \frac{V}{\alpha} \left(1 - e^{-\alpha t} \sum_{m=0}^{i-1} \frac{(\alpha t)^m}{m!} \right) \tag{5.55}$$

Substituting Eq. (5.46) and Eq. (5.55) into Eq. (5.44) gives the trajectory of the rest of the followers $x_i(t), i \geq 3$,

$$\begin{aligned} x_i(t) &= x_1(t) - \sum_{j=2}^{i} e_j(t) = x_1(t) - \frac{V}{\alpha} \left(i - 1 - e^{-\alpha t} \sum_{j=2}^{i} P_j(t) \right) \\ &= x_1(t) - \frac{V}{\alpha} \left(i - 1 - e^{-\alpha t} \sum_{j=2}^{i} \sum_{m=0}^{j-1} \frac{(\alpha t)^m}{m!} \right) \\ &= Vt - \frac{V}{\alpha} \left(i - e^{-\alpha t} \sum_{j=1}^{i} \sum_{m=0}^{j-1} \frac{(\alpha t)^m}{m!} \right), \qquad i = 2, \ldots, N+1. \end{aligned} \tag{5.56}$$

Defining the cumulative spacing error $f_{n,i}(t)$ for the i^{th} vehicle of the no-DSR AV network as

$$f_{n,i}(t) = i - e^{-\alpha t} \sum_{j=1}^{i} \sum_{m=0}^{j-1} \frac{(\alpha t)^m}{m!}. \tag{5.57}$$

The spacing loss function can be estimated from the following two cases:

1. The vehicle index i is small: Notice that the polynomial Eq. (5.54) is the Maclaurin series of $e^{\alpha t}$. Therefore, the sum of the polynomial is small compared with the $e^{-\alpha t}$, and the loss function can be approximated by

$$f_{n,i}(t) = i - e^{-\alpha t} \sum_{j=1}^{i} \sum_{m=0}^{j-1} \frac{(\alpha t)^m}{m!} \approx i. \tag{5.58}$$

2. The vehicle index i is large: The spacing loss $f_{n,i}$ has a limit given as

$$\begin{aligned}
\lim_{i\to\infty} f_{n,i}(t) &= \lim_{i\to\infty} i - e^{-\alpha t} \sum_{j=1}^{i} \sum_{m=0}^{j-1} \frac{(\alpha t)^m}{m!} \\
&= \lim_{i\to\infty} i - e^{-\alpha t} \left(\sum_{j=1}^{i} \left(\sum_{m=0}^{\infty} \frac{(\alpha t)^m}{m!} - \sum_{m=j}^{\infty} \frac{(\alpha t)^m}{m!} \right) \right) \\
&= \lim_{i\to\infty} i - e^{-\alpha t} \left(\sum_{j=1}^{i} \left(e^{\alpha t} - \sum_{m=j}^{\infty} \frac{(\alpha t)^m}{m!} \right) \right) \\
&= \lim_{i\to\infty} e^{-\alpha t} \sum_{j=1}^{i} \sum_{m=j}^{\infty} \frac{(\alpha t)^m}{m!} = e^{-\alpha t} \sum_{j=1}^{\infty} \sum_{m=j}^{\infty} \frac{(\alpha t)^m}{m!} \\
&= e^{-\alpha t} \sum_{m=1}^{\infty} \left(\sum_{j=1}^{m} \frac{(\alpha t)^m}{m!} \right) \text{ (by counting the number of each series term)} \\
&= e^{-\alpha t} \sum_{m=1}^{\infty} m \frac{(\alpha t)^m}{m!} = \alpha t e^{-\alpha t} \sum_{m=1}^{\infty} \frac{(\alpha t)^{m-1}}{(m-1)!} \\
&= \alpha t e^{-\alpha t} e^{\alpha t} = \alpha t
\end{aligned} \tag{5.59}$$

Therefore, the spacing loss function can be approximated by the piecewise linear function $\tilde{f}_{n,i}$ given by

$$f_{n,i}(t) \approx \tilde{f}_{n,i}(t) = \begin{cases} i & i \le \alpha t \\ \alpha t & i > \alpha t, \end{cases} \tag{5.60}$$

and Eq. (5.56) can be rewritten as

$$x_i(t) = Vt - \frac{V}{\alpha} f_{n,i}(t). \tag{5.61}$$

Substituting Eq. (5.61) into Eq. (5.26) and using the approximation $\tilde{f}_{n,i}(t)$ from Eq. (5.60), the traffic capacity $N_{p,n}$ of no-DSR AV network, is given as

$$\begin{aligned} N_{p,n} &= \arg\max_{i\in\mathbb{Z}} \{x_i(T) - (i-1)d_0 > 0\} \\ &= \arg\max_{i\in\mathbb{Z}} \left\{ f_{n,i}(T) < \alpha\left(T - \frac{d_0(i-1)}{V}\right)\right\} \\ &\approx \arg\max_{i\in\mathbb{Z}} \left\{ \tilde{f}_{n,i}(T) < \alpha\left(T - \frac{d_0(i-1)}{V}\right)\right\}. \end{aligned}$$

Since $\tilde{f}_{n,i} = \alpha t$ when $i > \alpha t$ in Eq. (5.60) does not satisfy the inequality $\tilde{f}_{n,i}(T) < \alpha(T - \frac{d_0(i-1)}{V})$, therefore using the other case of $\tilde{f}_{n,i} = i$ when $i \leq \alpha t$ in Eq. (5.60) results in,

$$\begin{aligned} N_{p,n} &\approx \arg\max_{i\in\mathbb{Z}} \left\{ i < \alpha\left(T - \frac{d_0(i-1)}{V}\right)\right\} \\ &= \text{floor}\left(\frac{\alpha(VT + d_0)}{V + \alpha d_0}\right) = \tilde{N}_{p,n}, \end{aligned} \tag{5.62}$$

where Eq. (5.62) provides an explicit (although approximate) estimate $\tilde{N}_{p,n}$ of the number of vehicles $N_{p,n}$ that can pass through the intersection in time T using the update dynamics from Eq. (5.16) for the all no-DSR AV network.

All DSR AVs with gain

For the followers of the all DSR AV network, the trajectory of the first follower $x_2(t)$ and the second follower $x_3(t)$ can be solved by substituting the leader trajectory $x_1(t)$ from Eq. (5.46) with $k = \alpha\gamma, b = \gamma$ into Eq. (5.34),

$$x_2(t) = \mathcal{L}(x_1(t), \alpha\gamma, \gamma)(t) = Vt - \frac{V}{\alpha\gamma}\left(1 - e^{-\alpha\gamma t}\right) \tag{5.63}$$

$$\begin{aligned} x_3(t) &= \mathcal{L}(x_2(t), \alpha\gamma, \gamma)(t) \\ &= x_2(t) - \frac{V}{\alpha\gamma}(1-\gamma)\left(1 - e^{-\alpha\gamma t}(1 + \alpha\gamma t)\right). \end{aligned} \tag{5.64}$$

Therefore, the spacing error of the first and the second followers, $e_2(t)$ and $e_3(t)$, are given as

$$e_2(t) = x_1(t) - x_2(t) = \frac{V}{\alpha\gamma}(1-\gamma)\left(1 - \frac{\gamma}{1-\gamma}\left(e^{-\alpha\gamma t} - e^{-\alpha t}\right)\right) \tag{5.65}$$

$$e_3(t) = x_2(t) - x_3(t) = \frac{V}{\alpha\gamma}(1-\gamma)\left(1 - e^{-\alpha\gamma t}(1+\alpha\gamma t)\right). \tag{5.66}$$

Although the spacing error $e_2(t)$ doesn't satisfy the general format in Eq. (5.39), $e_3(t)$ satisfies the general format in Eq. (5.39), with

$$c = \frac{V}{\alpha\gamma}(1-\gamma), \qquad P_3(t) = 1 + \alpha\gamma t. \tag{5.67}$$

Then, from Lemma 15, the spacing error $e_i(t),\ \forall i \geq 3$ preserves the same form as Eq. (5.39). However, there doesn't exist a closed form of the polynomial $P_i(t)$ in the spacing error $e_i(t)$ for DSR, as it does for the no-DSR method in Eq. (5.54). Therefore, the polynomial coefficients of $P_{i+1}(t)$ need to be solved by iterating the coefficients of $P_i(t)$. Let the coefficients of the i^{th} polynomial $P_i(t)$ be $[k_{0,i}, k_{1,i}, \ldots, k_{i-2,i}]$ such that

$$P_i(t) = \sum_{j=0}^{i-2} k_{j,i} t^j, \qquad i \geq 3. \tag{5.68}$$

Then, from Eq. (5.43), the coefficients for P_{i+1} can be solved as

$$k_{j,i+1} = \begin{cases} 1 - \gamma + \gamma k_{0,i} & j = 0 \\ (1-\gamma)\frac{\alpha\gamma}{j} k_{j-1,i} + \gamma k_{j,i} & 0 < j < i-1 \\ (1-\gamma)\frac{\alpha\gamma}{i+1} k_{i-1,i} & j = i-1 \end{cases} \tag{5.69}$$

such that

$$P_{i+1}(t) = \sum_{j=0}^{i-1} k_{j,i+1} t^j. \tag{5.70}$$

Therefore, trajectory $x_i(t)$ for any vehicle $i \geq 2$ with the DSR-based update in Eq. (5.32), can be solved as

$$\begin{aligned} x_i(t) &= x_2(t) - \sum_{j=3}^{i} e_j(t) \\ &= x_2(t) - \frac{V}{\alpha\gamma}(1-\gamma)(i-2-e^{-\alpha\gamma t}\sum_{j=3}^{i} P_j(t)) \\ &= Vt - \frac{V}{\alpha\gamma}\left(1 - e^{-\alpha\gamma t} + (1-\gamma)(i-2-e^{-\alpha\gamma t}\sum_{j=3}^{i} P_j(t))\right) \\ &= Vt - \frac{V}{\alpha} f_{d,i}(t), \qquad i = 2, \ldots, N \end{aligned} \tag{5.71}$$

where $f_{d,i}(t)$ is the cumulative spacing error at the i^{th} vehicle of the DSR AV network, defined as,

$$\begin{aligned} f_{d,i}(t) &= \frac{1}{\gamma}\left(1 - e^{-\alpha\gamma t} + (1-\gamma)(i-2-e^{-\alpha\gamma t}\sum_{j=3}^{i} P_j(t))\right) \\ &\approx \frac{1}{\gamma}\left(1 - e^{-\alpha\gamma t} + (1-\gamma)(i-2)\right) = \tilde{f}_{d,i}(t), \end{aligned} \tag{5.72}$$

where the approximation $\tilde{f}_{d,i}(t)$ of $f_{d,i}(t)$ tends to be accurate when time t is sufficiently large. Substituting Eq. (5.71), Eq. (5.72) into Eq. (5.26), the traffic capacity $N_{p,d}$ of the All DSR AV network is given as

$$\begin{aligned} N_{p,d} &= \arg\max_{i\in\mathbb{Z}} \left\{ f_{d,i}(T) < \alpha(T - \frac{d_0(i-1)}{V}) \right\} \\ &\approx \arg\max_{i\in\mathbb{Z}} \left\{ \tilde{f}_{d,i}(T) < \alpha(T - \frac{d_0(i-1)}{V}) \right\} \\ &= \arg\max_{i\in\mathbb{Z}} \left\{ 1 - e^{-\alpha\gamma T} + (1-\gamma)(i-2) < \alpha\gamma(T - \frac{d_0(i-1)}{V}) \right\} \\ &= \text{floor}\left(\frac{\alpha\gamma(VT+d_0) - V(2\gamma - 1 - e^{-\alpha\gamma T})}{V(1-\gamma)+\alpha\gamma d_0}\right) = \tilde{N}_{p,d}, \end{aligned} \tag{5.73}$$

where $\tilde{N}_{p,d}$ is an explicit approximation of the traffic capacity $N_{p,d}$ with the use of DSR.

5.4 Simulation Results and Discussion

This section provides comparative simulations of no-DSR AVs (Eq. (5.8)) and DSR AVs (Eq. (5.24)) in mixed traffic conditions to evaluate the improvement of traffic throughput with the use of DSR. The mixed traffic simulations are performed with different market-penetration rates of HDVs and CAVs, and random order of the vehicles in the network. The selection of the CAV and HDV models are provided in the Appendices.

5.4.1 System description

The mixed traffic simulations are implemented in MATLAB environment. The simulations include sufficient number of vehicles to flow through the signalized intersection within the green light phase. The traffic light signal additionally provides leader speed information to CAVs.

Traffic parameters

The traffic parameters are selected as discussed below.

1. Control gain α: The desired time period T_s of vehicles for accelerating to a target cruise speed varies from 5 to 10 seconds, depending on the surrounding traffic speed and the type of vehicles [68]. In the following, the control gain is selected as $\alpha = 2/3$ to match the desired time period T_s of 6 seconds. From Eq. (5.15), the equivalent headway time is given by $\lambda = 1/\alpha = 1.5$ s.

2. Signal time T: The traffic signal time, denoting the green phase of the intersection when vehicles are allowed to pass, depends on the location of the signalized intersection in the road network, as well as the speed limit of the road. In this following, the signal time is selected as $T = 25$ seconds [69].

3. Target inter-vehicle spacing d_0: The desired inter-vehicle constant spacing $d_0 = 10$

m_i (kg)	τ_i (s^{-1})	$k_{d,i}$ (kg/m)	$d_{m,i}$ (kgm/s^2)	$a_{max}(m/s^{-2})$	$a_{min}(m/s^{-2})$
1800	0.25	0.45	4	7	-7
$\lambda(s)$	$\bar{d}(m)$	$\bar{\tau}(s)$	$\Delta t(s)$	V_s	σ_r
1.5	10	20	0.01	0.01	0.05

Table 5.1: Vehicle model and improved intelligent driver model (IIDM) parameters

meters is selected as twice the mid-size vehicle length of a 2023 Toyota Camry as 192.1 inches (about 5 meters) [70].

Vehicle model

The vehicle dynamics in Eq. (5.3) for the simulations is considered to be, similar to [8],

$$\frac{d}{dt}\hat{a}_i = b(\hat{v}_i, \hat{a}_i) + a(\hat{v}_i)\hat{u}_i(t) \tag{5.74}$$

with

$$a(\hat{v}_i) = \frac{1}{m_i \tau_i} \tag{5.75}$$

$$b(\hat{v}_i, \hat{a}_i) = -2\frac{k_{d,i}}{m_i}\hat{v}_i\hat{a}_i - \frac{1}{\tau_i}\left(\hat{a}_i + \frac{k_{d,i}}{m_i}\hat{v}_i^2 + \frac{d_{m,i}}{m_i}\right) \tag{5.76}$$

where m_i is the mass of the i^{th} vehicle, τ_i is the vehicle's engine constant, $k_{d,i}$ is the drag coefficient, $d_{m,i}$ is the mechanical drag. The vehicle network is homogeneous and the values of above parameters are listed in Table 5.1, selected the same as in [8].

Control parameters

The control parameters for stable pole-zero cancellation using Eq. (5.7), and for the no-DSR (Eq. (5.16)) and DSR (Eq. (5.25)) control updates used in the simulations are discussed in this section.

1. Feedback controller $C_{fb}(s)$ and $C_{ff}(s)$: To place cancelled poles on the open-left-half plane, the feedback controllers are selected as

$$C_{ff}(s) = s^2 + 4s + 4, \qquad C_{fb} = 4s^2 + 4s \tag{5.77}$$

with $k_1 = k_0 = 4$. With above selections of $C_{fb}(s)$ and $C_{ff}(s)$, the cancelled poles $p_{1,2}$ are placed at

$$p_{1,2} = \{s \in \mathbb{R} | s^2 + k_1 s + k_0 = 0\} = -2. \tag{5.78}$$

For onboard implementation, the controllers need to compute the derivatives of incoming signal numerically. Therefore, a low-pass filter with cutoff frequency $w_f = 40\alpha$ (where $\alpha = 2/3$ is the control gain) is added to remove high-frequency noise before computing time derivatives, which results in a modified feedback controller

$$C_{ff}(s) = \frac{\omega_f}{s + \omega_f}(s^2 + 4s + 4). \tag{5.79}$$

2. DSR delay τ_d: The DSR delay depends on the update rate of the local sensors. Typically for vehicles with Advance Driver Assistance System (ADAS), the local sensing delay varies between 0.1 to 0.3 s [47, 48]. In this simulation, the DSR delay is selected as $\tau_d = 0.1s$.

3. Gain γ: According to the criterion established in [1], the gain γ is constrained by

$$\gamma < \gamma^* = \sqrt{1/(\alpha\tau_d + 1)} = 0.968 \tag{5.80}$$

for string stability. Besides, the gain γ is constrained within $\gamma \in (0.5, 1]$ for internal stability. To retain robustness of the network, the gain is selected as $\gamma = 0.95$ in order to satisfy above constraints and reduce the steady state error for decentralized vehicles.

5.4.2 Metrics for improvement in traffic capacity

The improvement I on recovering the ideal traffic capacity $N_{p,idl}$ with the use of DSR can be estimated using $N_{p,idl}$ from Eq. (5.49), traffic capacity estimate without DSR $\tilde{N}_{p,n}$ from

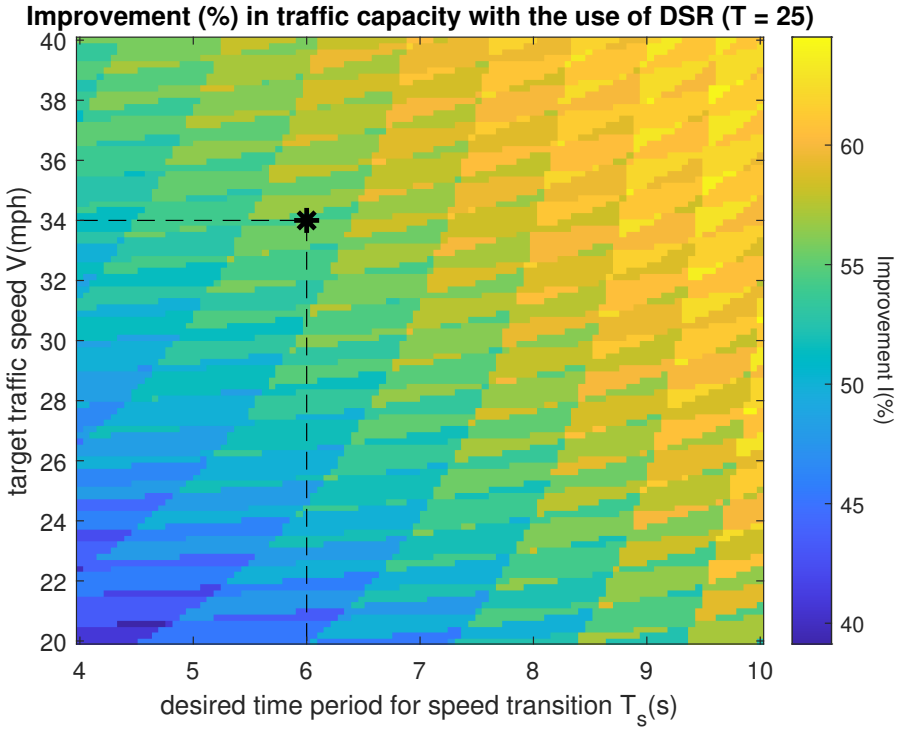

Figure 5.1: DSR improves traffic capacity (right vertical azis) over a wide range of desired time period T_s (horizontal axis), and target traffic speed V (left vertical axis), according to Eq. (5.81).

Eq. (5.62) and traffic capacity estimate with DSR $\tilde{N}_{p,d}$ from Eq. (5.73)

$$I = \left(\frac{\tilde{N}_{p,d} - \tilde{N}_{p,n}}{N_{p,idl}} \right) \times 100\%. \tag{5.81}$$

With the use of DSR on an all-AV network, improvement in the traffic capacity I, ranging from 40% to 60%, is seen over a large range of desired time period T_s from 4 s to 10 s, and target traffic speed V from 20 mph to 40 mph as seen in Fig. 5.1. For instance, with a desired time period $T_s = 6$ and target traffic speed $V = 34$ mph, the estimated improvement I with the use of DSR is 57%, as illustrated by the black star in Fig. 5.1.

5.4.3 Comparative simulations of single-lane capacity, with and without DSR

Comparative MATLAB simulations indicate the use of DSR reduces the cumulative spacing error of the all-AV network, therefore it improves the traffic capacity of the AV network, defined as number of vehicles passing through the intersection within the chosen traffic signal time. Furthermore, the benefits from using DSR is preserved when it is applied to the AVs in a mixed traffic network. DSR improves the traffic capacity of a mixed traffic network on average compared to the no-DSR approach.

To determine the average performance in mixed traffic with different market-penetration rates, the mean traffic capacity is computed from various simulations with random assigned order of vehicles in the network. In order to determine the number of simulations such that the mean traffic capacity converges, a pre-checked simulation is conducted at a selected market-penetration rate (CAVs:HDVs:AVs = 3:3:4) with different numbers of simulations. The result shows that the mean traffic capacity differs within ± 0.25 when the number of iteration is greater than 65 runs, as illustrated by Fig. 5.2. Therefore, the number of runs for the mixed traffic simulation is selected as 70 in the following.

Predicted traffic capacity matches simulation results

The explicit approximations of the cumulative spacing loss function $\tilde{f}_{n,i}$ in Eq. (5.60) and $\tilde{f}_{d,i}$ in Eq (5.72) provide good estimations for the actual cumulative spacing loss function $f_{n,i}$ and $f_{d,i}$, as shown in Fig. 5.3. Specifically, with α and d_0 selected the same as in Table. 5.1, and the target speed $V = 34$ mile-per-hour (mph), i.e., 15 m/s, the maximum approximation error using $\tilde{f}_{n,i}$ for no-DSR AV network ($|f_{n,i}(T) - \tilde{f}_{n,i}(T)|$) is within 7%, and within 1% using $\tilde{f}_{d,i}$ for DSR AV network ($|f_{d,i}(T) - \tilde{f}_{d,i}(T)|$). Furthermore, all DSR AV network results in smaller cumulative spacing loss, compared with all no-DSR AV network, and therefore better traffic capacity, as illustrated by Fig. 5.3.

The traffic capacity estimations for the ideal network Eq. (5.49), no-DSR network Eq. (5.62) and DSR network Eq. (5.73) are verified by the all-AV simulations, illustrated by Fig. 5.3

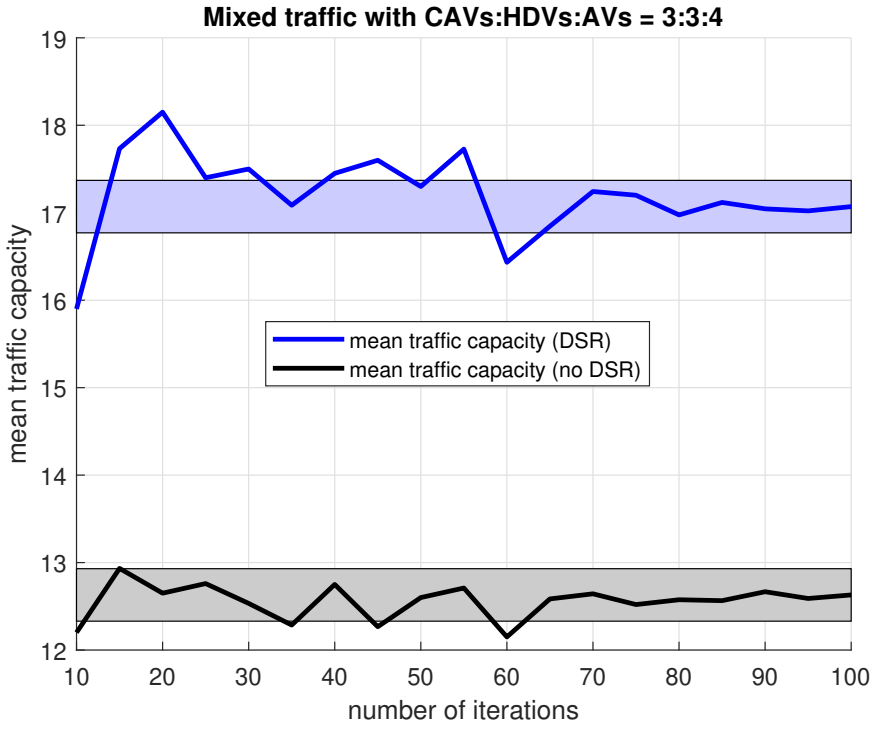

Figure 5.2: The mean capacity (for both cases with and without DSR) converges within ± 0.25 vehicles when the number of simulations are greater than 65 runs.

with selected parameters. Compared with no-DSR network, For instance, at the target speed $V = 34$ mph, the traffic capacity from numerical simulations with DSR is $N_{p,d} = 32$, which is the same as the estimated traffic capacity $\tilde{N}_{p,d} = 32$, computed by substituting $\alpha, \gamma, V, T, d_0$ into Eq. (5.73). In the meanwhile, without the use of DSR, the traffic capacity $N_{p,n} = 12$ from the simulations, which is very close to the predicted value $\tilde{N}_{p,n} = 11$ by substituting α, V, T, d_0 into Eq. (5.62), as illustrated by Fig. 5.4. The analytical prediction of the capacity improvement from Eq. (5.81) is small — difference from the simulation results is within 5%. For instance, at the target speed $V = 34$ mph, the predicted improvements from Eq. (5.81) is $(32 - 11)/36 \cdot 100\% = 58.3\%$, which compares well with the improvement computed from the simulation $(32 - 12)/36 \cdot 100\% = 55.5\%$, as illustrated by the right plot of Fig. 5.4.

Note that the capacity with AVs is not expected to be much higher than with HDVs since the response time and the range of the headway time of the ACC system (1.1 to 4.1s) is similar to human drivers (0.6s to 3.8s), as reported in [36]. Moreover, the inter-spacing distance between vehicles increases as the target speed V increases for no-DSR AVs and HDVs, which results in increased spacing. Therefore, the traffic capacity with no-DSR AVs and HDVs does not increase substantially with speed V when compared to DSR AVs and ideal CAVs.

DSR improves the traffic capacity of the all-AV network

The DSR method reduces the spacing loss of the agents to its leader, compared with no-DSR method. In low-speed zone when the traffic target speed $V = 20$ mph, the traffic capacity of the ideal network is $N_{p,idl} = 21$ vehicles. The traffic capacity of the DSR AV network is $N_{p,d} = 20$ vehicles, which is about 95% of the ideal case (with centralized communication), compared with the no-DSR AV network $N_{p,n} = 9$ vehicles, which is about 43% of the ideal cases. Therefore in this case, the use of DSR recovers the ideal traffic throughput by $I = (20 - 9)/21 \cdot 100\% = 52\%$. In the high-speed zone when the traffic target speed $V = 40$ mph, the traffic capacity of the ideal CAV network is $N_{p,idl} = 42$ vehicles. The traffic capacity of the DSR AV network is $N_{p,d} = 37$ vehicles, which is about 88% of the ideal case, compared

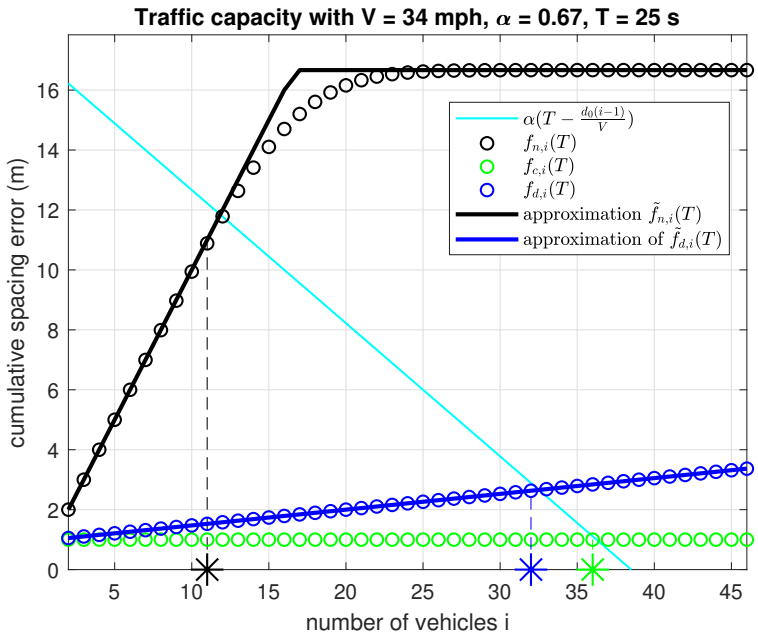

Figure 5.3: All DSR AV network achieves better traffic capacity N_p by reducing the cumulative spacing loss. The solid lines are the numerical solutions of the cumulative spacing loss $f_{c,i}(T)$ from Eq. (5.48) for ideal network, $f_{d,i}(T)$ from Eq. (5.72) for All DSR AV network and $f_{n,i}(T)$ from Eq. (5.60) for no-DSR AV network. Dashlines are the analytical approximation of the spacing loss $\tilde{f}_{d,i}(T)$ for All DSR AV network and $\tilde{f}_{n,i}(T)$ for no-DSR AV network. The star markers are the estimated traffic capacity $N_{p,idl} = 36$ for ideal network (green) from Eq. (5.49), $\tilde{N}_{p,n} = 11$ for no-DSR network (black) from Eq. (5.62) and $\tilde{N}_{p,d} = 32$ for DSR network (black) from Eq. (5.73).

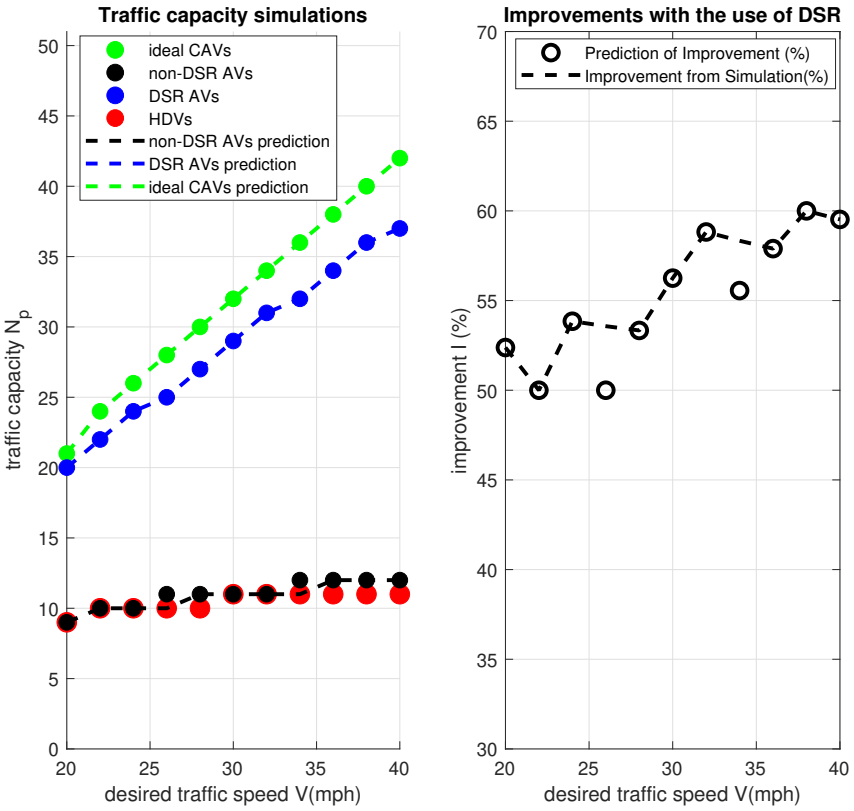

Figure 5.4: DSR improves the traffic capacity compared without the use of DSR on AVs with different target speed V (left plot) The dotted data points are from MATLAB simulations, while the dash-lines are computed from the capacity prediction Eqs. (5.49), (5.62) and (5.73), as well as the prediction of improvement I Eq. (5.81)(right plot)

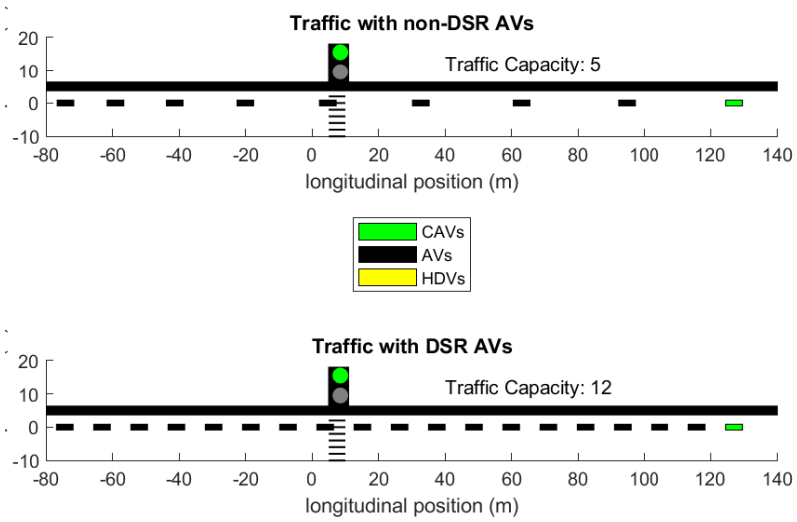

Figure 5.5: DSR AV network maintains higher traffic capacity compared with no-DSR network: With the target speed $V = 34$ mph and 10 s after the traffic signal turns green, the DSR AV network (bottom plot) has less spacing loss from the leader (the green box) and thus allows more vehicles (12) compared with the no-DSR AV network (top plot) with 5 vehicles during the same amount of time. Therefore, the use of DSR on AVs improves the traffic capacity of the all-AV network. Video is available at `https://youtu.be/xGiAI4IXVns` , as well as in supplementary material.

with the no-DSR AV network $N_{p,n} = 12$ vehicles, which is about 29% of the ideal cases. In this case, the use of DSR recovers the ideal traffic throughput by $I = (37 - 12)/42 \cdot 100\% = 59\%$. Therefore, the use of DSR improves the traffic capacity through different range of traffic speed. Fig. 5.5 demonstrates an example of the AV networks 10 s after the traffic light turning to green with the target traffic speed $V = 34$ mph. Overall, from Fig. 5.6, the use of DSR without V2I communication (32 vehicles for all DSR AVs) captures most of the capacity increase of CAVs (36 vehicles for all CAVs) with V2I communication.

DSR improves the traffic capacity of mixed traffic networks

The use of DSR on AVs improves the traffic capacity of a mixed network, with different market-penetration rate of HDVs and CAVs. The level of improvements decreases as the market-penetration rate of HDVs increases. However the use of DSR guarantees improvements on the traffic capacity N_p when the mixed traffic has at least 20% the AVs, or no more than 50% HDVs, as Fig. 5.6 illustrates. Specifically, when the mixed traffic has 30% CAVs, 30% HDVs and 40% AVs, the average improvement I from the use of DSR on AVs is 17% of the ideal capacity; and when the mixed traffic has 30% AVs, the average improvement I from the use of DSR varies from $6\% - 36\%$. The capacity improvement when using DSR also is not impacted significantly by the order of different types of vehicles in the network since the standard deviation shows that the traffic capacity varies within 14% of the mean capacity with different orders of vehicles, as illustrated by Fig. 5.7. Thus, the use of DSR on AVs improves the traffic capacity N_p of mixed traffic with various market-penetration rate of HDVs and CAVs.

5.4.4 Comparison of intersection capacity using SUMO, with and without DSR

The proposed DSR approaches ability to improve capacity at intersections is also assessed using Simulation of Urban MObility (SUMO), where the car-following dynamics are simulated together with lane-changing model, intersection models and collision avoidance models

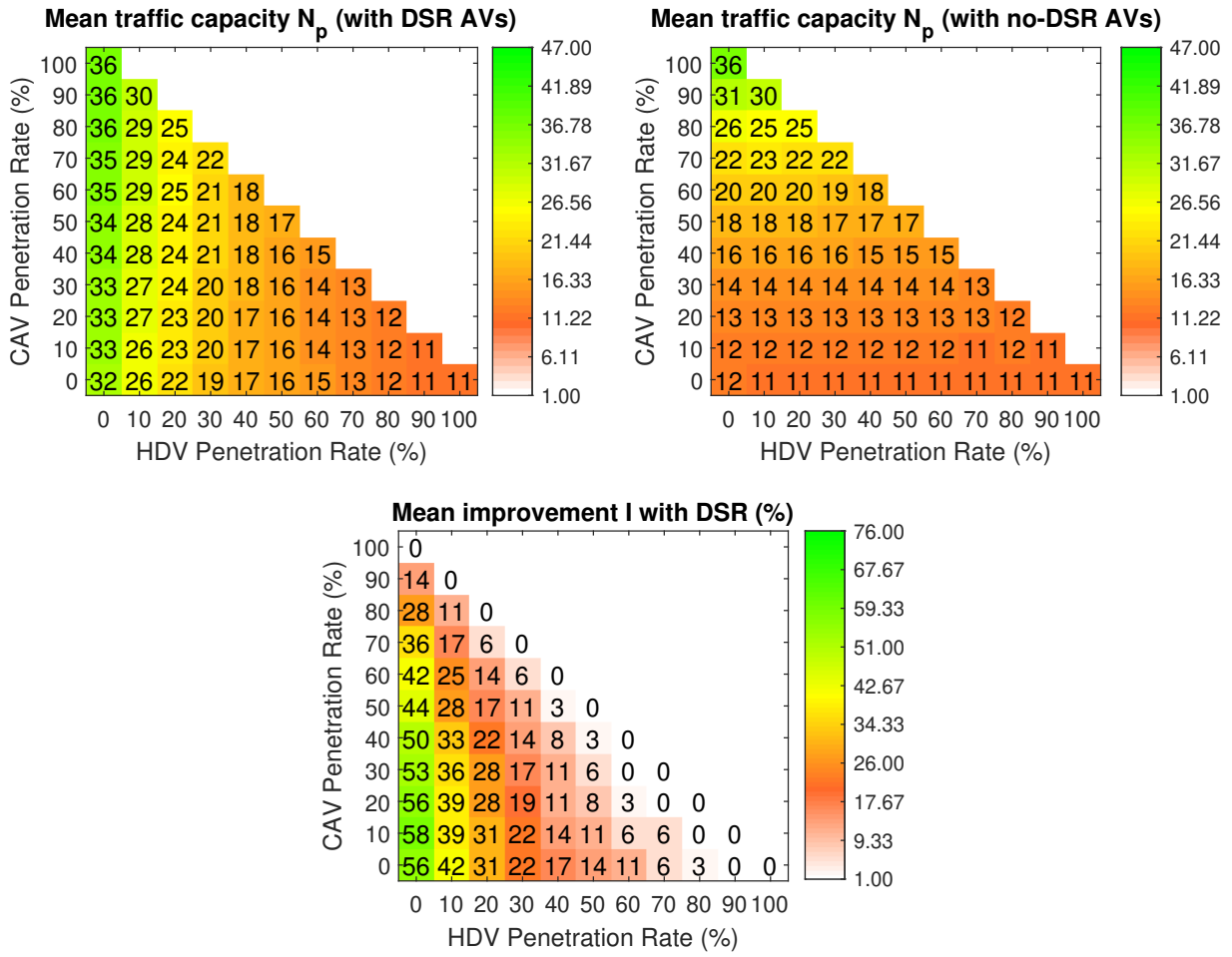

Figure 5.6: Mixed traffic capacity with $V = 34$ mph. DSR guarantees improvements on the traffic capacity N_p when the mixed traffic has no more than 50% of HDVs, or when the mixed traffic has at least 20% of the AVs with the use of DSR. DSR results in improvements even with 70% HDVs and 30% AVs .

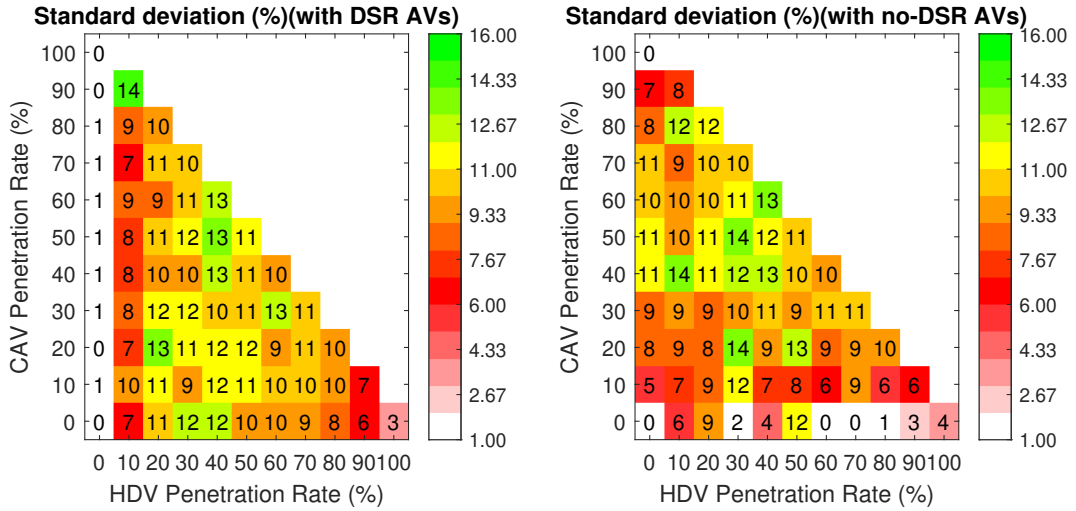

Figure 5.7: Standard deviation (as a percentage of the mean capacity) for the mixed traffic simulation.

to provide more realistic traffic simulations. Comparative evaluations are performed, with and without DSR, for mixed traffic with selected market penetration rates of HDVs.

SUMO settings

The satellite view and the snapshot of the SUMO intersection model of the intersection selected at Fairview Ave and Denny way, Seattle, WA as in [71] are shown in Fig. 5.8. The target traffic speed $V = 34$ mph, and the speed limit is set as 40 mph to match the conditions in Section 5.4.3. The phase information of the traffic light and the volume of the traffic are provided in Fig.5.9. The volume of the traffic is selected to be be high to evaluate the maximum capacity, and the volume ratios among different routes are selected as typical values [71]. Pedestrians in crossings are not modeled to focus the comparative evaluations with and without DSR. The intersection is defined as a 40 m $\times$ 40 m square area, and the vehicle is considered to have passed the intersection once it moves out of the square area. The net traffic capacity N_p is calculated by summing the vehicles passing through all the

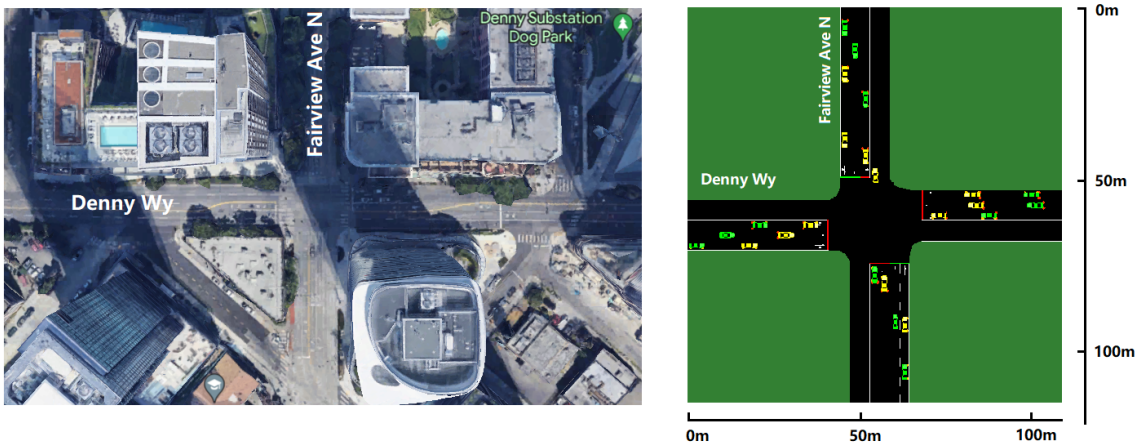

Figure 5.8: Satellite view [3] of the intersection (left) at Fairview and Denny way in Seattle, USA, evaluated with the intersection model in SUMO platform (right).

Light Phase	Time (s)	Volume (vehs/h, both directions)
Fairview Ave straight & right turn traffic	1-33, 37 - 108	1500 (straight) 250 (right turn)
Fairview Ave left turn traffic	1-36, 37-52, 56-110	250
Denny Way straight & right turn traffic	1-55, 56-89, 92-110	1500 (straight) 250 (right turn)
Denny Way left turn traffic	1-89, 92-107	250

Figure 5.9: The phase information of the traffic light (one cycle).

directions (North/South/West/East).

In the SUMO environment, DSR AV models are combined with lane-changing models and intersection models, which determines the right-of-way of the vehicles. Compared with MATLAB simulations in Section 5.4.3, SUMO simulations are different in terms of the engagement of autonomous car-following, specifically, AVs /CAVs will return to human-driven mode under the following three scenarios: (i) a neighbor vehicle is merging into the lane to the front, (ii) there is no preceding vehicle in front, or (iii) the traffic signal is red and the vehicle is within 50 meters of passing the intersection.

DSR improves intersection capacity

The use of DSR without V2I communication captures most of the improvements of CAVS with V2I communication – even in the real-world intersection simulations with SUMO. For instance, the DSR AV network has a capacity of 1248 which is close to 1302 (95.8%) of the all CAV network. Even when the mixed traffic has 30% CAVs, 30% HDVs and 40% AVs, the improvement I from the use of DSR is 15% from SUMO simulations as illustrated in Fig. 5.10, which is comparable to the improvement $I = 17\%$ for the single lane in Fig. 5.6. Therefore, capacity is increased with DSR even after considering realistic situations in intersections. Overall, the use of DSR enables close to CAV performance without the need for V2I communication.

5.5 Conclusion

This work investigates the use of delayed-self-reinforcement (DSR) on autonomous vehicles (AVs) within a mixed traffic network with AVs, connected AVs (CAVs) with communication to traffic signal and target traffic speed information, as well as human driven vehicles (HDVs). DSR mimics the ideal centralized control command in a decentralized manner and as a result, the spacing error of AVs with DSR is reduced compared to the case without DSR. Therefore, the use of DSR without V2I communication captures most of the capacity increase of CAVs with V2I communication. The improvement with DSR is shown with both analytical methods and numerical simulations and the improvement is seen even with mixed traffic conditions under realistic intersection simulations.

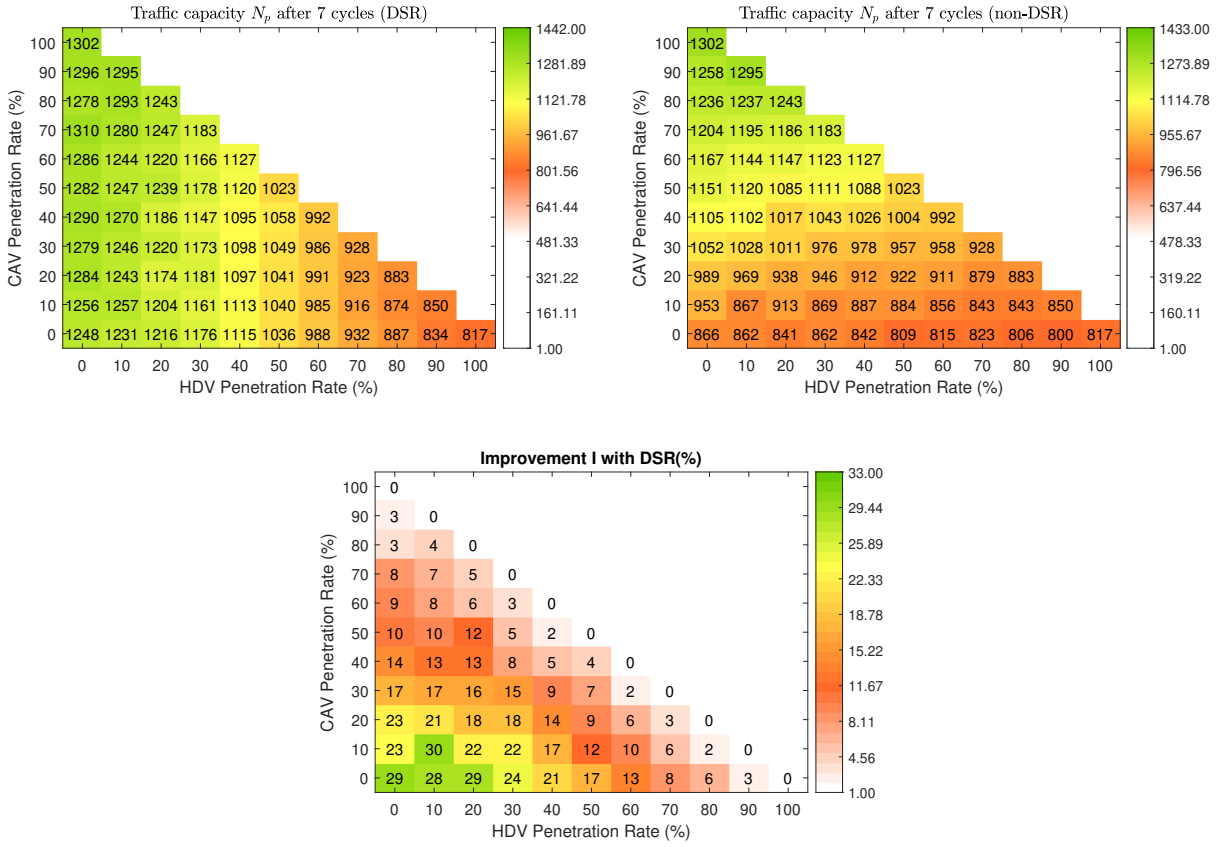

Figure 5.10: DSR improves the traffic capacity compared without the use of DSR on AVs from SUMO simulations. Capacity is evaluated after the intersection is loaded, for cycles 2-8.

Chapter 6

CONCLUSION AND FUTURE WORK

This thesis investigates the use of delayed-self-reinforcement (DSR) on autonomous vehicles (AVs), including its internal stability and string stability conditions. Furthermore, the performance of DSR has been examined via realistic simulation platform (SUMO) which constructs a mixed traffic network with AVs, connected AVs (CAVs) with communication to traffic signal and target traffic speed information, as well as human driven vehicles (HDVs). The improvement with DSR is shown via both analytical methods and numerical simulations and the improvement is seen even with mixed traffic conditions under realistic intersection simulations.

In the future work, drive quality and fuel economy will be considered in the design of DSR-based car-following approaches. The impact of the use of DSR can be further examined via larger-scale traffic simulations. The advantages brought by using DSR can be integrated with vehicle-to-infrastructure (V2I) control which shows great potential to improve the traffic coordination.

BIBLIOGRAPHY

[1] Yudong Lin, Anuj Tiwari, Brian Fabien, and Santosh Devasia. Constant-spacing connected platoons with robustness to communication delays. *IEEE Transactions on Intelligent Transportation Systems*, pages 1–13, 2023.

[2] Yudong Lin, Anuj Tiwari, Brian Fabien, and Santosh Devasia. Safely increasing capacity of traffic intersections with mixed autonomous vehicles using delayed self reinforcement. In *8th Indian Control Conference (ICC 2022)*, 2022.

[3] Google. Google maps locations for fairview ave n and denny way,seattle,wa. 2023.

[4] Darbha Swaroop and J Karl Hedrick. Constant spacing strategies for platooning in automated highway systems. *J. Dyn. Sys., Meas., Control*, 121(3):462–470, 1999.

[5] Assad Alam, Bart Besselink, Valerio Turri, Jonas Mårtensson, and Karl H Johansson. Heavy-duty vehicle platooning for sustainable freight transportation: A cooperative method to enhance safety and efficiency. *IEEE Control Systems Magazine*, 35(6):34–56, 2015.

[6] Shengbo Eben Li, Yang Zheng, Keqiang Li, Yujia Wu, J Karl Hedrick, Feng Gao, and Hongwei Zhang. Dynamical modeling and distributed control of connected and automated vehicles: Challenges and opportunities. *IEEE Intelligent Transportation Systems Magazine*, 9(3):46–58, 2017.

[7] Pete Seiler, Aniruddha Pant, and Karl Hedrick. Disturbance propagation in vehicle strings. *IEEE Transactions on Automatic Control*, 49(10):1835–1842, 2004.

[8] Petros A Ioannou and Cheng-Chih Chien. Autonomous intelligent cruise control. *IEEE Transactions on Vehicular technology*, 42(4):657–672, 1993.

[9] Lian Cui, Zheng Chen, Aobo Wang, Jia Hu, and Byungkyu Brian Park. Development of a robust cooperative adaptive cruise control with dynamic topology. *IEEE Transactions on Intelligent Transportation Systems*, pages 1–12, 2021.

[10] Yonggui Liu, Huanli Gao, Chunjie Zhai, and Wei Xie. Internal stability and string stability of connected vehicle systems with time delays. *IEEE Transactions on Intelligent Transportation Systems*, 22(10):6162–6174, 2021.

[11] Xiangheng Liu, A. Goldsmith, S.S. Mahal, and J.K. Hedrick. Effects of communication delay on string stability in vehicle platoons. In *ITSC 2001. 2001 IEEE Intelligent Transportation Systems. Proceedings (Cat. No.01TH8585)*, pages 625–630, 2001.

[12] Mate Boban and Pedro M. d'Orey. Exploring the practical limits of cooperative awareness in vehicular communications. *IEEE Transactions on Vehicular Technology*, 65(6):3904–3916, 2016.

[13] Johan Karedal, Nicolai Czink, Alexander Paier, Fredrik Tufvesson, and Andreas F. Molisch. Path loss modeling for vehicle-to-vehicle communications. *IEEE Transactions on Vehicular Technology*, 60(1):323–328, 2011.

[14] Sadayuki Tsugawa, Sabina Jeschke, and Steven E Shladover. A review of truck platooning projects for energy savings. *IEEE Transactions on Intelligent Vehicles*, 1(1):68–77, 2016.

[15] Santosh Devasia. Cohesive networks using delayed self reinforcement. *Automatica*, 112:108699, 2020.

[16] Bin Tian, Xiaofeng Deng, Zhigang Xu, Yuqin Zhang, and Xiangmo Zhao. Modeling and numerical analysis on communication delay boundary for CACC string stability. *IEEE Access*, 7:168870–168884, 2019.

[17] Yu Zhang, Yu Bai, Meng Wang, and Jia Hu. Cooperative adaptive cruise control with robustness against communication delay: An approach in the space domain. *IEEE Transactions on Intelligent Transportation Systems*, 22(9):5496–5507, 2021.

[18] Yongfu Li, Chuancong Tang, Srinivas Peeta, and Yibing Wang. Nonlinear consensus-based connected vehicle platoon control incorporating car-following interactions and heterogeneous time delays. *IEEE Transactions on Intelligent Transportation Systems*, 20(6):2209–2219, 2018.

[19] Jeroen Ploeg, Elham Semsar-Kazerooni, Guido Lijster, Nathan van de Wouw, and Henk Nijmeijer. Graceful degradation of cooperative adaptive cruise control. *IEEE Transactions on Intelligent Transportation Systems*, 16(1):488–497, 2014.

[20] Chaoxian Wu, Yuan Lin, and Azim Eskandarian. Cooperative adaptive cruise control with adaptive kalman filter subject to temporary communication loss. *IEEE Access*, 7:93558–93568, 2019.

[21] Jaswandi Sawant, Uttam Chaskar, and Divyesh Ginoya. Robust control of cooperative adaptive cruise control in the absence of information about preceding vehicle acceleration. *IEEE Transactions on Intelligent Transportation Systems*, 22(9):5589–5598, 2021.

[22] J Piao and Mike McDonald. Advanced driver assistance systems from autonomous to cooperative approach. *Transport reviews*, 28(5):659–684, 2008.

[23] Arash Olia, Saiedeh Razavi, Baher Abdulhai, and Hossam Abdelgawad. Traffic capacity implications of automated vehicles mixed with regular vehicles. *Journal of Intelligent Transportation Systems*, 22(3):244–262, 2018.

[24] Tessa Tielert, Moritz Killat, Hannes Hartenstein, Raphael Luz, Stefan Hausberger, and Thomas Benz. The impact of traffic-light-to-vehicle communication on fuel consumption and emissions. In *2010 Internet of Things (IOT)*, pages 1–8. IEEE, 2010.

[25] Behrang Asadi and Ardalan Vahidi. Predictive cruise control: Utilizing upcoming traffic signal information for improving fuel economy and reducing trip time. *IEEE transactions on control systems technology*, 19(3):707–714, 2010.

[26] Bokui Chen, Duo Sun, Jun Zhou, Wengfai Wong, and Zhongjun Ding. A future intelligent traffic system with mixed autonomous vehicles and human-driven vehicles. *Information Sciences*, 529:59–72, 2020.

[27] Todd Litman. *Autonomous vehicle implementation predictions*. Victoria Transport Policy Institute Victoria, Canada, 2017.

[28] Aidin Ferdowsi, Samad Ali, Walid Saad, and Narayan B Mandayam. Cyber-physical security and safety of autonomous connected vehicles: Optimal control meets multi-armed bandit learning. *IEEE Transactions on Communications*, 67(10):7228–7244, 2019.

[29] Ziran Wang, Guoyuan Wu, and Matthew J Barth. A review on cooperative adaptive cruise control (CACC) systems: Architectures, controls, and applications. In *2018 21st International Conference on Intelligent Transportation Systems (ITSC)*, pages 2884–2891. IEEE, 2018.

[30] Valerio Turri, Bart Besselink, and Karl H Johansson. Cooperative look-ahead control for fuel-efficient and safe heavy-duty vehicle platooning. *IEEE Transactions on Control Systems Technology*, 25(1):12–28, 2016.

[31] Santosh Devasia. Faster response in bounded-update-rate, discrete-time linear networks using delayed self-reinforcement. *International Journal of Control*, 94(5):1286–1296, 2021.

[32] Jakob Axelsson. Safety in vehicle platooning: A systematic literature review. *IEEE Transactions on Intelligent Transportation Systems*, 18(5):1033–1045, 2016.

[33] Pengyuan Sun, Daisik Nam, R Jayakrishnan, and Wenlong Jin. An eco-driving algorithm based on vehicle to infrastructure (v2i) communications for signalized intersections. *Transportation Research Part C: Emerging Technologies*, 144:103876, 2022.

[34] Jeroen Ploeg, Elham Semsar-Kazerooni, Guido Lijster, Nathan van de Wouw, and Henk Nijmeijer. Graceful degradation of cacc performance subject to unreliable wireless communication. In *16th International IEEE Conference on Intelligent Transportation Systems (ITSC 2013)*, pages 1210–1216. IEEE, 2013.

[35] Michail Makridis, Konstantinos Mattas, and Biagio Ciuffo. Response time and time headway of an adaptive cruise control. an empirical characterization and potential impacts on road capacity. *IEEE Transactions on Intelligent Transportation Systems*, 21(4):1677–1686, 2020.

[36] Michail Makridis, Konstantinos Mattas, Aikaterini Anesiadou, and Biagio Ciuffo. Openacc. an open database of car-following experiments to study the properties of commercial acc systems. *Transportation research part C: emerging technologies*, 125:103047, 2021.

[37] Ali Bidram, Frank L. Lewis, and Ali Davoudi. Synchronization of nonlinear heterogeneous cooperative systems using input–output feedback linearization. *Automatica*, 50(10):2578–2585, 2014.

[38] Linjun Zhang, Jing Sun, and Gábor Orosz. Hierarchical design of connected cruise control in the presence of information delays and uncertain vehicle dynamics. *IEEE Transactions on Control Systems Technology*, 26(1):139–150, 2018.

[39] H.K. Khalil. *Nonlinear Systems*. Pearson Education. Prentice Hall, 2002.

[40] W. T. Tuttle. *Graph Theory*. Cambridge University Press, Cambridge, 2001.

[41] Furqan Jameel, Muhammad Awais Javed, and Duy Trong Ngo. Performance analysis of cooperative V2V and V2I communications under correlated fading. *IEEE Transactions on Intelligent Transportation Systems*, 21(8):3476–3484, 2020.

[42] Frank L Lewis, Hongwei Zhang, Kristian Hengster-Movric, and Abhijit Das. *Cooperative control of multi-agent systems: optimal and adaptive design approaches*. Springer Science & Business Media, 2013.

[43] Tamás Insperger and Gábor Stépán. *Semi-discretization for time-delay systems: stability and engineering applications*, volume 178. Springer Science & Business Media, 2011.

[44] William S Levine. *The Control Handbook (three volume set)*. CRC press, 2018.

[45] Vicente Milanés, Steven E. Shladover, John Spring, Christopher Nowakowski, Hiroshi Kawazoe, and Masahide Nakamura. Cooperative adaptive cruise control in real traffic situations. *IEEE Transactions on Intelligent Transportation Systems*, 15(1):296–305, 2014.

[46] J. Zhang and P.A. Ioannou. Longitudinal control of heavy trucks in mixed traffic: environmental and fuel economy considerations. *IEEE Transactions on Intelligent Transportation Systems*, 7(1):92–104, 2006.

[47] Meng Wang, Serge Paul Hoogendoorn, Winnie Daamen, Bart van Arem, Barys Shyrokau, and Riender Happee. Delay-compensating strategy to enhance string stability of adaptive cruise controlled vehicles. *Transportmetrica B: Transport Dynamics*, 6(3):211–229, 2018.

[48] Lingyun Xiao and Feng Gao. Practical string stability of platoon of adaptive cruise control vehicles. *I1EEE Transactions on Intelligent Transportation Systems*, 12(4):1184–1194, 2011.

[49] Jurgen Hasch. Driving towards 2020: Automotive radar technology trends. In *2015 IEEE MTT-S International Conference on Microwaves for Intelligent Mobility (ICMIM)*, pages 1–4. IEEE, 2015.

[50] Richard D Braatz. On internal stability and unstable pole-zero cancellations [feedback]. *IEEE Control Systems Magazine*, 32(5):15–16, 2012.

[51] Gerrit J. L. Naus, René P. A. Vugts, Jeroen Ploeg, Marinus J. G. van de Molengraft, and Maarten Steinbuch. String-stable CACC design and experimental validation: A frequency-domain approach. *IEEE Transactions on Vehicular Technology*, 59(9):4268–4279, 2010.

[52] Srdjan S Stankovic, Milorad J Stanojevic, and Dragoslav D Siljak. Decentralized overlapping control of a platoon of vehicles. *IEEE Transactions on Control Systems Technology*, 8(5):816–832, 2000.

[53] Steven E Shladover. Longitudinal control of automotive vehicles in close-formation platoons. 1991.

[54] Y. Lin, A. Tiwari, B. Fabien, and S. Devasia. Constant-spacing connected platoons with robustness to communication delays. *IEEE Transactions on Intelligent Transportation Systems*, page submitted, 2022.

[55] Washington state commercial vehicle guide. https://www.wsdot.wa.gov/publications/manuals/fulltext/M30-39/CVG.pdf.

[56] Soufiene Djahel, Ronan Doolan, Gabriel-Miro Muntean, and John Murphy. A communications-oriented perspective on traffic management systems for smart cities: Challenges and innovative approaches. *IEEE Communications Surveys & Tutorials*, 17(1):125–151, 2014.

[57] Zhihong Yao, Yunxia Wu, Yi Wang, Bin Zhao, and Yangsheng Jiang. Analysis of the impact of maximum platoon size of cavs on mixed traffic flow: An analytical and simulation method. *Transportation Research Part C: Emerging Technologies*, 147:103989, 2023.

[58] Shian Wang, Mingfeng Shang, Michael W Levin, and Raphael Stern. A general approach to smoothing nonlinear mixed traffic via control of autonomous vehicles. *Transportation Research Part C: Emerging Technologies*, 146:103967, 2023.

[59] Ketan Savla, Lili Du, Samitha Samaranayake, Xuegang Jeff Ban, and Alexandre M. Bayen. Guest editorial special issue on modeling dynamic transportation networks in the age of connectivity, autonomy and data. *IEEE Transactions on Intelligent Transportation Systems*, 23(4):3802–3803, 2022.

[60] Mohammed Hamad Almannaa, Hao Chen, Hesham A Rakha, Amara Loulizi, and Ihab El-Shawarby. Field implementation and testing of an automated eco-cooperative adaptive cruise control system in the vicinity of signalized intersections. *Transportation research part D: transport and environment*, 67:244–262, 2019.

[61] Qinzheng Wang, Yaobang Gong, and Xianfeng Yang. Connected automated vehicle trajectory optimization along signalized arterial: A decentralized approach under mixed traffic environment. *Transportation research part C: emerging technologies*, 145:103918, 2022.

[62] Kay Massow, Ilja Radusch, and Robert Shorten. A numerical study on constant spacing policies for starting platoons at oversaturated intersections. *IEEE Access*, 10:43766–43786, 2022.

[63] Handong Yao and Xiaopeng Li. Decentralized control of connected automated vehicle trajectories in mixed traffic at an isolated signalized intersection. *Transportation research part C: emerging technologies*, 121:102846, 2020.

[64] Liangyao Yu and Ruyue Wang. Researches on adaptive cruise control system: A state of the art review. *Proceedings of the Institution of Mechanical Engineers, Part D: Journal of Automobile Engineering*, 236(2-3):211–240, 2022.

[65] P. Seiler, A. Pant, and K. Hedrick. Disturbance propagation in vehicle strings. *IEEE Transactions on Automatic Control*, 49(10):1835–1842, 2004.

[66] Fangfang Zheng, Can Liu, Xiaobo Liu, Saif Eddin Jabari, and Liang Lu. Analyzing the impact of automated vehicles on uncertainty and stability of the mixed traffic flow. *Transportation research part C: emerging technologies*, 112:203–219, 2020.

[67] Jian Wang, Wei Wang, Gang Ren, and Min Yang. Worst-case traffic assignment model for mixed traffic flow of human-driven vehicles and connected and autonomous vehicles by factoring in the uncertain link capacity. *Transportation research part C: emerging technologies*, 140:103703, 2022.

[68] Vicente Milanés, Steven E Shladover, John Spring, Christopher Nowakowski, Hiroshi Kawazoe, and Masahide Nakamura. Cooperative adaptive cruise control in real traffic situations. *IEEE Transactions on intelligent transportation systems*, 15(1):296–305, 2013.

[69] Ziran Wang, Guoyuan Wu, and Matthew J Barth. Cooperative eco-driving at signalized intersections in a partially connected and automated vehicle environment. *IEEE Transactions on Intelligent Transportation Systems*, 21(5):2029–2038, 2019.

[70] 2023 camry full specs, https://www.toyota.com/camry/features/mpg_other_price/2532/2559/2546. 2023.

[71] Qiangqiang Guo and Xuegang (Jeff) Ban. A multi-scale control framework for urban traffic control with connected and automated vehicles. *Transportation Research Part B: Methodological*, 175:102787, 2023.

[72] Ahmed MH Al-Jhayyish and Klaus Werner Schmidt. Feedforward strategies for cooperative adaptive cruise control in heterogeneous vehicle strings. *IEEE Transactions on Intelligent Transportation Systems*, 19(1):113–122, 2017.

[73] Holger H Meinel and Wolfgang Bösch. Radar sensors in cars. In *Automated driving*, pages 245–261. Springer, 2017.

[74] Guangchuan Yang, Hao Xu, Zhongren Wang, and Zong Tian. Truck acceleration behavior study and acceleration lane length recommendations for metered on-ramps. *International journal of transportation science and technology*, 5(2):93–102, 2016.

[75] Assad Alam, Jonas Mårtensson, and Karl H Johansson. Experimental evaluation of decentralized cooperative cruise control for heavy-duty vehicle platooning. *Control Engineering Practice*, 38:11–25, 2015.

[76] Shi-Yuan Han, Yue-Hui Chen, Lin Wang, and Ajith Abraham. Decentralized longitudinal tracking control for cooperative adaptive cruise control systems in a platoon. In *2013 IEEE International Conference on Systems, Man, and Cybernetics*. IEEE, 2013.

[77] Bart Besselink and Karl H Johansson. String stability and a delay-based spacing policy for vehicle platoons subject to disturbances. *IEEE Transactions on Automatic Control*, 62(9):4376–4391, 2017.

[78] DVAHG Swaroop, J Karl Hedrick, CC Chien, and Petros Ioannou. A comparision of spacing and headway control laws for automatically controlled vehicles1. *Vehicle system dynamics*, 23(1):597–625, 1994.

[79] Linjun Zhang and Gábor Orosz. Nonlinear dynamics of connected vehicle systems with communication delays. In *2015 American Control Conference (ACC)*, pages 2759–2764. IEEE, 2015.

[80] Gerrit JL Naus, Rene PA Vugts, Jeroen Ploeg, Marinus JG van De Molengraft, and Maarten Steinbuch. String-stable CACC design and experimental validation: A frequency-domain approach. *IEEE Transactions on vehicular technology*, 59(9):4268–4279, 2010.

[81] Mihailo R Jovanovic and Bassam Bamieh. On the ill-posedness of certain vehicular platoon control problems. *IEEE Transactions on Automatic Control*, 50(9):1307–1321, 2005.

[82] Prabir Barooah, Prashant G Mehta, and Joao P Hespanha. Mistuning-based control design to improve closed-loop stability margin of vehicular platoons. *IEEE Transactions on Automatic Control*, 54(9):2100–2113, 2009.

[83] W Levine and Michael Athans. On the optimal error regulation of a string of moving vehicles. *IEEE Transactions on Automatic Control*, 11(3):355–361, 1966.

[84] Kai-ching Chu. Decentralized control of high-speed vehicular strings. *Transportation science*, 8(4):361–384, 1974.

[85] Erik Hellström. *Look-ahead control of heavy vehicles*. Department of Eelectrical Engineering, Linköping University, 2010.

[86] ITF Transport Outlook. Int. transport forum, 2015.

[87] C Marcy and B Sanchez. Power sector carbon dioxide emissions fall below transportation sector emissions. *Energy Information Administration. Washington, DC*, 2017.

[88] Anshuman Sharma, Zuduo Zheng, Jiwon Kim, Ashish Bhaskar, and Md Mazharul Haque. Assessing traffic disturbance, efficiency, and safety of the mixed traffic flow of connected vehicles and traditional vehicles by considering human factors. *Transportation research part C: emerging technologies*, 124:102934, 2021.

[89] Dominik Salles, Stefan Kaufmann, and Hans-Christian Reuss. Extending the intelligent driver model in sumo and verifying the drive off trajectories with aerial measurements. In *SUMO User Conference*, 2020.

[90] Vittorio Marzano, Andrea Papola, and Fulvio Simonelli. Limits and perspectives of effective o–d matrix correction using traffic counts. *Transportation Research Part C: Emerging Technologies*, 17(2):120–132, 2009.

[91] Jinsoo You and Tschangho John Kim. Development and evaluation of a hybrid travel time forecasting model. *Transportation Research Part C: Emerging Technologies*, 8(1-6):231–256, 2000.

[92] Rachel M James, Christopher Melson, Jia Hu, and Joe Bared. Characterizing the impact of production adaptive cruise control on traffic flow: An investigation. *Transportmetrica B: Transport Dynamics*, 7(1):992–1012, 2019.

[93] David E Rumelhart, Geoffrey E Hinton, and Ronald J Williams. Learning internal representations by error propagation. parallel distributed processing: Exploration in the microstructure of cognition, vol. 1. *Foundations*, pages 318–362, 1986.

[94] Yurii Evgen'evich Nesterov. A method of solving a convex programming problem with convergence rate o\bigl(k^2\bigr). In *Doklady Akademii Nauk*, volume 269, pages 543–547. Russian Academy of Sciences, 1983.

.1 A:Car-following dynamics of CAV followers

In this section, the control update is developed for CAV followers based on previous work in [88] in which CAVs reduce the use of the leader information as the local inter-spacing decreases since the risk of colliding with the preceding vehicle increases.

Let $\mathcal{N}_c$ represent the set of CAVs in the network such that $1 < n(\mathcal{N}_c) \leq N$. For $i \in \mathcal{N}_c$, the vehicle i is connected to the traffic signal information which provides the leader speed information $\hat{v}_1(t)$. The control update for vehicle i, where $i \in \mathcal{N}_c$, is obtained by augmenting the decentralized PF control law in Eq. (5.8) with the cruise speed command $v_d(s) = \hat{v}_1(s)$

$$u_{c,i}(s) = v_d(s) + u_{std,i}(s), \qquad i \geq 2, \tag{1}$$

where in the simulations with a constant target cruise speed V, the leader speed $\hat{v}_1(s)$ is calculated from Eq. (5.14). Eq. (1) results in the control update $\tilde{u}_i(s)$ for the i^{th} CAV to be,

$$\tilde{u}_i(s) = C_{ff}(s)u_{c,i}(s) - C_{fb}(s)x_i(s). \tag{2}$$

Using the steps similar to Eq. (5.12), the control law in Eq. (2) results in the following CAV dynamics,

$$x_i(s) = \frac{v_d(s) + \alpha x_{i-1}(s)}{s + \alpha}. \tag{3}$$

However, in the mixed traffic environment with other types of vehicles, it is not guaranteed that the information $v_d(t)$ is transmitted to each CAV $i \in \mathcal{N}_c$ without delay. Besides, the predecessor $\hat{x}_{i-1}$ might not track the desired trajectory perfectly. Simply using the target cruise speed command $v_d(s)$ in addition to local sensing command $u_{std,i}$ could result in collisions.

To guarantee safety, the individual target speed for the i^{th} CAV $v_{d,i}(t)$ is scaled with a usefulness function $S(d_i)$ based on the relative spacing d_i, as

$$v_{d,i}(t) = S(d_i)v_d(t), \tag{4}$$

$$S(d_i) = \left(1 + e^{-h_1\left(\frac{d_i - d_0}{d_0} + h_2\right)}\right)^{-1}, \tag{5}$$

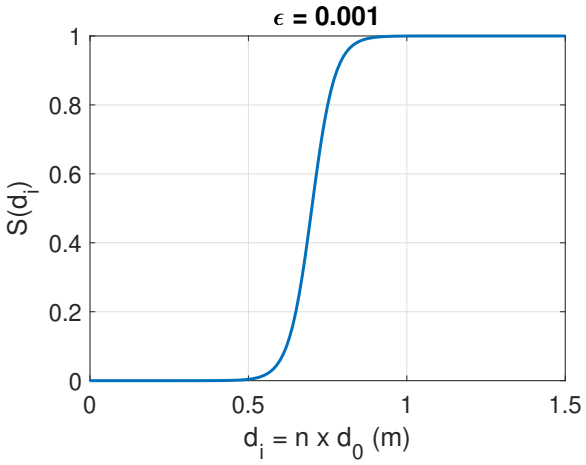

Figure 1: The value of $S(d_0)$ with $\epsilon = 10^{-3}$

where $S(d_i)$ is the usefulness function of the traffic light information $v_d(t)$ [88]. It is a deviated sigmoid function varying from 0 to 1, as shown in Fig. 1.

When the relative spacing of i^{th} vehicle is smaller than desired spacing, i.e. $d_i < d_0$, the V2I communication is less useful since the risk of collision increases, and vice versa. Therefore, the function parameters h_1, h_2 can be selected based on the usefulness of the traffic light information. For example, if the system requires that the traffic light information is fully utilized when $d_i > d_0$ and fully not utilized when $d_i < 0.5d_0$ with tolerance ϵ, then the required usefulness function $S(d_i)$ must satisfy

$$S(d_i) = \epsilon \approx 0, \qquad d_i = 0.5d_0 \tag{6}$$

$$S(d_i) = 1 - \epsilon \approx 1, \qquad d_i = d_0. \tag{7}$$

Then, substituting Eq. (6) and (7) into Eq. (5)

$$-h_1 \left(\frac{1}{2} + h_2 \right) = \ln \frac{1-\epsilon}{\epsilon}, \tag{8}$$

$$-h_1 h_2 = \ln \frac{\epsilon}{1-\epsilon}, \tag{9}$$

which provides a method to select the function parameters, h_1 and h_2, for the usefulness

function $S(d_i)$ based on a chosen tolerance ϵ. Solving Eq. (8), (9) for h_1 and h_2 yields

$$h_1 = 4 \ln \frac{1-\epsilon}{\epsilon}, \qquad h_2 = 0.25. \tag{10}$$

Fig. 1 shows an example usefulness function designed with a tolerance $\epsilon = 0.001$. Thus, using the individualized target speed $v_{d,i}$ for CAV i, which ensures no collision, the revised CAV control law with collision avoidance is given as

$$\tilde{u}_i(s) = C_{ff}(s)(v_{d,i}(s) + u_{std,i}(s)) - C_{fb}(s)x_i(s). \tag{11}$$

where $v_{d,i}(s)$ is the Laplace transform of $v_{d,i}(t)$ in Eq. (4).

.2 B: Human Intelligent Driver Model

The improved intelligent driver model (IIDM) from [89] is implemented to capture the car-following behaviors of the human driven vehicles in the mixed traffic. To model the imperfect estimation capability of human drivers, an estimation error model is implemented together with the IIDM. The IIDM model is a discrete model with time step Δt. Let $\mathcal{N}_h$ as the set of human-driven vehicles in the network such that $1 \leq n(\mathcal{N}_h) \leq N - n(\mathcal{N}_c)$. Then, for each vehicle $i \in \mathcal{N}_h$, the acceleration $\hat{a}_i(t)$ is updated as [88].

$$\hat{a}_i(t+\Delta t) = \begin{cases} a_{max}\left(1 - \left(\frac{d_i^*(t)}{\tilde{d}_i(t)}\right)^2\right), & d_i(t) \leq d_i^*(t), \\ a_{free}(t)\left(1 - \left(\frac{d_i^*(t)}{\tilde{d}_i(t)}\right)^{\frac{2a_{max}}{|a_{free}|}}\right), & \text{otherwise}, \end{cases} \tag{12}$$

with

$$d_i^*(t) = \bar{d} + \max\left(0, \hat{v}_{i-1}\lambda - \frac{\hat{v}_{i-1}\Delta\tilde{v}_i}{2\sqrt{a_{max}a_{min}}}\right), \tag{13}$$

$$a_{free}(t) = a_{max}\left(1 - \left(\frac{\hat{v}_{i-1}(t)}{\hat{v}_i(t)}\right)^{\delta}\right), \tag{14}$$

where a_{max} is the maximum acceleration of the vehicle, a_{min} is the maximum deceleration, $\bar{d}$ is the minimum gap , $\delta = 4$ is the acceleration exponent and λ is the desired headway time.

The variables $\tilde{d}_i$ and $\Delta\tilde{v}_i$ are the relative spacing and relative speed estimated by human drivers, which are given by the estimation model [88]

$$\tilde{d}_i(t) = d_i(t)e^{V_s w_s(t)}, \tag{15}$$

$$\Delta\tilde{v}_i(t) = \hat{v}_{i-1}(t) - \hat{v}_i(t) + \tilde{d}_i(t)\sigma_r w_l(t), \tag{16}$$

where $w_s(t), w_l(t) \in W$ belongs to the set of random variables generated by Wiener process, V_s is the coefficient variation of the Wiener process, σ_r is the constant standard deviation of the relative approach rate. The random variable $w(t) \in W$ produced by the Wiener process can be described by

$$w(t + \Delta t) = w(t)e^{\frac{-\Delta t}{\bar{\tau}}} + \eta\sqrt{\frac{2\Delta t}{\bar{\tau}}}, \tag{17}$$

where η is a random number which follows the uniform distribution with zero expectation and unit variance, and $\bar{\tau}$ is the correlation time. The estimation model in Eq. (15), (16) and (17) describes the stochastic aspects of human estimation [88].